学位論文

Study of Bulge Properties in Local Luminous Infrared Galaxies Based on Ground-based Paα Imaging Survey

水素パッシェン α 輝線サーベイ観測による 近傍高光度赤外線銀河バルジの研究

平成２６年１２月　博士（理学）申請

東京大学大学院理学系研究科
天文学専攻

舘内　謙

Author
Ken Tateuchi

Study of Bulge Properties in Local Luminous Infrared Galaxies Based on Ground-based Paα Imaging Survey

水素パッシェンα輝線サーベイ観測による近傍高光度赤外線銀河バルジの研究

Abstract

In recent years, many researches suggest that there are two types of bulges found at the center of galaxies, which are called “classical bulges” and “pseudobulges”. The classical bulges are dynamically hot, supported by stellar velocity dispersion rather than their systemic rotational motion, and characterized by steep increase in density towards their centers. In addition, they are red in color, old in population, high in metallicity and in α/Fe ratio. Also, it is suggested that their positons in the fundamental plane form a continuous sequence with those of elliptical galaxies. On the other hand, the pseudobulges are dynamically cold, supported by stellar systemic rotation, and have flat shapes resembling those of expotential disks. Also, they can be identified as outliers in the fundamental plane and generally have younger stellar populations than classical bulges. Theoretically, the classical bulges are considered to be formed by major merger processes, or by collapse of giant clumps in primordial disks to remove their angular momentum. Ellipticals are also considered to be formed by similar processes but they have poor molecular gas with dry merger. On the other hand, the pseudobulges are considered to be built by a secular evolution. From these results, the classical bulges and the pseudo-bulges are considered to have different formation processes, where the classical bulges are formed by drastic external factor such as major merger processes, which are similar process expected for the formation of ellipticals, and the pseudobulges by a secular evolution. However, there are few observational studies to verify the formation scenario of bulges and ellipticals.

The aim of this paper is to verify observationally the formation scenario of bulge drawn in theory, and to understand the formation process of bulges. We therefore focus on LIRGs in the local universe, which are ideal laboratories for studying bulge formation, because half of them are non-irregular galaxies where their bulge type can be evaluated, and they are considered to be current formation sites of bulges with on-going starburst.

However, LIRGs are affected by a large amount of dust, typically associated with the regions of active star formation. Therefore, optical hydrogen recombination lines that are direct probes of massive stars such as Hα and Hβ are easily attenuated by the dust. Wherein the hydrogen Paα emission line (1.8751 μm) is a good tracer of the dusty star-forming region because of its insensitivity to the dust-extinction and being the strongest emission line in the near-infrared wavelength range (NIR, $\lambda \sim 0.9$–2.5 μm), which can reach higher spatial resolution easily than in the MIR and FIR.

However, because of poor telluric atmospheric transmission around the wavelength of Paα due to absorptions mainly by water vapor, no Paα imaging from a ground-based telescope is reported so far.

Therefore, we have been carrying out Paα narrow-band imaging observations with

Atacama Near InfraRed camera (ANIR), on the University of Tokyo Atacama Observatory (TAO) 1.0m telescope (miniTAO) installed at the summit of Co. Chajnantor (5640m altitude) in northern Chile. Thanks to the high altitude and the extremely low water vapor content of the site we can stably observe Paα emission line has been observationally confirmed.

We have observed 38 galaxy system listed in *IRAS* RBGS catalog in Paα with a narrow-band filter at 1.91 μm (cz = 2800–8100 km s^{-1}, $L(\mathrm{IR}) = 4.5 \times 10^{10}$–$6.5 \times 10^{11}\ L_\odot$). Pa$\alpha$ fluxes are estimated from the narrow-band images with our newly developed flux calibration method, and find that $SFR(\mathrm{Pa}\alpha)_{\mathrm{corr}}$ which is star formation rate (SFR) obtained from Paα luminosity corrected for effect of dust extinction with balmer decrement method (Hβ/Hα) shows good agreement with $SFR(\mathrm{IR})$ which is SFR estimated from total infrared luminoisity. This result suggests that Paα with dust-extinction correction is sufficient for estimating SFR of whole the galaxy. However, some galaxies have large differences between the $SFR(\mathrm{Pa}\alpha)_{\mathrm{corr}}$ and the $SFR(\mathrm{IR})$, which may be caused by effect of AGNs, strong dust-extinction, or IR cirrus component. We also obtain surface densities of $L(\mathrm{IR})$ ($\Sigma_{L(\mathrm{IR})}$) and SFR obtained from Paα (Σ_{SFR}) for individual galaxies by measuring extension of distribution of star-forming regions within a galaxy with Paα emission line. The range of $SFR(\mathrm{Pa}\alpha)_{\mathrm{corr}}$ in our sample (from 0.6 to 104 $M_\odot$ yr^{-1}) fill the blank of the range of SFR in previous works. We find that most of the sample follow a sequence of local U/LIRGs on the $L(\mathrm{IR})$-$\Sigma_{L(\mathrm{IR})}$ and SFR-Σ_{SFR} plane. We confirm that a transition of the sequence from normal galaxies to U/LIRGs is seen at $L(\mathrm{IR}) = 8 \times 10^{10}\ L_\odot$.

Using this sample, we next estimate the properties of two types of bulges (classical and pseudo-bulges). To classify them, we remove 18 irregular galaxies from our sample and perform a two-demensional bulge-disk decomposition analysis in the K_{s}-band images with a combination of a Sérsic profile as the bulge component and an exponential profile as the disk component. We find that the Sérsic indices of LIRGs have bimodal ditribution with a separation of $n_b \sim 2.5$, which is consistent with the separation of bulges in the normal galaxies reported in previous works. Also, B/T increase with increasing Sérsic indices. These results suggest that properties of bulges in LIRGs are same as those of normal galaxies. Also, we measure the extents of distribution of star-forming regions in Paα emission line images, and find that extents normalized by the bulge sizes correlate with Sérsic indices of bulges, suggesting that pseudobulges have extended star-forming regions beyond the bulge, while classical bulges have compact star-forming regions concentrated at the centers of the galaxies. These results suggest that there are different star formation scenarios at work in classical and pseudo-bulges.

Furthermore, our results may support the hypothesis that there are two different modes of black hole feeding, where the growth of black holes and classical bulges are controlled by the same global process with major merging, while that of black holes and pseudobulges are independent or have a weak connection with secular evolution.

Contents

List of Figures

List of Tables

Acknowledgments

First and foremost I offer my sincerest gratitude to my supervisor, Dr. Kentaro Motohara, who has supported me during the graduate course with his patience and knowledge. I attribute the level of my PhD degree to his encouragement and effort and without him this thesis, too, would not have been completed or written. The members of the ANIR and SWIM-team have contributed immensely to my personal and professional time. The team has been a source of friendships as well as good advice and collaboration. I am especially grateful for Dr. Brian Gardner, Per Bjornsson, and Eric Straver. I would like to acknowledge honorary group member Doug Bonn who was here on sabbatical a couple years ago

I have been involved in the several research projects in these five years.

the quality of the paper, and we also thank M. Malkan (UCLA) and S. Howard (CfA) for enlightening discus- sions on this topic.

Also, this work is supported by Ministry of Education, Culture, Sports, Science and Tech- nology of Japan, Grant-in-Aid for Scientific Research (17104002, 20040003, 20041003, 21018003, 21018005, 21684006, 22253002, 22540258,and 23540261) from the Japan Society for the Promotion of Science (JSPS). Op- eration of ANIR on the miniTAO 1m telescope is also supported by NAOJ Research Grant for Universities and Optical & Near-Infrared Astronomy Inter-University Cooperation Program, supported by the MEXT of Japan. Part of this work has been supported by the Institutional Program for Young Researcher Overseas Visits operated by JSPS. The Image Reduction and Analysis Facility (IRAF) used in this paper is distributed by the National Optical Astronomy Observatories, which are operated by the Association of Universities for Research in Astronomy, Inc., under cooperative agreement with the National Science Foundation. We acknowledge the usage of the HyperLeda database (http://leda.univ-lyon1.fr).

Chapter 1

Introduction

1.1 Bulge Structure and Formation

What is a Bulge? Although there is no canonical interpretation, we have a common understanding that it appears legitimate to look at bulges as ellipticals in the Hubble-Sandage de Vaucouleurs classifications (e.g., Hubble, 1926, 1927). In recent years, many researches suggest that there are two types of bulges found at the center of galaxies, which are called "classical bulges" and "pseudobulges" (e.g. Kormendy & Kennicutt, 2004; Athanassoula, 2005; Kormendy & Fisher, 2005; Combes, 2009; Fisher & Drory, 2010). The classical bulges are dynamically hot, supported by stellar velocity dispersion rather than their systemic rotational motion, and characterized by a steep increase in density towards their centers. (Fisher & Drory, 2008; Guedes et al., 2013). In addition, they are red in color, old in population, high in metallicity and in α/Fe ratio (Moorthy & Holtzman, 2006; Zoccali et al., 2006; Ballero et al., 2007; Lecureur et al., 2007; McWilliam et al., 2008). Also, it is suggested that their positions in the fundamental plane form a continuous sequence with those of elliptical galaxies (Driver et al., 2007; Falcón-Barroso et al., 2002; Thomas & Davies, 2006; Jablonka et al., 2007; Gadotti, 2009). On the other hand, the pseudobulges are dynamically cold, supported by stellar systemic rotation, and have flat shapes resembling those of expotential disks. Also, they can be identified as outliers in the fundamental plane (Gadotti, 2009) and generally have younger stellar populations than classical bulges.

Kormendy & Kennicutt (2004) classify 75 normal galaxies obtained in V-band by their eyes, and report that 28.5% of their sample have classical bulges and 71.5% have pseudobulges. Using this sample, Fisher & Drory (2008) show that two kinds of bulges can be distinguished by Sérsic indices, and that a distribution of the indicies is bimodal, where the pseudobulges have $n_b < 2.2$, while the classical bulges $n_b \geq 2.2$.

Theoretically, the classical bulges are considered to be formed by major merger processes (e.g., Kormendy & Kennicutt, 2004; Naab & Trujillo, 2006; Hopkins et al., 2010), or by collapse of giant clumps in primordial disks (Bournaud et al. 2007) to remove their angular momentum. Ellipticals are also considered to be formed by similar processes but they have poor molecular gas with dry merger (e.g., Kormendy & Kennicutt, 2004). On the other hand, the pseudobulges are considered to be built by a secular evolution (e.g., Kormendy & Kennicutt, 2004). Okamoto (2013) shows that pseudobulges are formed by

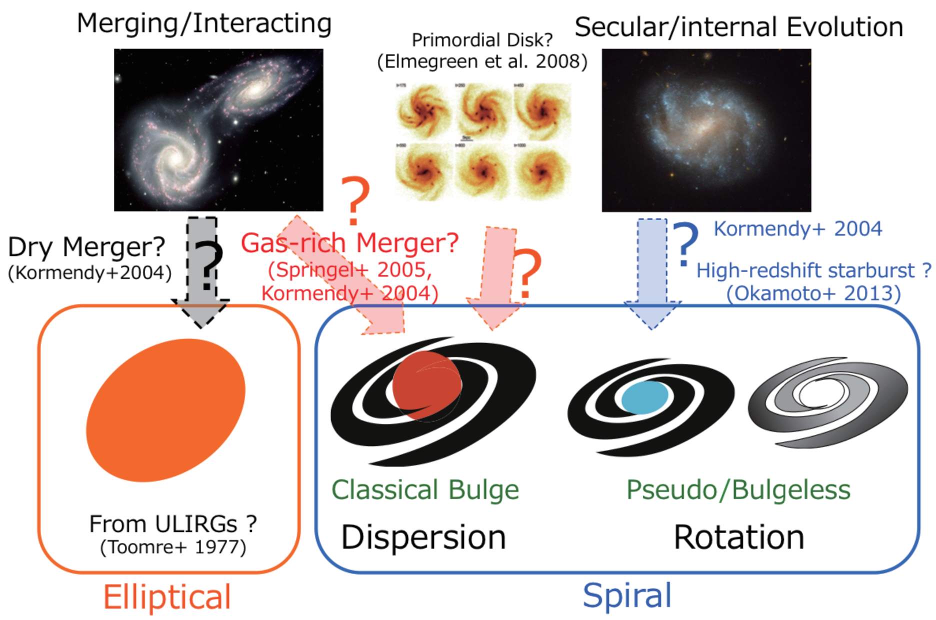

Figure 1.1: Schematic view of theoretical prospect of morphogenesis of galaxies. Classical bulges and ellipticals are thought to be end-products of galaxy mergers, and pseudobulges are considered that they have been formed without a major merging process with other galaxies.

drastic formation with starbursts at high-redshift of two, which may be an extreme example of secular evolution. Figure 1.1 shows the schematic view of theoretical prospect of galactic formation.

Furthermore, it is speculated that these two types of bulges have a deep relationship with the growth of supermassive black holes (SMBs). Magorrian et al. (1998) found that the relation between the mass of a central black hole and the mass of the host galaxy with 32 of the nearby galaxies, which is known as the 'Magorrian relation'. After that, many researcheres found an empirical correlation between the stellar velocity dispersion σ of a bulge in host galaxy and the mass (M) of the SMB, which is called "$M-\sigma$ relation", and these results suggest that the SMBs and their hosts are coevolve (e.g., Kormendy & Gebhardt, 2001; Ferrarese & Merritt, 2000; Gebhardt et al., 2000; Tremaine et al., 2002; Gültekin et al., 2009). Kormendy et al. (2011) find that the correlation between masses of SMBs $(M_\bullet)$ and velocity dispersions of a classical bulges have a tight correlation, while those of pseudobulges do not. They suggest that there are two fundamentally different feeding mechanisms for a black hole; one is that growth of the black hole and the galaxy is controlled by a same global process where large amounts of gas fall into the center of the galaxy via rapid feeding, and the other is that the growth of the black hole is controlled by a local process that feed gas from $\sim 10^2$ pc stochastically, and independent or have a weak connection to the growth of the mass of SMBs.

Thus, the classical bulges and the pseudobulges are considered to have different formation processes, where the classical bulges are considered to be formed by drastic external factor such as major merger processes, which are the similar process with ellipticals, and the pseudobulges are considered to be built by a secular evolution. However, there are few observational studies to verify the formation scenario of bulges and ellipticals.

1.2 Luminous Infrared Galaxy

The dawn of infrared astronomy for galaxy is brought with the first discoveries of some extra-galactic sources (e.g., Kleinmann & Low, 1970a,b; Becklin et al., 1971; Becklin & Neugebauer, 1972; Rieke & Low, 1972). Following these results, researches find that the radiation mechanism of these infrared sources are explained by models of thermal reradiation from dust (e.g., Rees et al., 1969; Burbidge & Stein, 1970) and the infrared emissions from interacting galaxies are enhanced more than those from isolated galaxies (e.g., Joseph et al., 1984; Lonsdale et al., 1984; Cutri & McAlary, 1985). In January 25 1983, the Infrared Astronomical Satellite (*IRAS*) has been lunched by the United States, United kingdom and Netherlands to perform an unbiased and sensitive all sky survey at 12, 25, 60 and 100 μm (Soifer et al., 1987). This satellite find that there are many galaxies which are bright in the infrared in the universe and these luminous infrared sources are defined as ULIRGs (Ultra Luminous Infrared Galaxies; $L(\mathrm{IR}) \equiv L$ (8–1000 μm) $\geq 10^{12}$ $L_\odot$) and LIRGs (Luminous Infrared Galaxies; $L(\mathrm{IR}) \equiv 10^{11}$–$10^{12}$ $L_\odot$). Sanders & Mirabel (1996) suggest that local ULIRGs are produced by major-merger events, and a large fraction of ellipticals could be formed via merging, while most of LIRGs do not show obvious appearance of current or past interaction, being consistent with the result from recent research (e.g., Wang et al., 2006). They also claimed that the infrared activity in U/LIRGs come from starburst and/or active galactic nulcei (ANG), whose details are still an open question. In addition, normal galaxies show extended star-forming regions over a few kilo-parsecs along the spiral arms, while distributions of star-forming regions of LIRGs at the high infrared luminosity end ($\log(L(\mathrm{IR})/L_\odot)$ = 11.8–12.0) and ULIRGs, which are considered to be in the starburst sequence, become very compact and concentrated at central regions (e.g., Soifer et al., 2000; Díaz-Santos et al., 2010; Rujopakarn et al., 2011; Alonso-Herrero et al., 2012). However, the relationship between star formation activities and spatial distribution of star-forming regions, and the mechanism of starburst is still an open question. Some simulations of galaxy formation suggest that the central concentration of stars and gases is formed by interacting/merging events, which accumulate dense gas clouds and triggers starburst (Barnes & Hernquist, 1996). However, there have been not enough observational studies to reveal the relationship between star formation activities and spatial distribution of star-forming regions. From these results, it is considered that ULIRGs and LIRGs have an important role for understanding the formation and evolution of galaxies, although their contribution to the infrared emission in the local universe is only about 6$\sim$7% (e.g., Soifer & Neugebauer, 1991; Goto et al., 2010).

In recent years, many large deep cosmological surveys have been performed in various wavelengths, including ultraviolet, visible, infrared and submillimeter. These surveys have revealed that the star formation rate (SFR) density of the universe (cosmic SFR density, cSFRD) increases with redshift, and peaks at $1 < z < 3$ (e.g., Hopkins &

Beacom, 2006; Rujopakarn et al., 2010). It is also found that the cSFRD at the high-redshift universe is dominated by bright infrared galaxies; ULIRGs and LIRGs dominate 80% of total star formation activities at $z \sim 1$ (e.g., Caputi et al., 2007; Goto et al., 2010), and these galaxies are in the starburst sequence which have high star formation efficiency (SFE = SFR ($M_\odot$ yr^{-1})/$M_{\rm gas}$ ($M_\odot$)) of around 10^{-8} yr^{-1} (e.g., Lada et al., 2012; Daddi et al., 2010) in contrast to 10^{-9} yr^{-1} for normal galaxies.

1.3 Aim of this Thesis

The aim of this paper is to verify observationally the formation scenario of bulge drawn in theory, and is to understand the formation process of bulges. We therefore focus on LIRGs in the local universe, which are ideal laboratories for studying bulge formation, because half of them are non-irregular galaxies (Wang et al., 2006) where their bulge type can be evaluated, and they are considered to be current formation sites of bulges with on-going starburst. Also, nearby U/LIRGs are ideal laboratories to study the detailed properties of galaxy formation, as they can be spatially resolved easily. Especially, to understand the detailed mechanism of starburst activities in LIRGs, star formation rate is one of the most important parameters. Many indicators for estimation of star formation rate, such as X-ray, ultraviolet (UV), Hα, mid-infrared (MIR), and far-infrared (FIR) emission have been used. Hydrogen recombination lines, which is emitted from the current star-forming regions within 10 Myr (Sanders & Mirabel, 1996), are direct tracers of star-forming regions. Especially, optical hydrogen recombination lines such as Hα and Hβ are usually used because they can be observed easily.

However, LIRGs are affected by a large amount of dust (extinction of $A_V \sim 3$ mag for LIRGs; Alonso-Herrero et al., 2006, and $A_V > 10$ mag for ULIRGs; Piqueras López et al., 2013), typically associated with the regions of active star formation. Therefore, optical hydrogen recombination lines that are direct probes of massive stars such as Hα and Hβ are easily attenuated by the dust. Wherein the hydrogen Paα emission line (1.8751 μm) is a good tracer of the dusty star-forming region (Alonso-Herrero et al., 2006) because of its insensitivity to the dust-extinction ($A_{\rm Pa\alpha}/A_{\rm H\alpha} = 5.68$) and being the strongest emission line in the near-infrared wavelength range (NIR, $\lambda \sim 0.9$–2.5 μm), which can reach higher spatial resolution easily than in the MIR and FIR. Figure 1.2 shows the intensities of hydrogen recombination lines compare to the intrinsic Hα intensity, suggesting that Paα intensity is the strongest beyond $A_V \sim 3.5$.

However, because of poor telluric atmospheric transmission around the wavelength of Paα emission line (Figure 3.1) due to absorptions mainly by water vapor, no Paα imaging from a ground-based telescope is reported so far, although there are some spectroscopic observations of Paα in redshifted galaxies (e.g., Hill et al., 1996; Falcke et al., 1998; Murphy et al., 1999; Kim et al., 2010). To overcome these difficulties, it is necessary to observe the emission line by either a space-borne facilities such as the Near Infrared Camera and Multi-object Spectrometer (NICMOS) on *Hubble Space Telescope* (*HST*) (e.g., Scoville et al., 2001; Alonso-Herrero et al., 2006; Liu et al., 2013a) or facilities built at sites with low precipitable water vapor (PWV). However, some researchers have pointed out that *HST*/NICMOS (already decommissioned in 2010) may be insensitive to diffuse Paα emis-

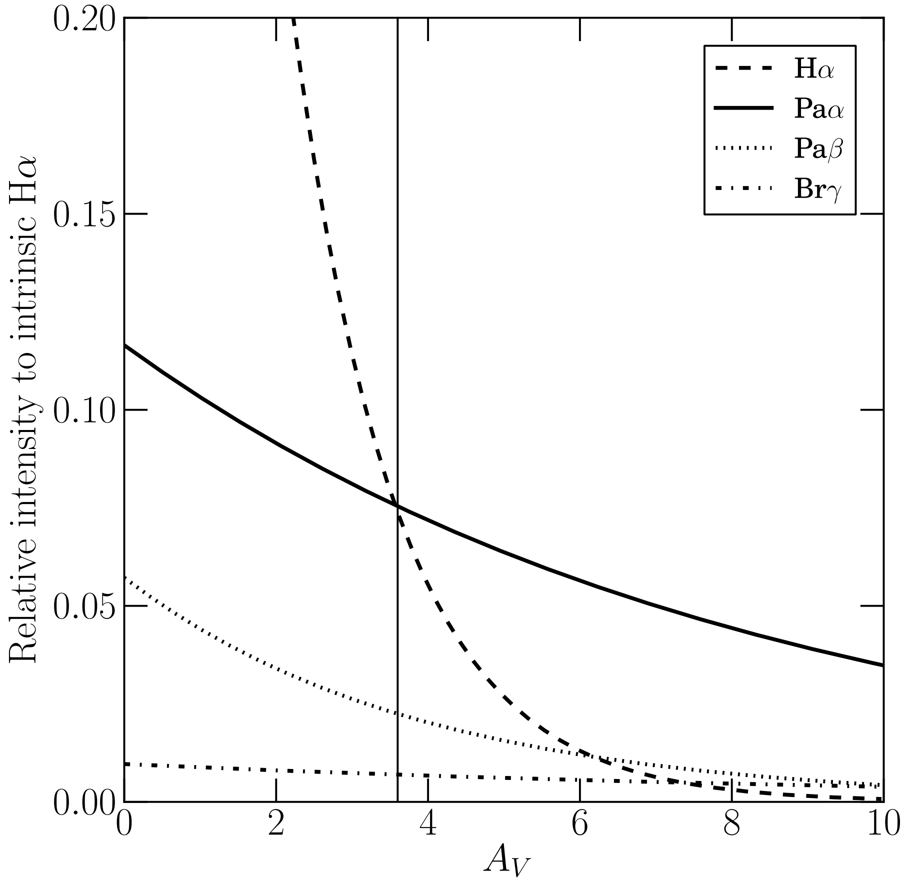

Figure 1.2: Comparison between the dust extinction (A_V) and the the intensities of hydrogen recombination lines compare to the intrinsic Hα intensit. To estimate for the dust extinction, we adopt the extinction curve of Calzetti et al. (2000) with $R_V = 4.05$, and Case-B.

sion due to its intrinsic high angular resolution (e.g., Alonso-Herrero et al., 2006; Calzetti et al., 2007; Kennicutt et al., 2007; Rieke et al., 2009).

Therefore, we have been carrying out Paα narrow-band imaging observations with Atacama Near InfraRed camera (ANIR; Motohara et al. 2008, Konishi et al. 2014; K14), on the University of Tokyo Atacama Observatory (TAO, Yoshii et al. 2010) 1.0m telescope (miniTAO; Minezaki et al. 2010) installed at the summit of Co. Chajnantor (5640m altitude) in northern Chile to understand distributions of star-forming region and properties of dust-enshrouded infrared galaxies in the local universe. Thanks to the high altitude and the extremely low water vapor content of the site we can stably observe Paα emission line has been observationally confirmed (Motohara et al., 2010, 2011; Tanabé et al., 2013; Konishi et al., 2014; Tateuchi et al., 2015).

In the following chapters, we describe our sample of luminous infrared galaxies and the observation procedure in Part 2, the method of data reduction and flux calibration in Part 3, and the derived Paα flux, properties of individual galaxies and the result of bulge-disk decomposition for some LIRGs in Part 4. In Part 5, we evaluate the selection bias due to our luminosity-limited sample, the effects of dust-extinction, the relationship between SFRs estimated from Paα and those from FIR fluxes, the properties of surface densities of SFR, the properties of bulges and the relationship between the sizes of star-forming regions and the Sérsic indices of bulges. Then, we summarize and conclued them in Par 6.

Throughout this paper, we use a Λ-CDM cosmology with $\Omega_m = 0.3$, $\Omega_\Lambda = 0.7$, and $H_0 = 70$ km s^{-1} Mpc^{-1}.

Chapter 2

Data

2.1 Atacama Near Infrared Camera

The observations have been carried out using Atacama NIR camera (ANIR; Motohara et al. 2008,Konishi et al. 2014) installed at the Cassegrain focus of the University of Tokyo Atacama Observatory (TAO, P.I.:Yuzuru Yoshii; Yoshii et al. e.g., 2002, 2010) 1.0 m telescope (miniTAO; Minezaki et al. 2010). The observatory is located at the summit of Co. Chajnantor (5640m altitude) in northern Chile.

The high altitude and the extremely low precipitable water vapor (PWV = 0.5 mm) of the site enable us to perform observation of Paα. Figure 3.1 shows the simulated atmospheric transmittance with the ATRAN (Lord , 1992) at the TAO site. It can be seen that the site (bold line) shows higher transmission than at the lower site (dotted line), especially at the wavelength range around Paα. The first light observation was carried out in July 2009, and Paα images have been successfully obtained using the narrow-band filters (N1875 for Galactic objects and $N191$ for extragalactic objects redshifted by $cz = 2800 \sim 8100$ km s^{-1} (Motohara et al., 2010)).

2.2 Paα Survey of Local LIRGs

We have selected the target galaxies from the $IRAS$ Revised Bright Galaxy Sample (RBGS : Sanders et al. 2003). The location of the observatory limits the declination of the targets to be $< 30°$. The wavelength range of the $N191$ narrow-band filter limits the recession velocity to be 2800 km s^{-1} – 8100 km s^{-1}, corresponding to the distances of 46.6 Mpc – 109.6 Mpc. From these conditions, the observable galaxies in the RBGS is 151, and we have observed 38 galaxies out of them at random, corresponding 25% out of the all 151 galaxies.

The selected galaxies are listed in Table 2.1. Figure 2.2 shows the distribution of the distance of the sample. The gray is the 629 galaxies from the RBGS catalog cut within the $cz < 1000$ km s^{-1}, the gray-red 151 galaxies selected by the limits of the wavelenght range of the $N191$ narro-band filter, the gray-blue 24 galaxies selected by the limits of the wavelength range of the $N1875$ narrow-band filter, and the red 38 galaxies our selected targets. Our 38 targets are uniformly distributed whithin the recession velocity.

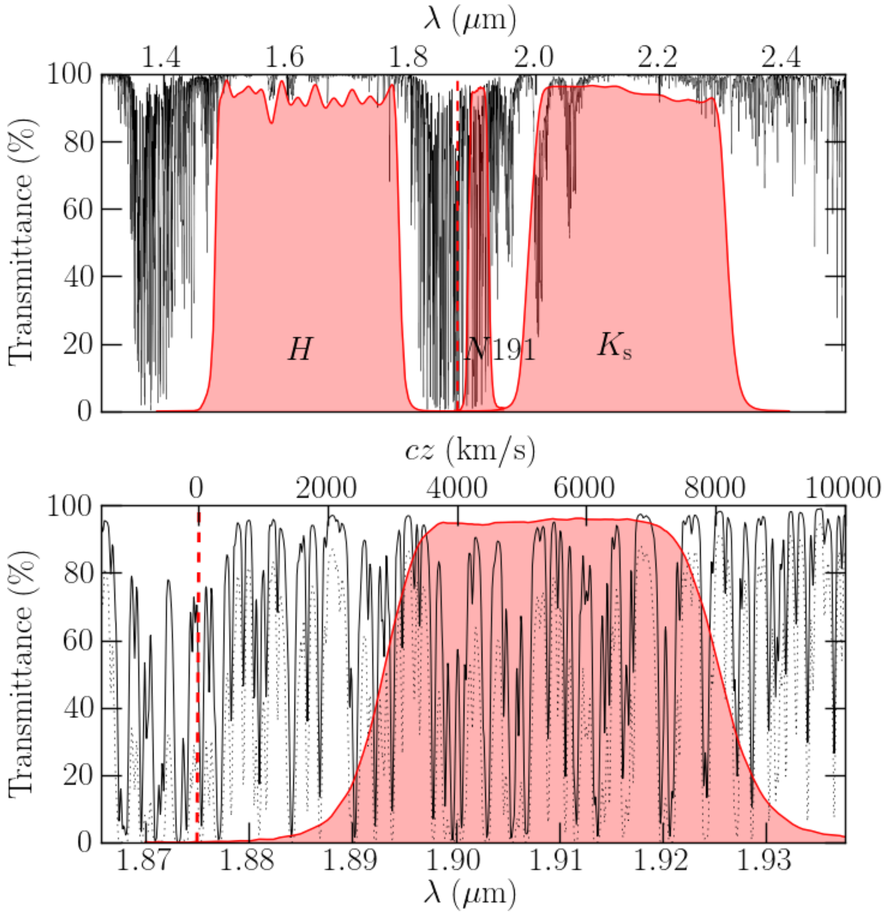

Figure 2.1: Top: atmospheric transmittance in the wavelength range containing the H- and the K_s-band. The area shaded with cyan represents the difference of the median value of the transmittance at the miniTAO site (altitude of 5,640 m, PWV = 0.5 mm) and that at the VLT site (2,600 m, PWV = 2.0 mm), both calculated by ATRAN (Lord , 1992). The bold lines shows the filter transmittance curve of the H-band, $N191$, and K_s-band filters. Bottom: atmospheric transmittance around the $N191$ filter. The cyan line corresponds to that at the TAO site, and the thin-gray at the VLT site. The overlaid thick red line shows the transmittance of the $N191$ filter. The dashed vertical red line in the both plots represents the wavelength of the rest-frame Paα (1.8751 μm).

Table 2.1: Sample of Local Luminous Infrared Galaxies

ID (1)	Galaxy Name (2)	IRAS Name (3)	R.A. (J2000) (4)	Dec. (J2000) (5)	cz (km s^{-1}) (6)	Dist. (Mpc) (7)	log(L(IR)) (log($L_\odot$)) (8)	Spectral Class (9)	Obs. Date (10)
1	NGC 23	F00073+2538	00 09 55.1	+25 55 37	4536	65.6	11.13	HII	2009-10-26
2	NGC 34	F00085−1223	00 11 06.6	−12 06 27	5931	86.0	11.52	Sy2	2011-10-22
3	NGC 232	F00402−2349	00 42 46.5	−23 33 31	6047	87.7	11.39	HII	2009-10-21
4	IC 1623A/B	F01053−1746	01 07 46.3	−17 30 32	6028	87.4	11.74	HII	2009-10-17
5	ESO 244-G012	F01159−4443	01 18 08.6	−44 27 40	6866	99.8	11.48	LINER	2009-10-21
6	UGC 2238	F02435+1253	02 46 17.0	+13 05 45	6436	93.5	11.33	LINER	2009-10-27
7	IRAS F02437+2122	F02437+2122	02 46 38.3	+21 35 06	6987	101.6	11.21	LINER	2009-10-22
8	UGC 2982	F04097+0525	04 12 22.4	+05 32 49	5161	74.7	11.20	HII	2011-10-19
9	NGC 1614	F04315−0840	04 34 00.1	−08 34 46	4746	68.6	11.66	HII/Sy2	2009-10-15
10	MCG −05-12-006	F04502−3304	04 52 06.8	−32 59 24	5622	81.5	11.17	HII	2009-10-14
11	NGC 1720	F04569−0756	04 59 19.9	−07 51 34	4186	60.4	10.90	N	2011-10-19
12	ESO 557-G002	F06295−1735	06 31 46.3	−17 37 15	6339	92.0	11.24	HII	2009-10-19
13	IRAS F06592-6313	F06592−6313	06 59 40.3	−63 17 53	6882	100.0	11.20	HII	2009-10-27
14	NGC 2342	07063+2043	07 09 19.6	+20 38 12	5276	76.4	11.40	HII	2009-10-23
15	ESO 320-G030	F11506−3851	11 53 12.0	−39 07 54	3232	46.6	11.28	HII	2011-04-21
16	NGC 4922	F12590+2934	13 01 25.9	+29 18 46	7071	102.8	11.33	LINER	2009-06-13
17	MCG −03-34-064	F13197−1627	13 22 23.5	−16 43 34	5152	74.6	11.28	Sy1	2011-04-28
18	NGC 5135	F13229−2934	13 25 43.0	−29 49 54	4114	59.4	11.27	Sy2	2011-04-28
19	NGC 5257/8	F13373+0105	13 39 54.9	+00 50 07	6798	98.8	11.54	HII	2011-04-27
20	IC 4518A/B	F14544−4255	14 57 43.1	−43 08 01	4715	68.2	11.09	Sy2	2011-04-24
21	IC 4687/86	F18093−5744	18 13 38.6	−57 43 36	5188	75.0	11.55	HII (both)	2011-04-25
22	IRAS F18293-3413	F18293−3413	18 32 40.2	−34 11 26	5449	78.9	11.82	HII	2009-06-12
23	ESO 339-G011	F19542−3804	19 57 37.5	−37 56 10	5722	82.9	11.14	Sy2	2009-10-25
24	NGC 6926	F20304−0211	20 33 04.8	−02 01 39	5970	86.6	11.32	Sy2	2009-06-12
25	IC 5063	F20482−5715	20 52 03.5	−57 04 03	3380	48.7	10.86	Sy2	2010-10-15
26	ESO 286-G035	F21008−4347	21 04 11.2	−43 35 34	5208	75.4	11.25	HII	2009-10-27
27	ESO 343-IG013	F21330−3846	21 36 10.8	−38 32 38	5714	82.8	11.10	HII	2009-10-25
28	NGC 7130	F21453−3511	21 48 19.6	−34 57 05	4824	69.8	11.39	LINER/Sy1	2009-10-26
29	IC 5179	F22132−3705	22 16 10.0	−36 50 35	3398	49.0	11.21	HII	2010-10-14
30	ESO 534-G009	F22359−2606	22 38 40.8	−25 51 05	3393	48.9	10.70	LINER	2010-10-07
31	NGC 7469	F23007+0836	23 03 15.5	+08 52 25	4922	71.2	11.67	Sy1	2009-10-22
32	CGCG 453-062	F23024+1916	23 04 55.2	+19 33 01	7524	109.6	11.41	LINER	2010-10-19
33	NGC 7591	F23157+0618	23 18 15.7	+06 35 06	4961	71.8	11.11	LINER	2011-10-16
34	NGC 7678	F23259+2208	23 28 27.0	+22 25 09	3482	50.2	10.84	HII	2010-10-20
35	MCG −01-60-022	F23394−0353	23 42 02.2	−03 36 48	6966	101.3	11.29	HII	2009-10-17
36	NGC 7771	F23488+1949	23 51 24.7	+20 06 39	4336	62.6	11.42	HII	2009-10-27
37	Mrk 0331	F23488+2018	23 51 26.1	+20 35 08	5371	77.8	11.48	HII/Sy2	2010-10-15
38	UGC 12914/15	F23591+2312	00 01 40.7	+23 29 37	4534	65.5	10.99	LINER	2010-10-09

Column (1): Galaxy ID in this paper. Column (2): Galaxy name. Column (3): IRA catalog ID. Column (4): Right Ascension for the epoch 2000. Column (5): Declination for the epoch 2000. Column (6): Recession velocity. Column (7): Luminosity distance based on the parameters of Λ-CDM cosmology (e.g., Spergel et al., 2003). Column (8): Bolometric Infrared luminosities ($L_{\mathrm{IR}(8-1000\mu\mathrm{m})}$ ($L_\odot$)) in Sanders et al. (2003) corrected for the different cosmic parameters. Column (9): Classification by optical spectroscopic observation taken from Kim et al. (1998) and Alonso-Herrero et al. (2006). Sy1: Seyfert 1, Sy2: Seyfert 2, LINER: LINER, HII: HII region. (10): Observation date, yyyy-mm-dd.

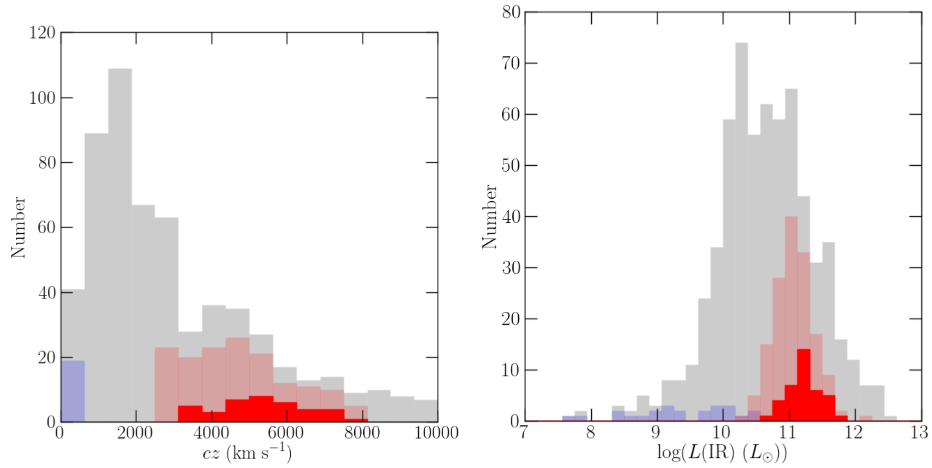

Figure 2.2: Left: histogram of cz in RBGS catalog (Sanders et al., 2003). The gray show the 629 galaxies from the RBGS catalog cut within the $cz < 1000$ km s^{-1}, the gray-red 151 galaxies selected by the limits of the wavelenght range of the $N191$ narro-band filter, the gray-blue 24 galaxies selected by the limits of the wavelength range of the $N1875$ narrow-band filter, and the red 38 galaxies our selected targets. Right: histogram of infrared luminosity in RBGS catalog. The gray is the 629 galaxies from the RBGS catalog, the gray-red 151 galaxies selected by the limits of the wavelenght range of the $N191$ narro-band filter, the gray-blue 24 galaxies selected by the limits of the wavelength range of the $N1875$ narrow-band filter, and the red 38 galaxies our selected targets.

Also, our sample distribute the bolometric infrared luminosity ($L(\mathrm{IR})$) ranges between 4.5×10^{10} $L_\odot$ and 6.5×10^{11} $L_\odot$, which is from the high luminosity end of normal galaxies to LIRGs. Figure 2.2 shows the distribution. The gray is the 629 galaxies from the RBGS catalog, the gray-red 151 galaxies selected by the limits of the wavelenght range of the $N191$ narro-band filter, the gray-blue 24 galaxies selected by the limits of the wavelength range of the $N1875$ narrow-band filter, and the red 38 galaxies our selected targets. Our targets show that 33 galaxies in our sample are LIRGs, corresponding 87 % in our 38 targets, and there are no ULIRGs.

Figure 2.3 shows the sky position of the galaxies. The dot shows the 629 galaxies from the RBGS catalog, the red diamond 151 galaxies selected by the limits of the wavelenght range of the $N191$ narro-band filter, the bule diamond 24 galaxies selected by the limits of the wavelength range of the $N1875$ narrow-band filter, and the filled-red diamond 38 galaxies our selected targets. Although the location of miniTAO/ANIR are limitted, our targets are uniformly distributed whithin the limitation.

We have carried out 5 observation runs from 2009 to 2011 to observe these 38 targets (44 individual galaxies). They have been observed with the $N191$ narrow-band filter, which has the central wavelength (λ_{c}) of 1.9105 μm with a FWHM of 0.0079 μm ($\Delta\lambda$) to cover redshifted Paα line. Also, we have carried out the observations with the H and K_{s} broad-band filters to obtain stellar continuum images. Typical seeing size is

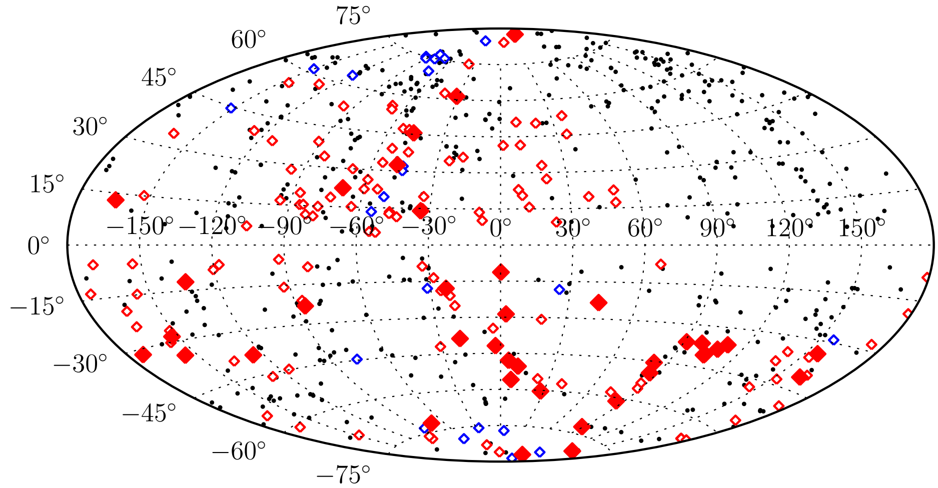

Figure 2.3: Sky location of galaxies in RBGS catalog (Sanders et al., 2003). The dot shows the 629 galaxies from the RBGS catalog, the red diamond 151 galaxies selected by the limits of the wavelenght range of the $N191$ narro-band filter, the bule diamond 24 galaxies selected by the limits of the wavelength range of the $N1875$ narrow-band filter, and the filled-red diamond 38 galaxies our selected targets.

$0''.8$ during the observations. The total integration time for each galaxy is 540 s (60 s $\times$ 9 dithering) for the H and K_s filters, and 1620 s (180 s $\times$ 9 dithering) for the $N191$ except for UGC 12914/5 which is observed with longer integration time of 12420 s for a detailed study (Komugi et al., 2012). As the Paα emission line is strongly affected by the PWV, the observations have been carried out during nights with low PWV. The value of the PWV is 0.1–0.7 mm (Konishi et al., 2014), and the atmospheric window opens around the wavelength of Paα. The median value of the PWV during the observation is 0.5 mm.

Chapter 3

Reduction

3.1 The Procedure

The data are reduced using the standard IRAF software packages. In the first step of the data reduction, flat pattern and sky background are removed from raw images. A flat pattern image is made from a sky image produced by stacking all object-masked images per observation run for each filter. The skybackground is removed using a self-sky image which is made by stacking object-masked images in the same dither sequence. We do not correct the image distortions because it is negligible on ANIR. Each image is matched with World Coordinate System (WCS) using position of 2MASS stars (Skrutskie et al., 2006). Then, these images are shifted according to WCS and co-added. In the second step, the flux scale of the combined image is calibrated by 2MASS stars. Comparing stars in the image with those in the 2MASS catalog, zero-point magnitude and system efficiency are derived. Because reference magnitudes of the $N191$ filter are not available we derived them by interpolating the H- and $K_{\rm s}$- band magnitudes in the 2MASS catalog. Details of this flux calibration procedure are described in K14, arguing that the interpolating calibration technique produces negligible (< 0.01 mag) systematic error. We develop a script called Anir Redcution tool for Imaging data Analysis (ARIA) that automatically proceed these reduction (see Apendix B). The final H, $K_{\rm s}$ and $N191$ images are convolved with a Gaussian function to match the Point Spread Function (PSF) to the worst among the images (typical spatial resolution of the convolved images is $0''.9$). Then, a continuum image is made by interpolating between H and $K_{\rm s}$ images, and we derive a Paα line image by subtracting the continuum image from the $N191$ image.

3.2 Flux Calibration Method for Ground-based Paα Imaging

3.2.1 Derivation of Paα Flux Affected by Atmospheric Absorptions

The TAO site is a suitable place for ground-based Paα observation thanks its low PWV. Still, there are many atmospheric absorption features within the wavelength range of the narrow-band filter (Figure 3.1) which vary temporally due to change of PWV, and it is difficult to obtain the emission-line flux accurately. To recover the intrinsic Paα fluxes

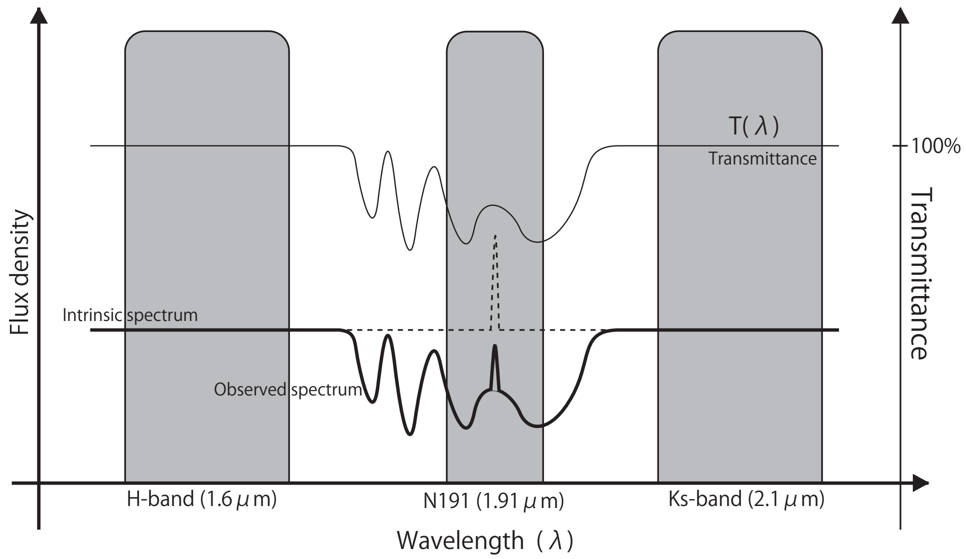

Figure 3.1: Cartoon of a model spectrum around the wavelength of Paα emission line, affected by the atmospheric absorption. H and $K_{\rm s}$ are the broad-band filters, and $N191$ is a narrow-band filter installed used for our observations. The thin curve represents the atmospheric transmittance, the dashed curve the intrinsic spectrum of the target, and the thick line the observed spectrum.

accurately, we then estimate the intrinsic Paα flux as follows.

Figure 3.1 represents a cartoon of a spectrum affected by the atmospheric absorption. The thin-solid curve represents the atmospheric transmittance, the dashed curve an intrinsic spectrum of a target, bold-solid an observed spectrum affected by the atmosphere, and the shaded areas the wavelength ranges of the H-, $N191$- and $K_{\rm s}$-band filters.

The intrinsic Paα flux in the narrow-band filter ($F_{\rm int}^{N191}$) can be divided into two components; one is continuum ($F_{\rm int}^{c}$) and the other is emission line ($F_{\rm int}^{l}$). Then, the intrinsic flux can be written as

$$F_{\rm int}^{N191} = F_{\rm int}^{c} + F_{\rm int}^{l}. \tag{3.1}$$

We also assume that the wavelength dependence of the continuum within the $N191$ filter is negligible. To derive $F_{\rm int}^{l}$ it is necessary to estimate the effect of instrumental absorption and atmospheric absorption due to PWV. The throughput ($\zeta_{\rm ANIR}$) can be written as

$$\zeta_{\rm ANIR} = T_{\rm Tel}^{N191} \times T_{\rm ANIR}^{N191} \times T_{\rm filter}^{N191} \tag{3.2}$$

where $T_{\rm Tel}^{N191}$, $T_{\rm ANIR}^{N191}$, and $T_{\rm filter}^{N191}$ represent transmittance of the telescope, the instrument except the filter, and the $N191$ filter. The averaged atmospheric transmittance toward the zenith (X = airmass = 1) within the wavelength of the $N191$ narrow-band filter $(T_{\rm atm}^{{\rm PWV},N191})^X$ can be written as

$$(T_{\rm atm}^{{\rm PWV},N191})^X = \frac{\int_{\lambda_1}^{\lambda_2} T_{\rm atm}(\lambda)d\lambda}{\int_{\lambda_1}^{\lambda_2} d\lambda}, \tag{3.3}$$

λ_1 and λ_2 represent cut-on and cut-off wavelength of the $N191$ narrow-band filter. Then the observed flux density of $N191$ can be written as follows,

$$F_{\rm obs}^{N191} = F_{\rm int}^{c}\zeta_{\rm ANIR}(T_{\rm atm}^{{\rm PWV},N191})^X + F_{\rm int}^{l}\zeta_{\rm ANIR}T_{\rm line} \tag{3.4}$$

$$F_{\rm int}^{l} = \frac{1}{\zeta_{\rm ANIR}T_{\rm line}}(F_{\rm obs}^{N191} - F_{\rm int}^{c}\zeta_{\rm ANIR}(T_{\rm atm}^{{\rm PWV},N191})^X), \tag{3.5}$$

where the factor $T_{\rm line}$ is effective atmospheric transmittance at the wavelength of redshifted Paα emission line. In a narrow-band filter observation, an observed flux is the averaged flux of emission line within the wavelength range from λ_1 to λ_2, and the flux are calibrated by using the flux of 2MASS stars. The relation between observed flux and calibrated flux ($f_{\rm cal}^{N191}$) is as follows,

$$F_{\rm obs}^{N191} = \zeta_{\rm ANIR}(T_{\rm atm}^{{\rm PWV},N191})^X f_{\rm cal}^{N191}\Delta\lambda. \tag{3.6}$$

where $\Delta\lambda$ is FWHM of the $N191$ narrow-band filter. We can derive a calibrated flux of continuum ($f_{\rm cal}^{c}$) obtained by interpolating H and $K_{\rm s}$ broad-band images ($f_{\rm cal}^{H-K_{\rm s}}$), which are not affected by the atmospheric absorption ($f_{\rm cal}^{c} \equiv f_{\rm cal}^{H-K_{\rm s}}$). (Konishi et al., 2014) argues the interpolating calibration technique produce negligible (< 0.01 mag) systematic error. The relation between intrinsic flux of continuum ($F_{\rm int}^{c}$) and calibrated flux is as follows,

$$F_{\rm int}^{c} = \zeta_{\rm ANIR}f_{\rm cal}^{c}\Delta\lambda \tag{3.7}$$

$$= \zeta_{\rm ANIR}f_{\rm cal}^{H-K_{\rm s}}\Delta\lambda. \tag{3.8}$$

Then, we can obtain the following relation by using the equations 3.5, 3.6 and 3.8,

$$F_{\rm int}^{l} = \frac{(T_{\rm atm}^{{\rm PWV},N191})^X}{T_{\rm line}}(f_{\rm cal}^{N191} - f_{\rm cal}^{H-K_{\rm s}})\Delta\lambda. \tag{3.9}$$

To obtain the Paα flux, we have to estimate $(T_{\rm atm}^{{\rm PWV},N191})^X$ and $T_{\rm line}$.

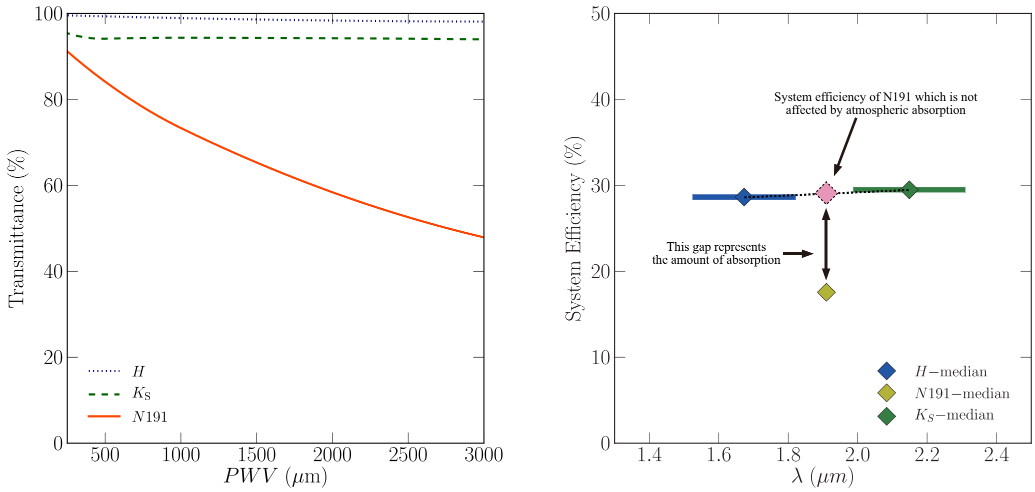

Figure 3.2: Left : PWV dependence of atmospheric transmittance. Dotted, dashed and solid lines represent those of the H-band, the Ks-band and the $N191$ narrow-band filter, respectively. Only the $N191$ filter is strongly affected by PWV. Right : Diagram to show how the atmospheric absorption of the $N191$ filter is derived. The gap between the interpolated and the observed $N191$ system efficiency is due to the effect of the atmospheric absorption.

3.2.2 Estimate PWV from System Efficiency

System efficiency is the ratio of the number of detected photons to that which falls into the Earth atmosphere. The number of incident photons on the telescope is

$$n_{\rm tel} = \pi \left(\frac{D}{2}\right)^2 \frac{F_\lambda \Delta\lambda}{h\nu} \tag{3.10}$$

where D is the diameter of the telescope. On the other hand, the number of the detected photons can be written as

$$n_{\rm ANIR} = \frac{f_{\rm ANIR} N_{\rm c}}{t} \tag{3.11}$$

where $f_{\rm ANIR}$ is the conversion factor between number of count and the amount of electron converted from photon. In the case of ($f_{\rm ANIR} = 3.4$ [e^{-1} ADU^{-1}]). $N_{\rm c}$ (ADU) is the count rate from the object, and t is the exposure time. Then, the observed system efficiency of $N191(\eta)$ can be derived as

$$(\eta^{\rm N191})^X = \frac{n_{\rm ANIR}}{n_{\rm tel}}, \tag{3.12}$$

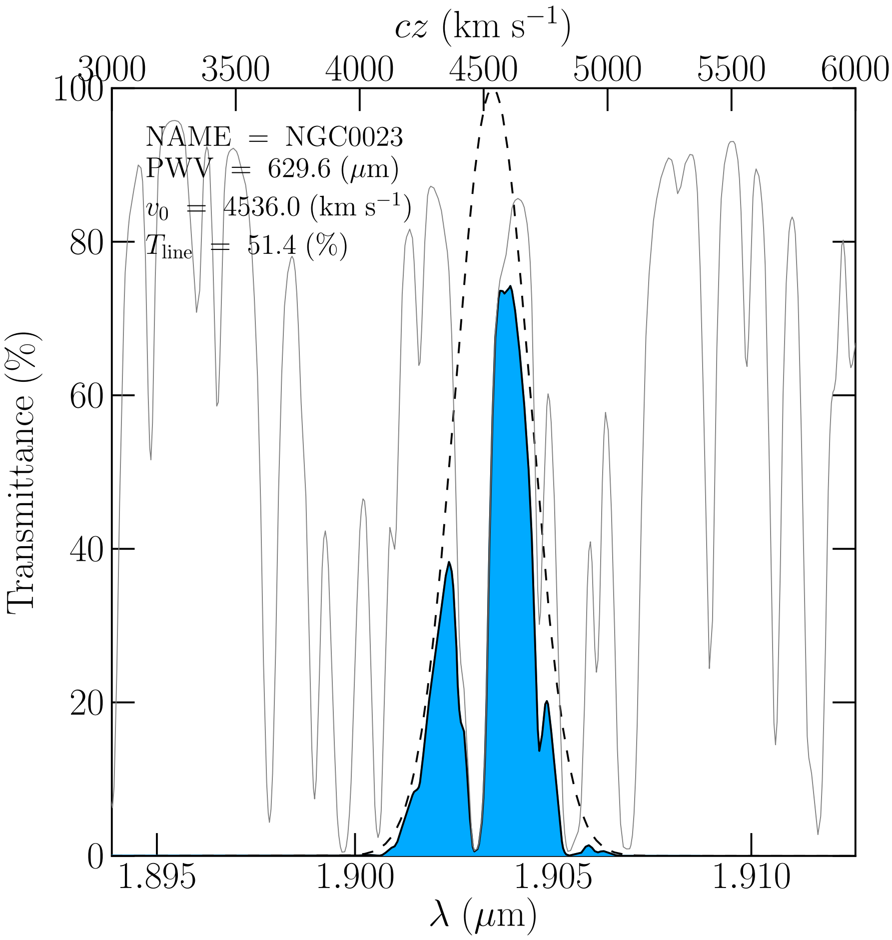

Figure 3.3: An example of Paα emission line we assume a redshifted Paα emission line of NGC 0023, convolved with atmospheric transmittance curve, are shown with the thick solid line. The solid-thin line represents the atmospheric transmittance at PWV = 629.6 (μm) calculated by ATRAN. The dashed line represents an intrinsic Paα line profile without atmospheric absorption. The recession velocity v_0 is set to be 4536 (km s^{-1}), and σ of the intrinsic profile is assumed to be 150 (km s^{-1}).

The system efficiency of $N191$ filter is found to be correlated with PWV Motohara et al. (2011). Left panel of Figure 3.2 shows the PWV dependency of the effective atmospheric transmittance for each filter. The transmittance of the $N191$ narrow-band filter shows strong dependence on PWV. To derive PWV, we first estimate $(\eta_{\rm int}^{N191})^X$, the system efficiency of $N191$ which is not affected by atmospheric absorption by interpolating those of the H- and $K_{\rm s}$- bands as shown in the right panel of Figure 3.2. The effective atmospheric transmittance within $N191$ filter can be obtained by,

$$(T_{\rm atm}^{{\rm PWV},N191})^X = \frac{(\eta^{N191})^X}{(\eta_{\rm int}^{N191})^X} \tag{3.13}$$

Then, PWV can be derived from $(T_{\rm atm}^{{\rm PWV},N191})^X$ using the relation shown in the left panel of Figure 3.2.

3.2.3 Estimate the Atmospheric Absorption

In a real galaxy, width of an emission line is broadened by more than $\sigma = 100$ km s^{-1} due to internal rotation and velocity dispersion of their emission line clouds. To incorporate this effect, the factor $T_{\rm line}$ is estimated from a model transmittance curve assuming the Paα emission line profile with the PWV obtained above. Figure 3.3 shows the assumed intrinsic emission-line profile (dashed line), atmospheric transmittance (solid line) and estimated emission-line profile affected by atmospheric absorption (dark-shaded area). The factor $T_{\rm line}$ within the bandpass $[\lambda_1, \lambda_2]$ of the $N191$ filter is then calculated as follows;

$$T_{\rm line} = \frac{\int_{\lambda_1}^{\lambda_2} \exp\left[-\left(\frac{\lambda-(1+z)\lambda_{\rm Pa\alpha}}{\sqrt{2}\sigma}\right)^2\right] T_{\rm atm}(\lambda) d\lambda}{\int_{\lambda_1}^{\lambda_2} \exp\left[-\left(\frac{\lambda-(1+z)\lambda_{\rm Pa\alpha}}{\sqrt{2}\sigma}\right)^2\right] d\lambda}, \tag{3.14}$$

where z is the redshift obtained from *IRAS* RBGS catalog (Sanders et al., 2003), $T_{\rm atm}(\lambda)$ represents the model atmospheric transmittance curve, and $\lambda_{\rm Pa\alpha}$ is the intrinsic wavelength of Paα (1.8751 μm).

3.3 Comparison with *HST*/NICMOS Data

3.3.1 Sample data

Table 3.1: Sample data of galaxies obeserved by miniTAO/ANIR

Galaxy (1)	R.A. (2)	Dec. (3)	cz (km s^{-1}) (4)	EXP. (second) (5)	OBS. (date) (6)	PWV (μm) (7)	$(T_{\rm atm}^{{\rm PWV},N191})^X$ (%) (8)	$T_{\rm line}$ (%) (9)
NGC 23 . .	00 09 55.1	+25 55 37	4536	1080	2009-10-26	629.6	57.3	51.4
NGC 1614	04 34 00.1	−08 34 46	4746	1080	2009-10-15	507.5	62.3	50.1
NGC 7130	21 48 19.6	−34 57 05	4824	1080	2009-10-26	491.2	62.9	44.1
IC 5179 . .	22 16 10.0	−36 50 35	3398	4320	2010-10-14	501.6	62.5	82.4
NGC 7469	23 03 15.5	+08 52 25	4922	1080	2009-10-22	156.7	77.1	58.9
NGC 7771	23 51 24.7	+20 06 39	4336	1080	2009-10-27	674.1	55.9	53.5

Column (1): Galaxy name. Column (2): Right ascension . Column (3): Declination. Column (4): Recession velocity. Column (5): Total exposure time. Column (6): Observed date. Column (7): PWV estimated by the flux calibration method. Column (8): Averaged Transmittance within the $N191$ narrow-band filter. Column (9): Transmittance of Paα emission-line

Table 3.2: Sample Data of *HST*/NICMOS and Calculated Fluxes

Galaxy (1)	Aperture (2)	$F(Pa\alpha)_{HST}$ (ergs cm^{-2} s^{-1}) (3)	$F(Pa\alpha)_{ANIR-r}$ (ergs cm^{-2} s^{-1}) (4)	$F(Pa\alpha)_{error}$ (ergs cm^{-2} s^{-1}) (5)	$F(Pa\alpha)_{ANIR-c}$ (ergs cm^{-2} s^{-1}) (6)
NGC 23....	5.3″	2.13×10^{-13}	2.61×10^{-13}	$\pm1.44\times10^{-14}$	2.91×10^{-13}
NGC 1614..	2.4″	8.08×10^{-13}	7.10×10^{-13}	$\pm7.01\times10^{-15}$	8.83×10^{-13}
NGC 7130 a	2.2″	1.06×10^{-13}	9.27×10^{-14}	$\pm5.37\times10^{-15}$	1.32×10^{-13}
NGC 7130 b	2.2″	3.75×10^{-14}	2.72×10^{-14}	$\pm5.37\times10^{-15}$	3.88×10^{-14}
IC 5179 a ..	3.1″	5.79×10^{-14}	7.70×10^{-14}	$\pm4.00\times10^{-15}$	5.84×10^{-14}
IC 5179 b ..	3.1″	3.35×10^{-14}	4.88×10^{-14}	$\pm4.00\times10^{-15}$	3.70×10^{-14}
IC 5179 c ..	2.2″	6.78×10^{-14}	9.02×10^{-14}	$\pm2.49\times10^{-15}$	6.84×10^{-14}
IC 5179 d ..	1.6″	7.78×10^{-15}	1.02×10^{-14}	$\pm1.64\times10^{-15}$	7.74×10^{-15}
IC 5179 e ..	1.6″	8.46×10^{-15}	1.02×10^{-14}	$\pm1.64\times10^{-15}$	7.74×10^{-15}
IC 5179 f...	1.6″	1.22×10^{-14}	1.39×10^{-14}	$\pm1.64\times10^{-15}$	1.05×10^{-14}
IC 5179 g ..	1.6″	7.78×10^{-15}	1.27×10^{-14}	$\pm1.64\times10^{-15}$	9.63×10^{-15}
IC 5179 h ..	1.6″	1.17×10^{-14}	1.61×10^{-14}	$\pm1.64\times10^{-15}$	1.22×10^{-14}
NGC 7469..	10.6″	5.57×10^{-13}	5.43×10^{-13}	$\pm5.80\times10^{-14}$	7.11×10^{-13}
NGC 7771..	5.0″	1.86×10^{-13}	1.18×10^{-13}	$\pm2.04\times10^{-14}$	1.99×10^{-13}

Note.— Column (1): Name of galaxies. Column (2): Radius of Photometry Aperture. Column (3): Paα flux observed by HST/NICMOS. Column (4): Paα flux observed by miniTAO/ANIR with no correction of atmospheric absorption. Column (5): Photometric error of Paα flux observed by miniTAO/ANIR. Column (6): Paα flux observed by miniTAO/ANIR with correction of atmospheric absorption.

In order to evaluate the feasibility of the above method, we compared the fluxes of galaxies obtained by our method using miniTAO/ANIR data with those by HST/NICMOS which, are not affected by the atmospheric absorption. Table 3.1 is the list of comparison sample. Out of 38 galaxies observed in our Paα survey of local LIRGs, 6 have *HST*/NICMOS 190N narrow-band imaging data. For the data of miniTAO/ANIR, standard reduction procedures (see Sec.3.1) are carried out to obtain a final image for each band. The 187N and 190N narrow-band data of *HST*/NICMOS are obtained from the archive. 187N is the Paα continuum, and 190N is for the redshifted Paα line including continuum. Paα emission line images are obtained by subtracting the image of 187N from 190N.

Paα emission line fluxes of miniTAO/ANIR and HST/NICMOS are measured by aperture photometry whose sizes are listed in Table 3.2. However, as the field of view of HST/NICMOS is limited, some of the data do not cover the entire galaxy. For such data, we compare each HII region in the image, and these regions are shown in Figure 3.4.

3.3.2 Comparison between miniTAO/ANIR and *HST*/NICMOS Paα Flux

First, we compare Paα flux derived from HST/NICMOS with those from miniTAO/ANIR with no atmospheric absorption correction in Figure 3.5. It can be seen that the dispersion of the flux ratios between NICMOS and ANIR data is large as 28.0%. On other hand, Figure 3.6 represents the comparison of the fluxes with atomospheric absorption correction, where the dispersion becomes as low as 9.4% compared to the Figure 3.5.

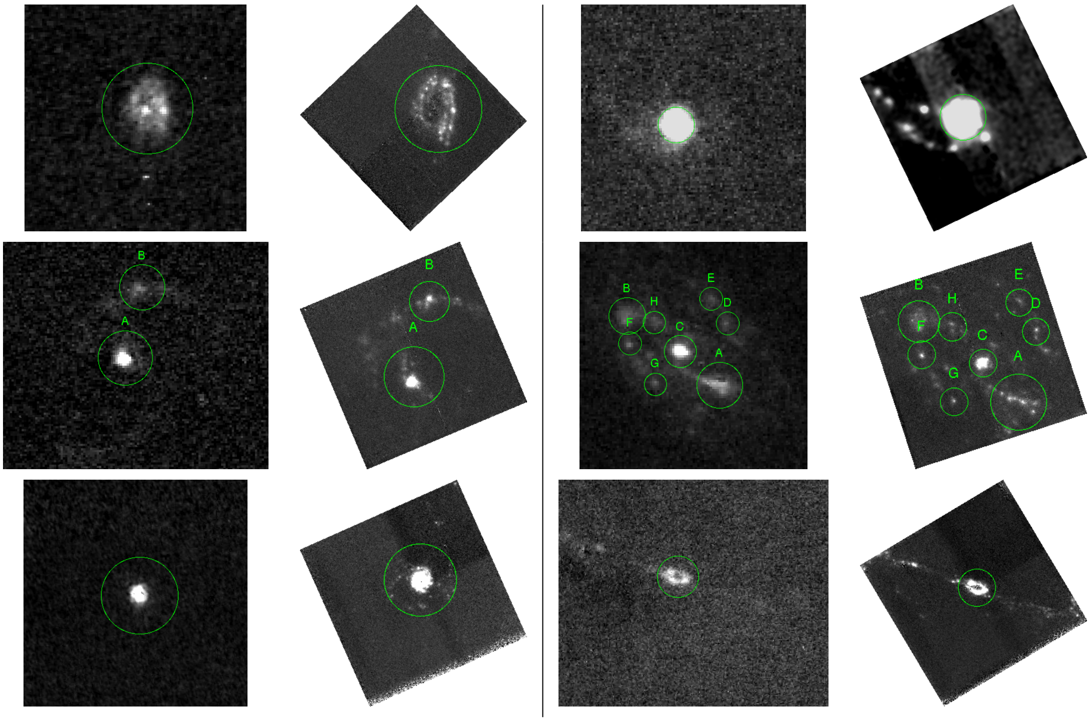

Figure 3.4: Left rows represent the Paα emission-line images observed by miniTAO/ANIR, and the right rows represents those observed by HST/NICMOS. Each circles show the apertures used for the measurements.

However, these results depend on the line profile we assumed (see section **??**). According to Kennicutt et al. (2009)Kennicutt et al. (2009), the median line width of starburst galaxies is 100 $\sim$ 200 km s^{-1} mesured by Hα emission line. We then varied the width of line profile from 50 km s^{-1} to 250 km s^{-1}, and the results of the flux ratios between NICMOS and ANIR are listed in Table 3.3. Within the assumed range of FWHM, the flux does not change so largely except for v=50 km s^{-1}. By assuming v=150 km s^{-1} which is the average velocity within of (Kennicutt et al., 2009), Paα fluxes are calibrated within the accuracy of about 10%.

Table 3.3: Dependence of the flux ratio between that derived from HST/NICMOS and miniTAO/ANIR on the assumed FWHM of the emission line

FWHM (km s^{-1}) (1)	Median (%) (2)	Error (1σ) (3)	Max (%) (4)	Min (%) (5)
50	108.2	$\pm$33.8	176.2	67.8
100	100.3	$\pm$13.0	114.5	85.0
150	98.3	$\pm$9.4	110.0	91.3
200	98.9	$\pm$9.9	112.8	85.6
250	102.2	$\pm$12.0	119.3	79.7

Note.— Assumed FWHM of line profile

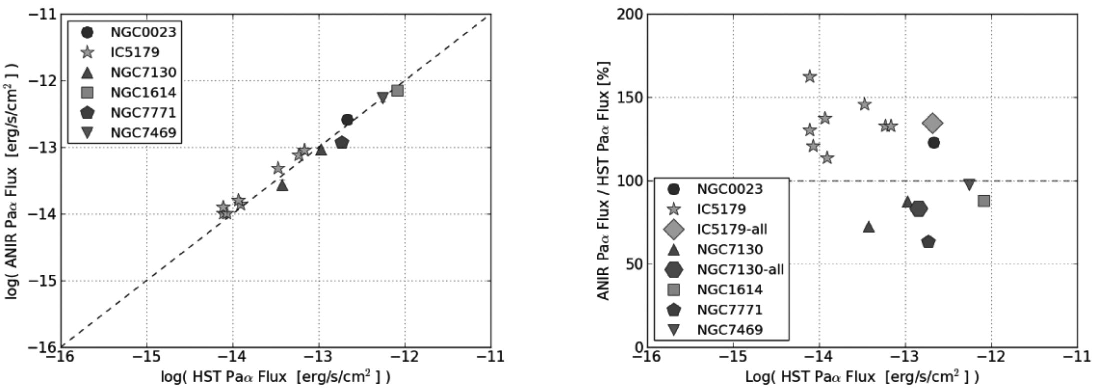

Figure 3.5: Left: Correlation relation between Paα fluxes derived from HST/NICMOS and from miniTAO/ANIR. Right : Ratios of the fluxes from HST/NICMOS and from miniTAO/ANIR. The atmospheric absorption is not corrected.

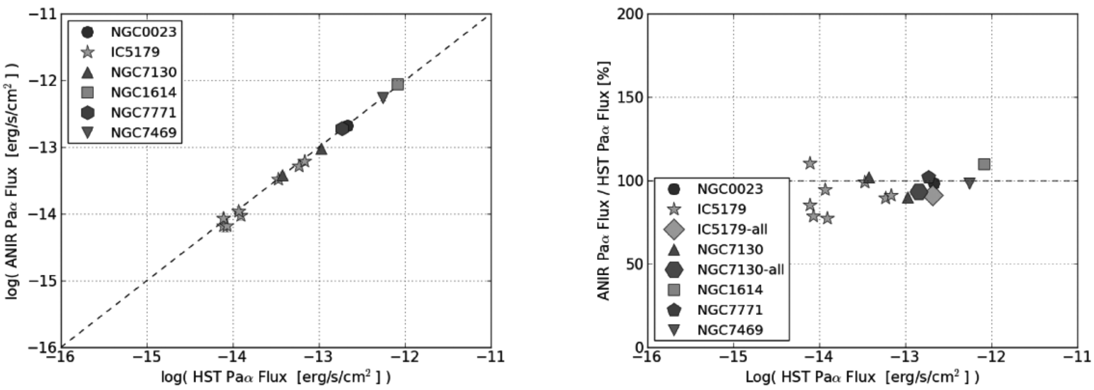

Figure 3.6: Left : Correlation relation between Paα fluxes derived from HST/NICMOS and from miniTAO/ANIR. Right : Ratios of the fluxes from HST/NICMOS and from miniTAO/ANIR. The atmospheric absorption is corrected.

Chapter 4

Results

4.1 Paα Line Images

4.1.1 Final Images

In Figure 4.1, all of our 44 individual galaxies in 38 systems are shown. The continuum images made by interpolating the H and K_s images are shown on the left side and the Paα line images, which is derived by subtracting continuum image from the $N191$ image, on the right.

4.1.2 Paα Flux

To estimate a total Paα flux of a galaxy, we first estimate how extended emission-line distributions are. Because there are large diversity in Paα morphology, we use isophotal photometry technique for our image, where 5σ isophotal area above the sky background level for Paα image is used. The 1σ noise level is measured in each Paα image convolved with a Gaussian function with a FWHM of 8 pixels to reduce the noise level, and the 5σ area is defined in this convolved line image.

The results are shown in Table 4.1 and Figure 4.1. Photometric uncertainties, $\sigma(\mathrm{Pa}\alpha)_\mathrm{phot}$, are defined as 1σ noise level measured by applying many apertures having the same area size as that used for the measurement of the total Paα flux at blank sky positions. These values are not so large ($\sim 0.5\%$ on average). The $\sigma(\mathrm{Pa}\alpha)_\mathrm{atm}$ is an error due to our Paα correction method mentioned in Section 3 and set to be 12.2% (Tateuchi et al., 2012b). We use the combination of them,

$$\sigma_\mathrm{total} = \sqrt{\sigma(\mathrm{Pa}\alpha)^2_\mathrm{phot} + \sigma(\mathrm{Pa}\alpha)^2_\mathrm{atm}}, \tag{4.1}$$

as the total uncertainties on the measurement of the Paα flux.

Our results may miss any diffuse Paα emission whose surface brightness is lower than the 5σ threshold. In the *HST*/NICMOS images, missing the diffuse Paα flux is also pointed out by Alonso-Herrero et al. (2006). In order to evaluate the maximum missing flux of Paα line emission ($f(\mathrm{Pa}\alpha)_\mathrm{miss}$), we assume the diffuse emission is spread over an aperture,

Table 4.1: Paα fluxes and derived quantities of atmospheric condition with miniTAO/ANIR.

ID	Galaxy Name	$f(\mathrm{Pa}\alpha)$ (ergs cm^{-2} s^{-1})	$\sigma(\mathrm{Pa}\alpha)_{\mathrm{phot}}$ (ergs cm^{-2} s^{-1})	$\sigma(\mathrm{Pa}\alpha)_{\mathrm{atm}}$ (ergs cm^{-2} s^{-1})	$f(\mathrm{Pa}\alpha)_{\mathrm{miss}}$ (ergs cm^{-2} s^{-1})	PWV (μm)	$(T_{\mathrm{atm}}^{\mathrm{PWV},N191})^X$ (%)	T_{line} (%)
(1)	(2)	(3)	(4)	(5)	(6)	(7)	(8)	(9)
1	NGC 23...........	2.28×10^{-13}	$\pm\ 2.42\times10^{-15}$	$\pm\ 2.79\times10^{-14}$	$+\ 1.03\times10^{-14}$	629.6	57.3	51.4
2	NGC 34...........	3.73×10^{-13}	$\pm\ 2.56\times10^{-15}$	$\pm\ 4.55\times10^{-14}$	$+\ 9.23\times10^{-15}$	485.7	63.2	55.6
3	NGC 232..........	8.66×10^{-14}	$\pm\ 1.59\times10^{-15}$	$\pm\ 1.06\times10^{-14}$	$+\ 5.98\times10^{-15}$	197.3	74.1	66.3
4	IC 1623A/B.......	6.58×10^{-13}	$\pm\ 4.33\times10^{-15}$	$\pm\ 8.03\times10^{-14}$	$+\ 7.74\times10^{-14}$	446.3	64.7	55.4
5	ESO 244-G012.....	3.63×10^{-13}	$\pm\ 1.60\times10^{-15}$	$\pm\ 4.43\times10^{-14}$	$+\ 5.64\times10^{-15}$	385.6	67.1	85.6
6	UGC 2238.........	3.71×10^{-13}	$\pm\ 3.87\times10^{-15}$	$\pm\ 4.53\times10^{-14}$	$+\ 6.80\times10^{-15}$	576.6	59.2	60.6
7	IRAS F02437±2122	1.99×10^{-14}	$\pm\ 5.79\times10^{-16}$	$\pm\ 2.42\times10^{-15}$	$+\ 3.42\times10^{-15}$	359.7	68.1	81.4
8	UGC 2982.........	4.00×10^{-13}	$\pm\ 3.03\times10^{-15}$	$\pm\ 4.88\times10^{-14}$	$+\ 5.39\times10^{-15}$	82.7	83.4	80.2
9	NGC 1614.........	1.06×10^{-12}	$\pm\ 4.64\times10^{-15}$	$\pm\ 1.29\times10^{-13}$	$+\ 1.38\times10^{-14}$	507.5	62.3	50.1
10	MCG −05-12-006..	1.61×10^{-13}	$\pm\ 1.18\times10^{-15}$	$\pm\ 1.97\times10^{-14}$	$+\ 4.31\times10^{-15}$	1035.1	48.1	55.5
11	NGC 1720.........	7.60×10^{-14}	$\pm\ 6.61\times10^{-16}$	$\pm\ 9.28\times10^{-15}$	$+\ 5.59\times10^{-15}$	74.9	84.3	82.9
12	ESO 557-G002.....	8.90×10^{-13}	$\pm\ 1.43\times10^{-15}$	$\pm\ 1.09\times10^{-14}$	$+\ 5.37\times10^{-15}$	435.0	65.2	61.9
13	IRAS F06592-6313.	6.17×10^{-14}	$\pm\ 1.33\times10^{-15}$	$\pm\ 7.53\times10^{-15}$	$+\ 4.03\times10^{-15}$	701.3	55.1	78.4
14	NGC 2342.........	2.22×10^{-13}	$\pm\ 3.14\times10^{-15}$	$\pm\ 2.71\times10^{-14}$	$+\ 9.96\times10^{-15}$	1307.5	43.9	56.1
15	ESO 320-G030.....	1.64×10^{-13}	$\pm\ 1.61\times10^{-15}$	$\pm\ 2.00\times10^{-14}$	$+\ 6.25\times10^{-15}$	532.5	61.2	81.9
16	NGC 4922.........	4.35×10^{-14}	$\pm\ 1.04\times10^{-15}$	$\pm\ 5.30\times10^{-15}$	$+\ 8.55\times10^{-15}$	516.2	61.9	65.9
17	MCG −03-34-064..	1.12×10^{-13}	$\pm\ 1.03\times10^{-15}$	$\pm\ 1.37\times10^{-14}$	$+\ 8.44\times10^{-15}$	512.2	62.0	57.8
18	NGC 5135.........	4.09×10^{-13}	$\pm\ 2.70\times10^{-15}$	$\pm\ 4.99\times10^{-14}$	$+\ 1.47\times10^{-14}$	759.3	53.4	39.0
19a	NGC 5257.........	2.27×10^{-13}	$\pm\ 1.94\times10^{-15}$	$\pm\ 2.76\times10^{-14}$	$+\ 4.30\times10^{-15}$	913.5	50.2	70.5
19b	NGC 5258.........	1.66×10^{-13}	$\pm\ 1.42\times10^{-15}$	$\pm\ 2.02\times10^{-14}$	$+\ 4.67\times10^{-15}$	913.5	50.2	70.5
20a	IC 4518A..........	8.11×10^{-14}	$\pm\ 1.52\times10^{-15}$	$\pm\ 9.89\times10^{-15}$	$+\ 8.60\times10^{-15}$	547.2	60.5	50.6
20b	IC 4518B..........	5.15×10^{-14}	$\pm\ 1.54\times10^{-15}$	$\pm\ 6.28\times10^{-15}$	$+\ 1.12\times10^{-14}$	547.2	60.5	50.6
21a	IC 4686	1.31×10^{-13}	$\pm\ 1.01\times10^{-15}$	$\pm\ 1.60\times10^{-14}$	$+\ 3.10\times10^{-15}$	923.8	50.0	50.9
21b	IC 4687	8.04×10^{-13}	$\pm\ 2.39\times10^{-15}$	$\pm\ 9.80\times10^{-14}$	$+\ 5.19\times10^{-15}$	923.8	50.0	50.9
21c	IC 4689	2.21×10^{-13}	$\pm\ 1.79\times10^{-15}$	$\pm\ 2.57\times10^{-14}$	$+\ 4.31\times10^{-15}$	923.8	50.0	50.9
22	IRAS F18293-3413.	8.44×10^{-13}	$\pm\ 2.94\times10^{-15}$	$\pm\ 1.03\times10^{-13}$	$+\ 5.31\times10^{-15}$	621.7	57.5	73.6
23	ESO 339-G011.....	8.95×10^{-14}	$\pm\ 1.68\times10^{-15}$	$\pm\ 1.09\times10^{-14}$	$+\ 7.33\times10^{-15}$	596.7	58.3	57.5
24	NGC 6926.........	1.29×10^{-13}	$\pm\ 2.52\times10^{-15}$	$\pm\ 1.57\times10^{-14}$	$+\ 1.15\times10^{-14}$	441.3	64.9	57.2
25	IC 5063	9.30×10^{-14}	$\pm\ 1.25\times10^{-15}$	$\pm\ 1.13\times10^{-14}$	$+\ 8.34\times10^{-15}$	350.5	68.4	86.8
26	ESO 286-G035.....	2.59×10^{-13}	$\pm\ 2.14\times10^{-15}$	$\pm\ 3.16\times10^{-14}$	$+\ 4.78\times10^{-15}$	526.5	61.4	64.7
27	ESO 343-IG013....	8.64×10^{-14}	$\pm\ 2.23\times10^{-15}$	$\pm\ 1.05\times10^{-14}$	$+\ 7.52\times10^{-15}$	469.7	63.8	63.8
28	NGC 7130.........	2.32×10^{-13}	$\pm\ 3.48\times10^{-15}$	$\pm\ 2.83\times10^{-14}$	$+\ 1.63\times10^{-14}$	491.2	62.9	44.1
29	IC 5179	5.65×10^{-13}	$\pm\ 2.83\times10^{-15}$	$\pm\ 6.89\times10^{-14}$	$+\ 5.72\times10^{-15}$	501.6	62.5	82.4
30	ESO 534-G009.....	2.28×10^{-14}	$\pm\ 8.26\times10^{-16}$	$\pm\ 2.78\times10^{-15}$	$+\ 6.61\times10^{-15}$	255.4	71.5	88.6
31	NGC 7469.........	6.11×10^{-13}	$\pm\ 3.71\times10^{-15}$	$\pm\ 7.45\times10^{-14}$	$+\ 1.14\times10^{-14}$	156.7	77.1	58.9
32	CGCG 453-062....	8.59×10^{-14}	$\pm\ 1.28\times10^{-15}$	$\pm\ 1.05\times10^{-14}$	$+\ 2.82\times10^{-15}$	172.5	76.0	85.4
33	NGC 7591.........	1.10×10^{-13}	$\pm\ 1.41\times10^{-15}$	$\pm\ 1.34\times10^{-14}$	$+\ 6.64\times10^{-15}$	37.4	90.4	81.4
34	NGC 7678.........	1.13×10^{-13}	$\pm\ 1.79\times10^{-15}$	$\pm\ 2.38\times10^{-14}$	$+\ 5.77\times10^{-15}$	301.2	70.2	83.0
35	MCG −01-60-022..	1.31×10^{-13}	$\pm\ 1.43\times10^{-15}$	$\pm\ 1.60\times10^{-14}$	$+\ 3.86\times10^{-15}$	328.9	69.2	83.8
36a	NGC 7770.........	1.87×10^{-13}	$\pm\ 4.19\times10^{-15}$	$\pm\ 2.28\times10^{-14}$	$+\ 7.19\times10^{-15}$	674.1	55.9	53.5
36b	NGC 7771.........	3.78×10^{-13}	$\pm\ 4.56\times10^{-15}$	$\pm\ 4.61\times10^{-14}$	$+\ 2.01\times10^{-14}$	674.1	55.9	53.5
37	MrK 331	2.96×10^{-13}	$\pm\ 2.36\times10^{-15}$	$\pm\ 3.60\times10^{-14}$	$+\ 6.96\times10^{-15}$	377.1	67.4	81.2
38a	UGC 12914........	1.23×10^{-13}	$\pm\ 1.30\times10^{-15}$	$\pm\ 1.51\times10^{-14}$	$+\ 2.96\times10^{-15}$	364.9	67.9	62.8
38b	UGC 12915........	7.49×10^{-14}	$\pm\ 9.75\times10^{-16}$	$\pm\ 9.14\times10^{-15}$	$+\ 3.88\times10^{-15}$	364.9	67.9	62.8

Column (1): Galaxy ID in this paper. Column (2): Galaxy name. Column (3): Observed Paα total flux corrected for atmospheric absorption. Column (4): 1σ photometric error of Paα flux. Column (5): Estimated error by the atmospheric absorption correction of the Paα flux. Column (6): 5σ error by continuum subtraction of the Paα flux. Column (7): Estimated PWV using the calibration method described in K14, submitted. Column (8): Estimated effective atmospheric transmittance within the $N191$ filter. Column (9): Estimated the effective line transmittance.

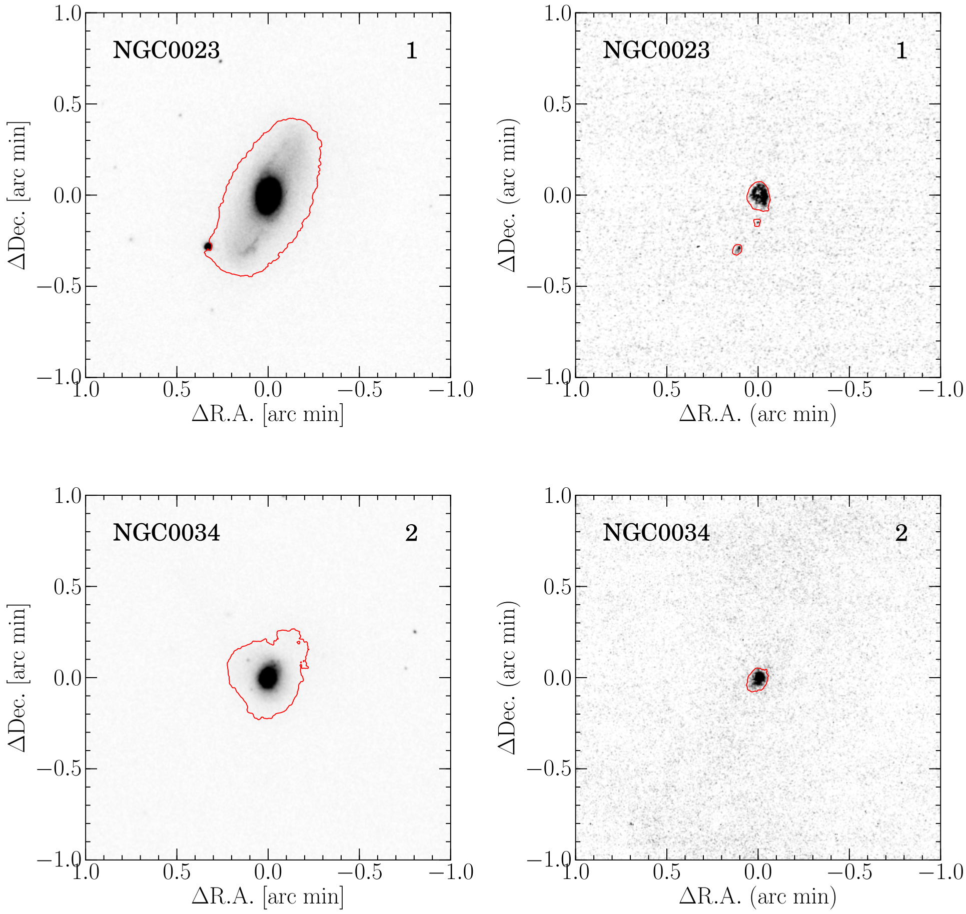

Figure 4.1: Continuum and Paα line images of our sample of 44 individual LIRGs in 38 systems observed with miniTAO/ANIR. The continuum images are listed on the left side and Paα line images on the right. The name of a galaxy is shown at the top-left corner and ID number at the top-right corner in each figure. The solid red lines represent 10σ surface brightness level for the continuum image and 5σ for the Paα line image measured on convolved images. The 1σ levels are calculated on the convolved images (see text).

whose area is defined by 10σ isophote for each continuum image. Then, the amount of the missing diffuse component is estimated to be 1.8% on average at a maximum.

4.1.3 Notes on Individual Objects

Following are notes on the individual galaxies, where the number at the top represents our sample ID. Continuum and $N191$ images are shown in Figure 4.1.

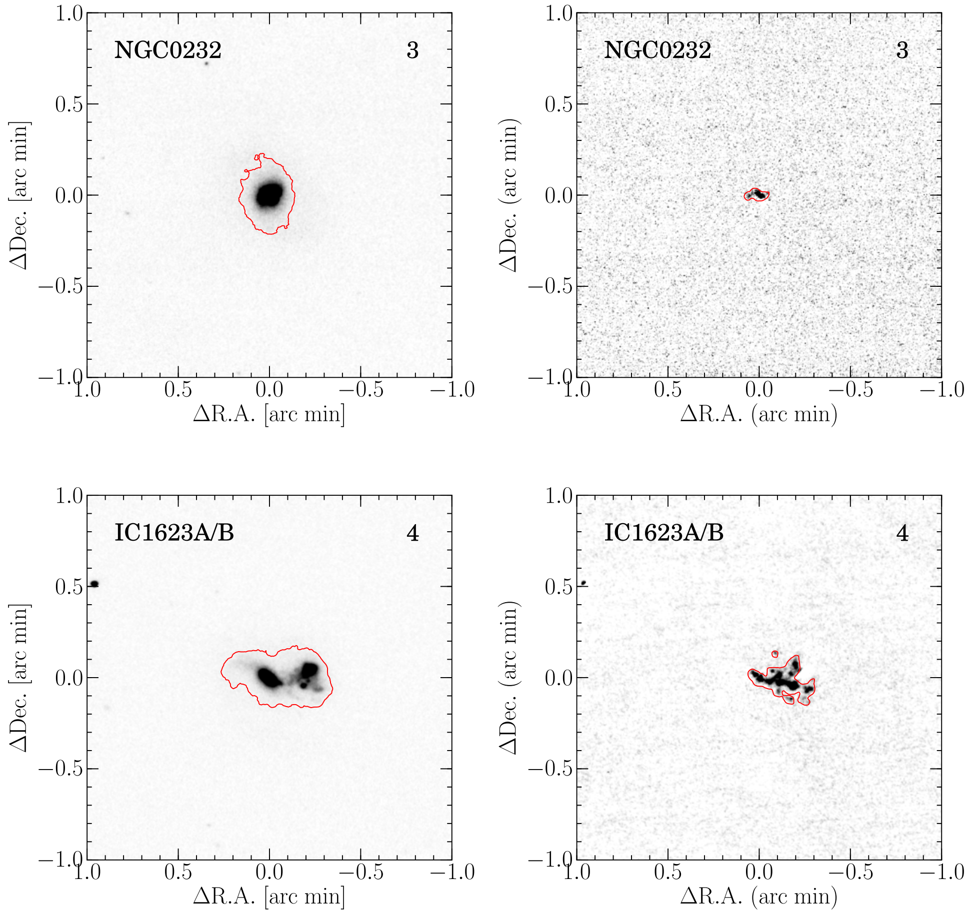

Figure 4.1: Continued

1. NGC 23 (IRAS F00073+253; Mrk 545): This is a paired galaxy with NGC 26 (Alonso-Herrero et al. 2006) at a distance of 9$'$.1. It is a barred spiral (Sa; HyperLeda[1]) classified as an HII galaxy by a long-slit spectroscopic study (Veilleux et al., 1995). X-ray emission is not detected by Swift/BAT (Koss et al., 2013). A ring starburst region are detected at the center of the galaxy. In addition to this structure, we find an extended Paα emission-line region along the southern spiral arm which is located outside the field of view of the *HST*/NICMOS observation.

2. NGC 34 (IRAS F00085−1223; Mrk 938; VV 850): This galaxy, hosting a strong starburst and a weak AGN, as evidenced by its optical, infrared, radio, and X-ray properties, is known as a remnant of unequal gas-rich merger (e.g., Fernández et al., 2010; Schweizer & Seitzer, 2007). It is an S0/a (HyperLeda) and classified as a Seyfert 2 by a

[1]database for physics of galaxies; http://leda.univ-lyon1.fr (Paturel et al., 2003)

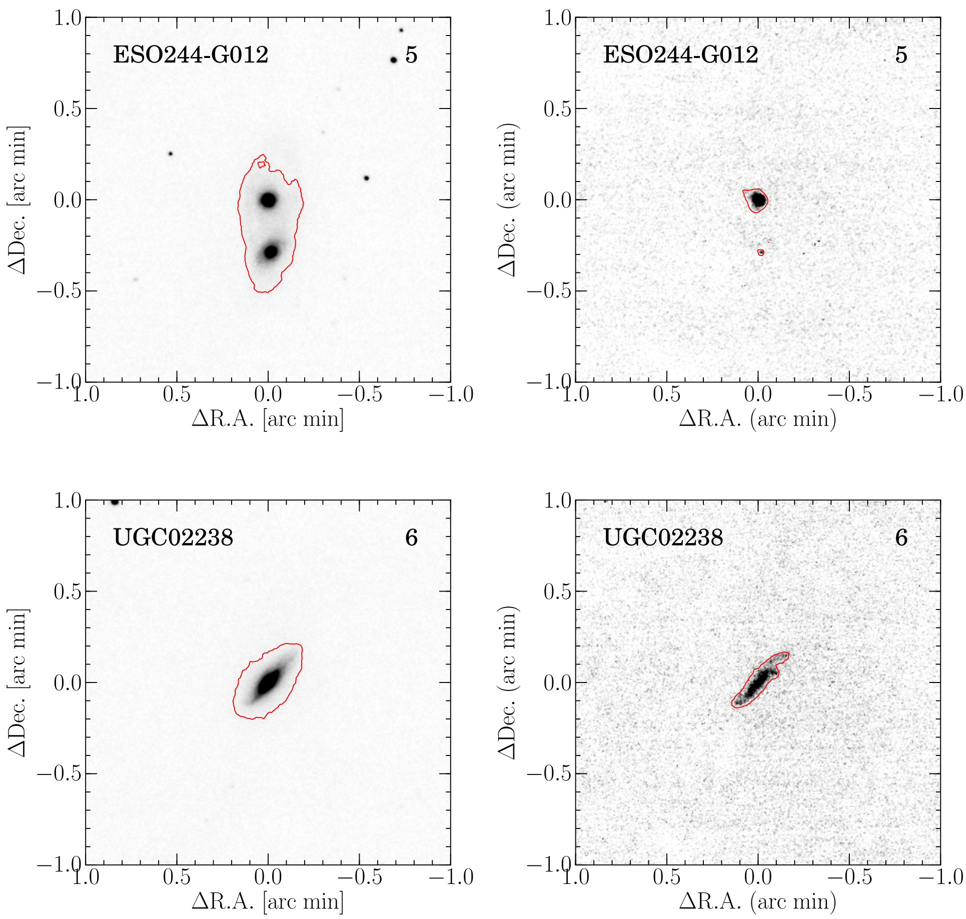

Figure 4.1: Continued

long-slit spectroscopic study (Veilleux et al., 1995). Paα emission-line region is concentrated at the center of the galaxy.

3. NGC 232 (IRAS F00402−2349; VV 830; AM 0040-234): This has a companion galaxy (NGC 235) at a distance of 2′. It is a barred spiral (SBa; HyperLeda) classified as an HII galaxy (Corbett et al., 2003; Veilleux et al., 1995). HII blobs, suggested as optical debris, between these two galaxies are detected in Hα (e.g., Dopita et al., 2002; Richter et al., 1994), but the Paα data is not enough deep to detect the blobs. While NGC 232 has bright FIR emission, NGC 235 has no FIR flux though it has bright HII blobs (Richter et al., 1994).

4. IC 1623A/B (IRAS F00402−2349; VV 114; Arp 236): This system is known as a merger at its middle or late stage, and consists of two galaxies, IC 1623B

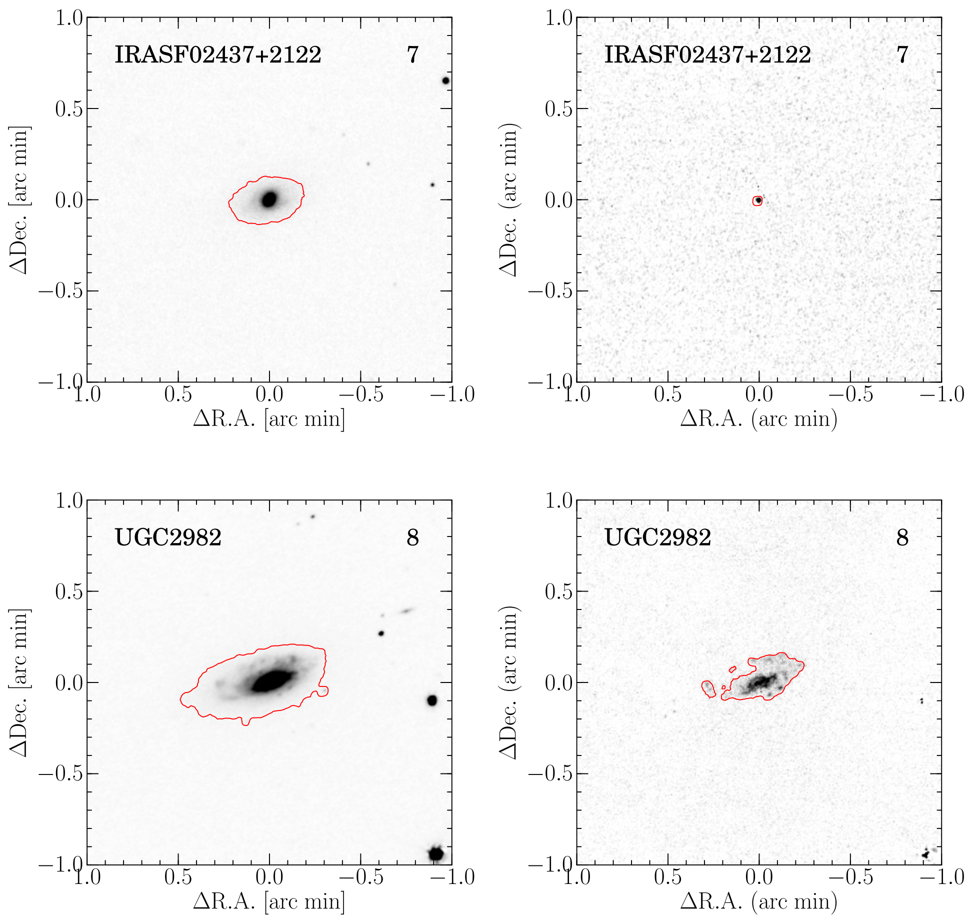

Figure 4.1: Continued

and IC 1623A. An obscured AGN in IC 1623B is revealed by MIR spectroscopy and X-ray observations (e.g., Alonso-Herrero et al., 2002; Grimes et al., 2006) suggesting that both starburst and AGN activities might be triggered by the ongoing merger. These galaxies are classified as an HII galaxy (Corbett et al., 2003; Veilleux et al., 1995). The diffuse component of Paα emission is distributed between the two galaxies over 10 kpc (Iono et al., 2013; Saito et al., 2013).

5. ESO 244-G012 (IRAS F01159−4443; VV 827; AM 0115-444): This system is on-going interacting paired galaxies (Agüero et al., 2000), separated by 17″. Both are spirals (Sc; HyperLeda), and the northern galaxy is classified as an HII galaxy (Corbett et al., 2003), while the class of the southern galaxy is ambiguous (Corbett et al., 2003). The northern galaxy has bright concentrated Paα emission at its center, while the southern source is faint.

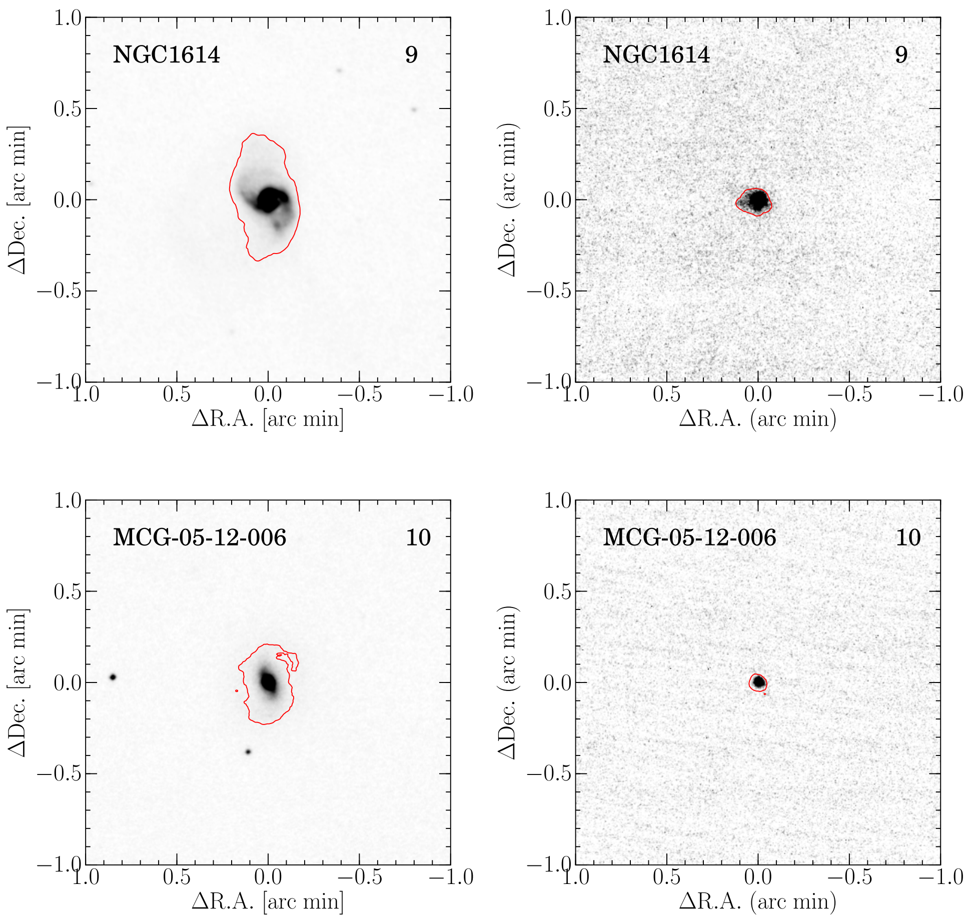

Figure 4.1: Continued

6. UGC 2238 (IRAS F02435+1253): This object is known as a merger remnant, and it is questionable whether it is undergoing or has undergone any amount of violent relaxation (Rothberg & Joseph, 2004). It is an edge-on disk galaxy (Sm; HyperLeda) classified as a LINER (Veilleux et al., 1995). Strong Paα emission are detected not only from the central region, but also from the disk component.

7. IRAS F02437+2122: This is an elliptical galaxy (E; HyperLeda) classified as a LINER (Veilleux et al., 1995). X-ray emission is detected (S/N=2.7, $L_{14-195\mathrm{keV}} < 10^{42.9}$ (erg s^{-1})) by Swift/BAT (Koss et al., 2013), but no high-quality X-ray data is obtained. The Paα morphology is compact and concentrated at the central region.

8. UGC 2982 (IRAS F04097+0525): This is a barred spiral (SABa; Hyper-

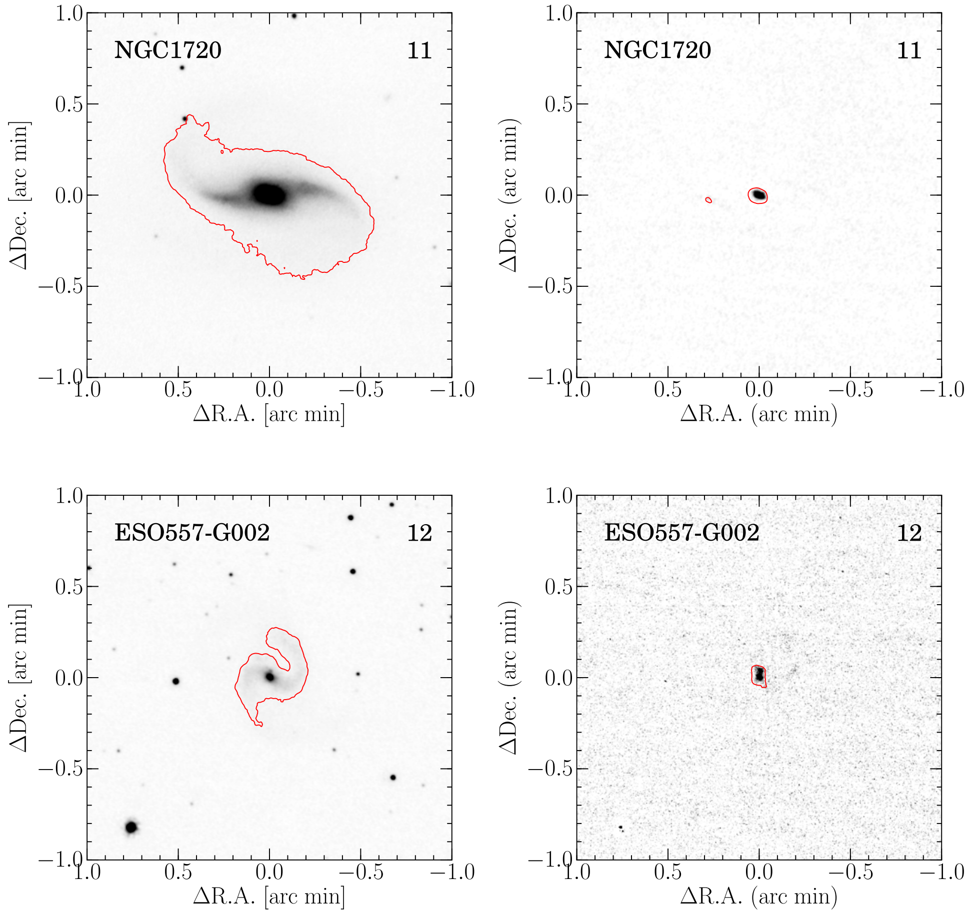

Figure 4.1: Continued

Leda) classified as an HII galaxy by a long-slit spectroscopic study (Veilleux et al., 1995). It is a diffuse isolated system having extended HII gas (Chaboyer & Vader, 1991) and 850 μm emission extends to the periphery of a optical disk (Thomas et al., 2004). Paα emission-line region is also extended out to the disk with clumpy blobs.

9. NGC 1614 (IRAS F04315−0840; ARP 186; Mrk 617; IIZW 015): This is a well known merger at its late stage, and found to be a minor merger system with a mass ratio of 5:1∼3:1 (Väisänen et al., 2012). It is a barred spiral (SBc; HyperLeda) classified as an HII galaxy (Veilleux et al., 1995; Alonso-Herrero et al., 2001; Corbett et al., 2003). A tidal tail can be seen in our continuum image, which is consistent with other broad-band images (Dopita et al., 2002; Rodríguez-Zaurín et al., 2011). A ring-like structure surrounding a nuclear region is discovered in a Paα image with *HST*/NICMOS (Alonso-Herrero et al., 2001). An extended star-forming region is detected in the Paα image, but the

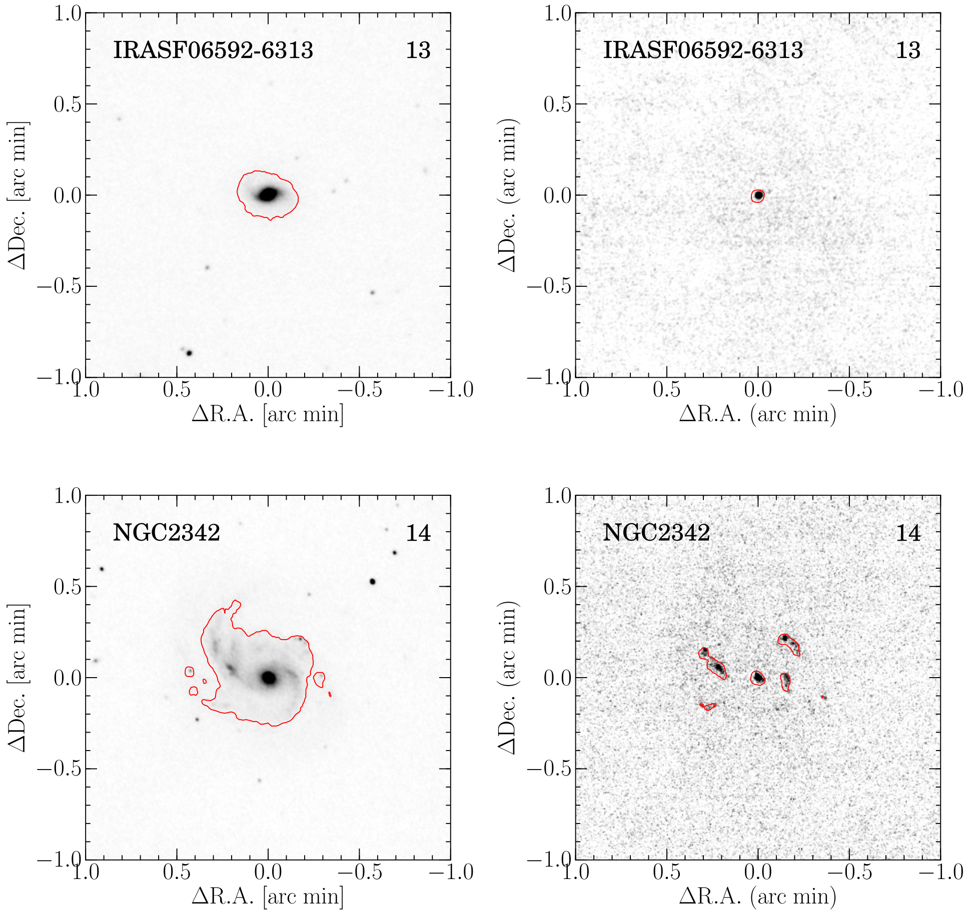

Figure 4.1: Continued

ring-like structure can not be detected in the 0.″8 spatial resolution of ANIR. Alonso-Herrero et al. (2001) describes that the growth of the ring structure is "inside-out", but Olsson et al. (2010) suggests that the ring is the result of a resonance.

10. MCG −05-12-006 (IRAS F04502−3304): This is an isolated barred spiral (SBb; HyperLeda) with a tidal tail (Yuan et al., 2010) and classified as an HII galaxy (Yuan et al., 2010). Paα emission is compact and concentrated at the center of the galaxy.

11. NGC 1720 (IRAS F04569−0756): This is a paired galaxy with NGC 1726 at a distance of 8.″2. It is a barred spiral (SBab; HyperLeda), but its energy source is not identified. The Paα emission is concentrated at the center of the galaxy, and little emission can be seen at the spiral arm.

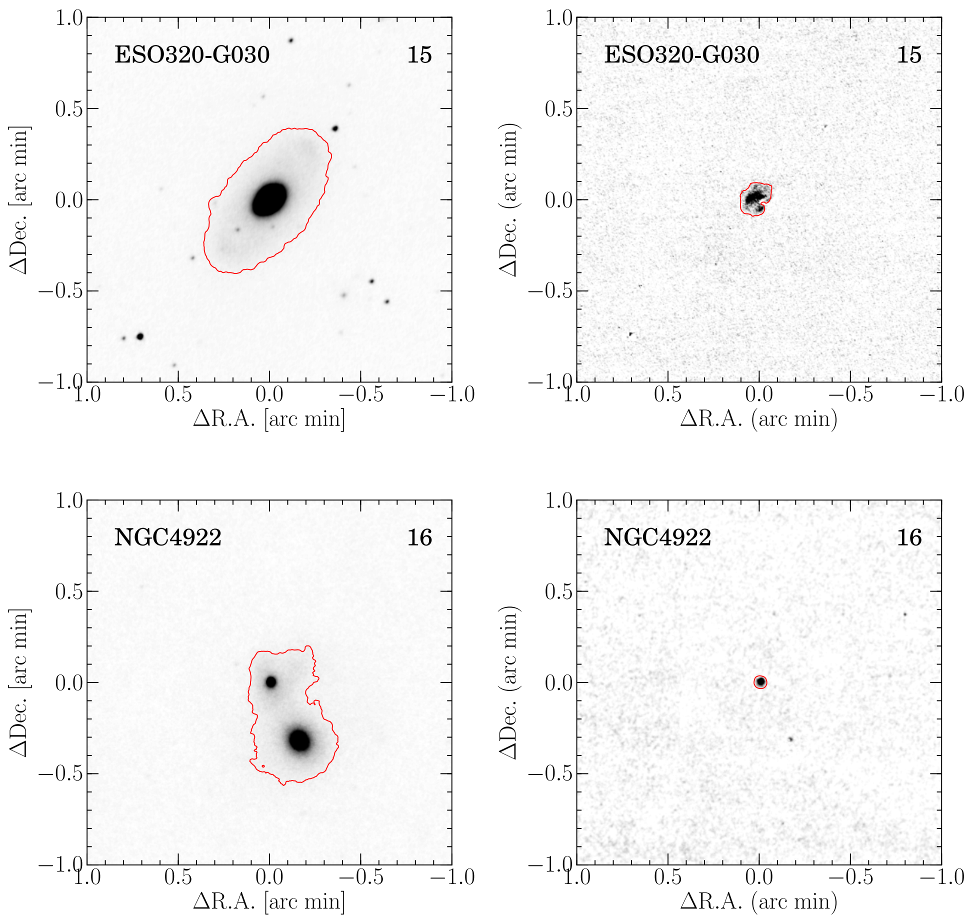

Figure 4.1: Continued

12. ESO 557-G002 (IRAS F06295−1735): This galaxy has a companion galaxy (ESO 557-G001) at a distance of $1'.6$ towards the south. It is a barred spiral (SBbc; HyperLeda) classified as an HII galaxy by a long-slit spectroscopic study (Corbett et al., 2003). Ultra-hard X-ray (14-195 keV) emission cannot be detected by Swift/BAT (Koss et al., 2013). The companion shows tidal distortion in the R-band and an Hα image (Dopita et al., 2002) but does not show clearly in the K_s-band and the Paα image. Two strong concentrated peaks at the center of the galaxy is detected on the Paα image.

13. IRAS F06592−6313: This is an isolated barred spiral (SABb; HyperLeda) with a tidal tail (Yuan et al., 2010) classified as an HII galaxy (Yuan et al., 2010). It has Hα condensation outside its main body at $7''.0$ towards the north (Rodríguez-Zaurín et al., 2011), of which the Paα image is not enough deep to detect. Distribution of Paα emission is concentrated at the center of the galaxy.

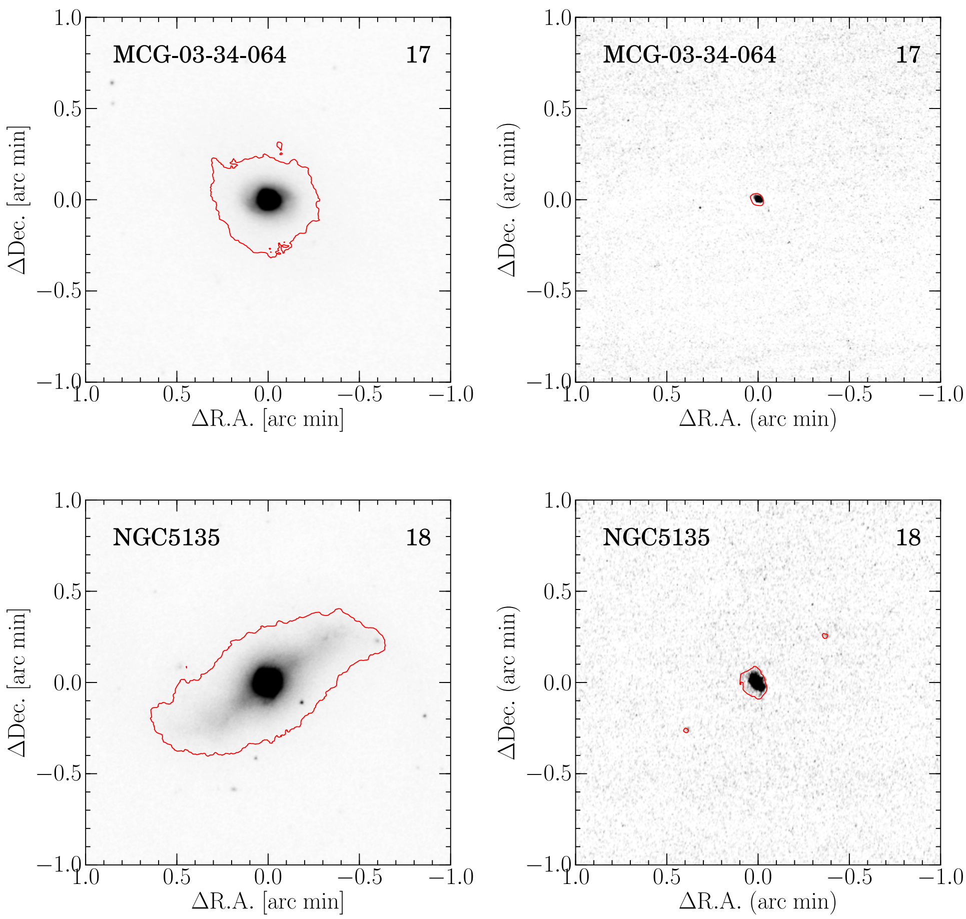

Figure 4.1: Continued

14. NGC 2342 (IRAS 07063+2043): This is a spiral (Sc; HyperLeda) classified as an HII galaxy (Ho et al., 1997) without an AGN activity at any wavelength, having a paired galaxy (NGC 2341; Alonso-Herrero et al. 2006) at a distance of 2$'$.5. This is not a well studied pair (Jenkins et al., 2005). The both galaxies have high IR luminosities of $\log(L_{\rm FIR}/L_{\odot}) = 10.8$ (Sanders et al., 2003). Paα emission is extended along the spiral arms over 10 kpc.

15. ESO 320-G030 (IRAS F11506−3851): This is a barred spiral (SBb; HyperLeda) classified as an HII galaxy (van den Broek et al., 1991). VLT-VIMOS/Hα (Rodríguez-Zaurín et al., 2011) and *HST*/NICMOS Paα (Alonso-Herrero et al., 2006) observations report starburst regions distributed in a ring-like shape, while they can not be seen in continuum images. In the Paα image, the same ring structure can be seen, and the

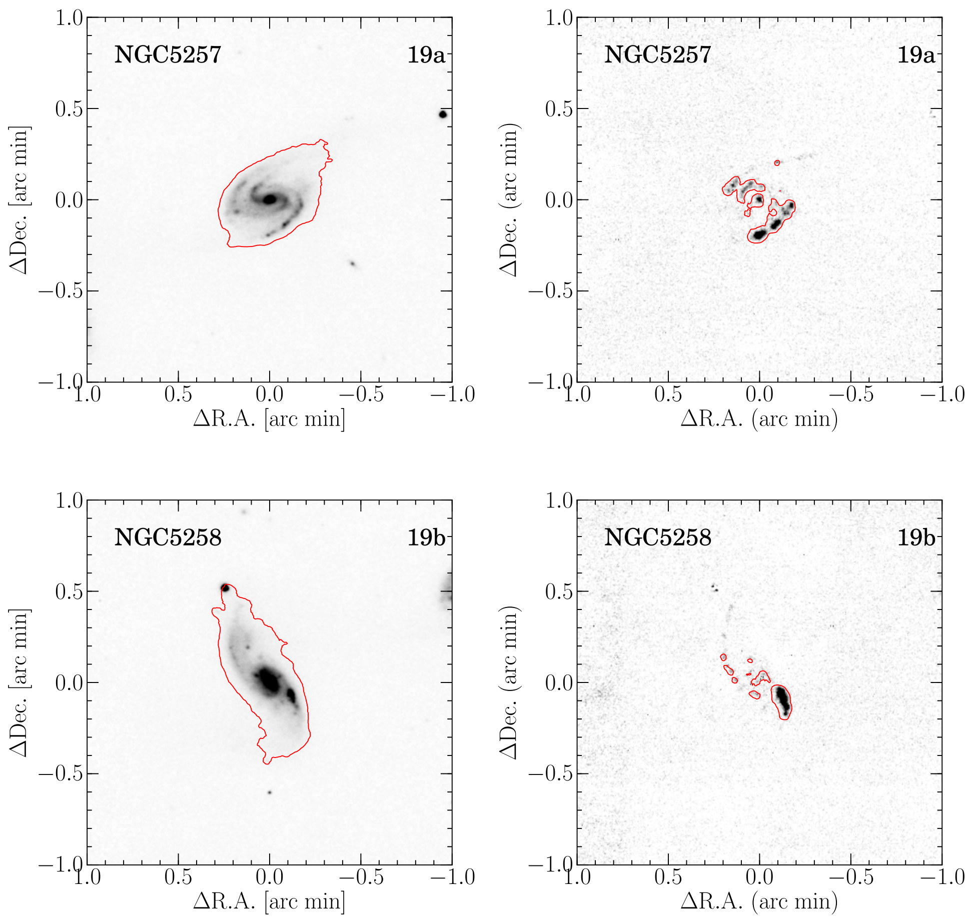

Figure 4.1: Continued

emission line region is extended beyond the ring.

16. NGC 4922 (IRAS F12590+2934; VV 609; KPG 363A/B): This is known as a post-merger between an early-type and a spiral, located at the outskirts of the Coma cluster (Sheen et al., 2009). It is an elliptical (E; HyperLeda) classified as a LINER (van den Broek et al., 1991), and shows extended soft X-ray emission not originated from an AGN but possibly related to the on-going star formation (Alonso-Herrero et al., 1999) in the northern galaxy, especially. In the Paα image, the concentrated northern nucleus has strong and extended emission, but the southern one is faint.

17. MCG −03-34-064 (IRAS F13197−1627): This galaxy forms a wide binary system with MCG −30-34-063 (Yuan et al., 2010), and is an S0/a (Naim et al., 1995) classified as a Seyfert 1 spectroscopically (Véron-Cetty & Véron, 2006). Paα emission is

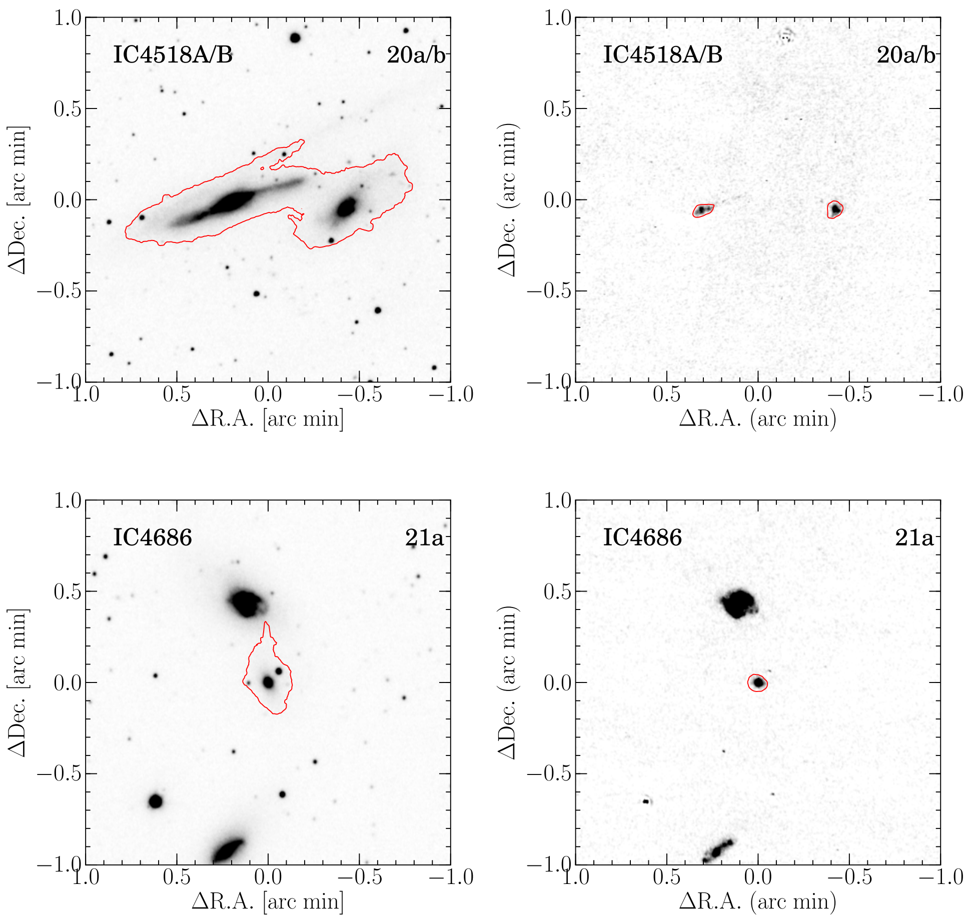

Figure 4.1: Continued

compact and concentrated at the center of the galaxy. In addition, a paired galaxy located 1′.8 away are found have a compact Paα source.

18. NGC 5135 (IRAS F13229−2934): This galaxy is an isolated system (Yuan et al., 2010), and is an SB(s)ab (de Vaucouleurs et al., 1991) classified as a Seyfert 2 (Corbett et al., 2003). In the Paα image, clumpy blobs are detected at the central region which have been already reported in previous Hα and Paα imaging observations (e.g., Rodríguez-Zaurín et al., 2011; Alonso-Herrero et al., 2006). Also, a mini-spiral structure can be seen in our Paα image.

19. NGC 5257/8 (IRAS F13373+0105 NW/SE; Arp 240; VV 055; KPG 389): These galaxies form an interacting pair with a separation of 1′.3. NGC 5258 is an SA(s)b; peculiar, and NGC 5257 is an SAB(s)b; peculiar (de Vaucouleurs et al., 1991) both

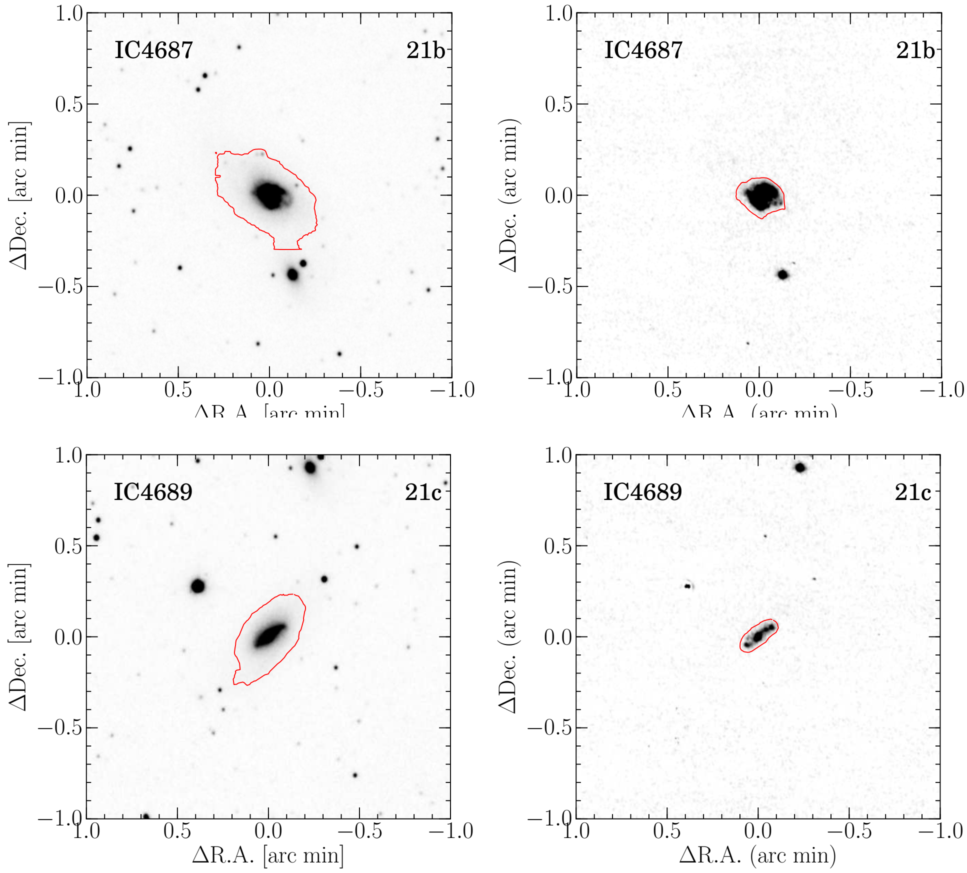

Figure 4.1: Continued

are classified as HII galaxies (Corbett et al., 2003; Veilleux et al., 1995). While a tidal tail between these galaxies can be seen in the continuum image, Paα emission is not detected there, which is consistent with Hα imaging observations (Dopita et al., 2002). NGC 5257 has Paα blobs along the spiral arms and the southern arm has stronger and bigger clumps of emission. NGC 5258 also has Paα blobs along spiral arms, with the southern arm having stronger Paα emission where larger amount of CO$(1-0)$ emission is detected (Iono et al., 2005).

20. IC 4518A/B (IRAS F14544−4255; VV 780; AM 1454−425): This is a strongly interacting pair of galaxies with a separation of 37.″6. Both are spirals (Sc; HyperLeda) classified as Seyfert 2 (Corbett et al., 2003). Although tidal tails exist not only between these galaxies but also at spiral arms of each galaxy as can be seen in the continuum image, the Paα emission is not detected there, being consistent with Hα imaging

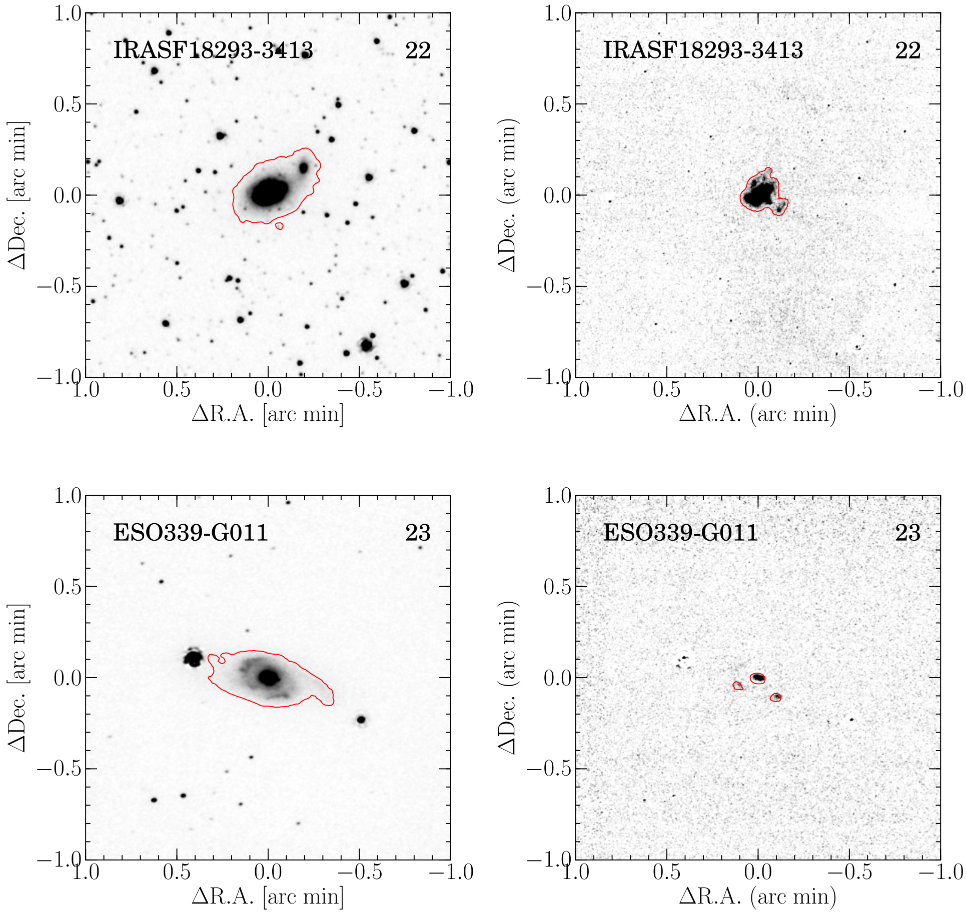

Figure 4.1: Continued

observations (Dopita et al., 2002). While the western galaxy has a strong and concentrated Paα emission at the central region, the eastern galaxy has extended Paα emission not only at its center but also along its spiral arms.

21. IC 4687/6 (IRAS F18093−5744; AM 1809−574): This is a system of three interacting galaxies (IC 4687; IC 4686; IC 4689) (West, 1976). The separation between the northern (IC 4687) and center (IC 4686) galaxy is 27.″8, and between the center and the southern (IC 4689) galaxy is 56.″8. The northern galaxy is a barred spiral (SABb; HyperLeda), the center is an elliptical (E; HyperLeda), and the southern is a barred spiral (SABa; HyperLeda), all classified as an HII galaxies (Yuan et al., 2010; Veilleux et al., 1995). These galaxies show strong Paα emission; the northern galaxy has disturbed blobs like a ring starburst, which is consistent with a Paα image of *HST*/NICMOS (Alonso-Herrero et al., 2006), the central galaxy has concentrated Paα emission at the center, and

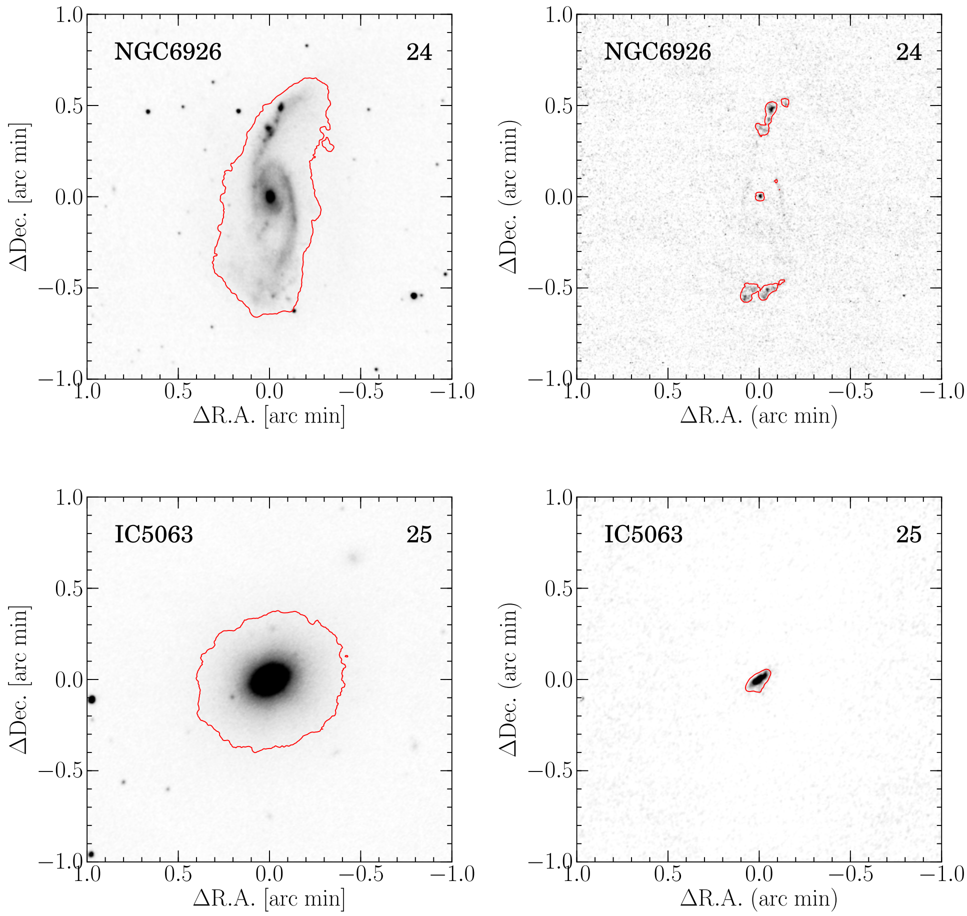

Figure 4.1: Continued

the southern galaxy has extended emission regions along the spiral arms. We can not see the Paα emission between these galaxies, which is consistent with Hα imaging observations (Rodríguez-Zaurín et al., 2011; Dopita et al., 2002).

22. IRAS F18293−3413: This galaxy is an S0/a (HyperLeda) classified as an HII galaxy (Veilleux et al., 1995). It shows a concentrated Paα emission region at the center and diffuse region along the disk.

23. ESO 339-G011 (IRAS F19542−3804): This is an isolated barred galaxy (SBb, HyperLeda) with a tidal tail (Yuan et al., 2010) classified as a Seyfert 2 (Yuan et al., 2010). It has disturbed Paα emission at the center and some blobs can be detected along the disk. It seems to have a companion with a separation of $14''.3$ with a tidal tail. The Paα emission region possibly were induced by merger, but the emission can not be detected in

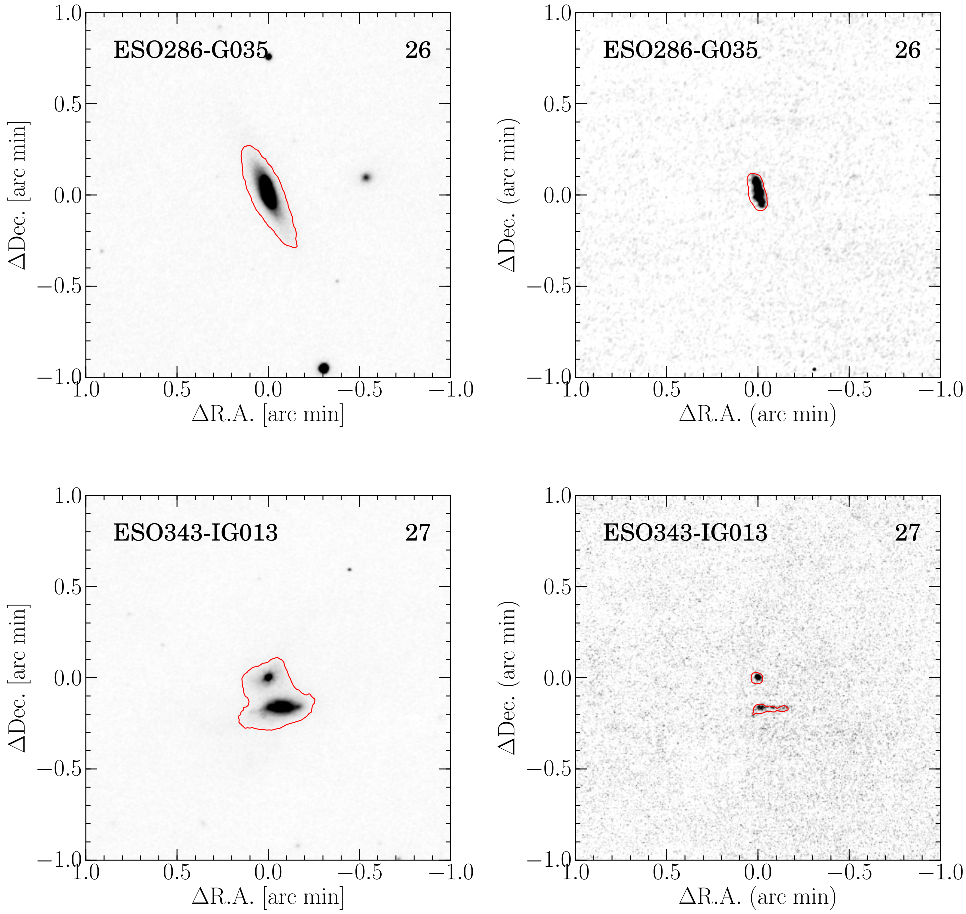

Figure 4.1: Continued

the companion.

24. NGC 6926 (IRAS F20305−0211; VV 621): This is a barred galaxy (Sc; HyperLeda) and has a companion of dwarf elliptical (NGC 6929) at a distance of $\sim 4'$ towards east. The starburst activity of this galaxy has presumably been triggered by a M51-type density wave induced by the companion (Lutz, 1991). This is classified as a Seyfert 2 (Veilleux et al., 1995) or an H II galaxy (Corbett et al., 2003). While strong Hα emissions are seen along the spiral arms especially in the northern part, no emission is detected in the nucleus (Dopita et al., 2002). However, bright Paα emission is detected not only at the spiral arms but also in the nucleus.

25. IC 5063 (IRAS F20481−5715; AM2048−571): This is an S0/a (HyperLeda) considered as a merger remnant (Colina et al., 1991) and classified as a Seyfert

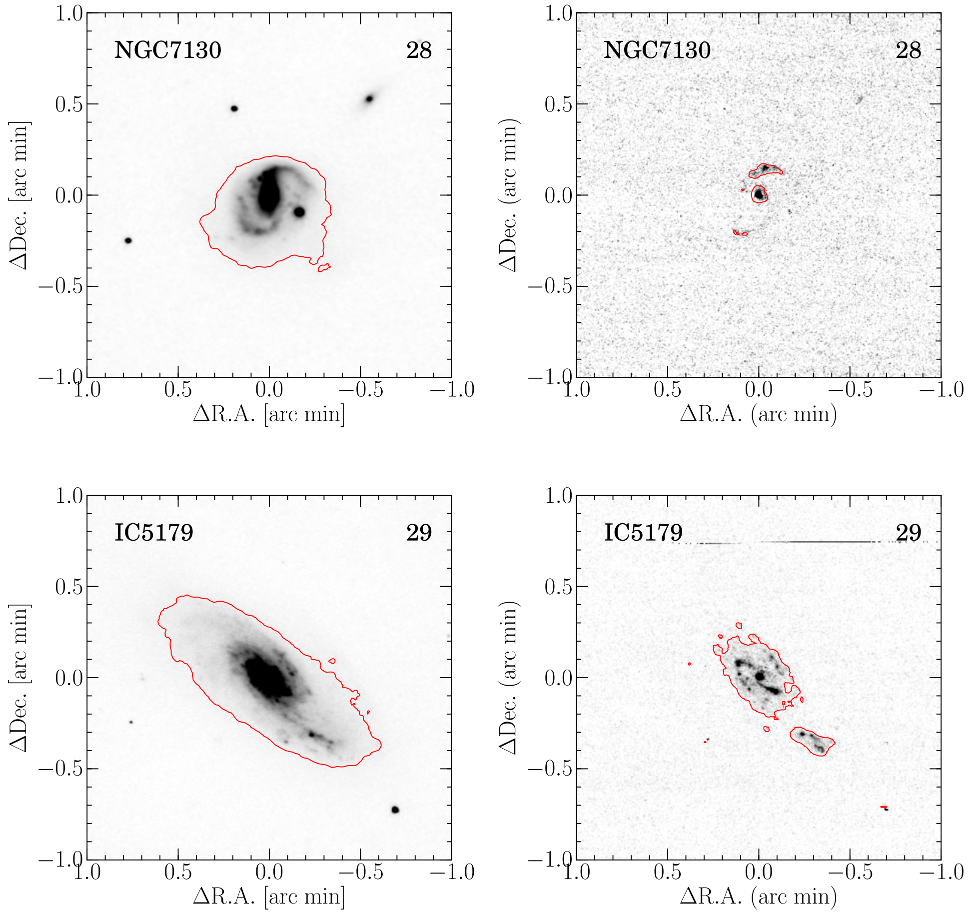

Figure 4.1: Continued

2. It shows high polarization in the near IR continuum (Hough et al., 1987) and strong broad Hα emission in polarized flux (Inglis et al., 1993). These results suggest that there is an obscured hidden broad-line region (HBLR) (e.g., Tran, 2001; Lumsden et al., 2001; Antonucci & Miller, 1985) and the broad emission line is scattered into our line of sight by scatters outside the obscured regions (Morganti et al., 2007). Also, this object is the first galaxy where a fast gas outflow has been discovered (Morganti et al., 1998). A Paα emission is strongly concentrated at the center and extended towards NW-SE direction, which may consistent with the direction of extend NLR reported by Colina et al. (1991).

26. ESO 286-G035 (IRAS F21008−4347): This is a spiral (Sc; HyperLeda) classified as an HII galaxy (Veilleux et al., 1995). In the Paα image, there is a strong emission line region at the center extended along the disk.

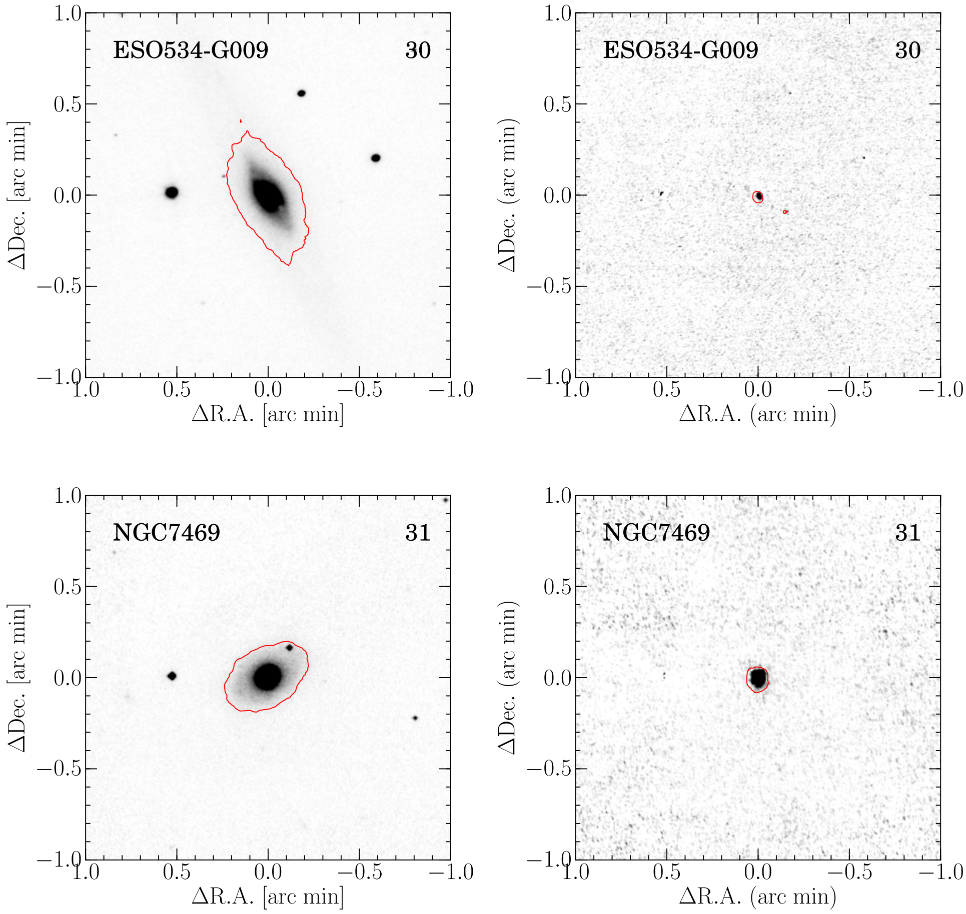

Figure 4.1: Continued

27. ESO 343-IG013 (IRAS F21330−3846; VV 714; AM 2133−384): This is a barred spiral (Sbc; HyperLeda) classed as an HII galaxy (Yuan et al., 2010; Veilleux et al., 1995). It is known as a strongly interacting pair (Vorontsov-Vel'Yaminov & Arkhipova, 1974) with a separation between the two galactic nuclei of 10.″9 in the K_s-band image. The northern part of the galaxy has concentrated Paα emission at its center, while the southern part has strong Paα emission at the its center and extended region along spiral arms.

28. NGC 7130 (IRAS F21453−3511; AM 2145−351; NED 02): This is a spiral (Sc; HyperLeda) classified as LINER/Seyfert 1 (Corbett et al., 2003; Veilleux et al., 1995). It is known as a peculiar/disturbed spiral (Lauberts, 1982) and a starburst/AGN composite galaxy (Levenson et al., 2005). In the Paα image, strong emission exists at the central region, as well as along the spiral arms, especially at the northern arm which is consistent with an Hα image (Rodríguez-Zaurín et al., 2011), and a Paα image by *HST*/NICMOS

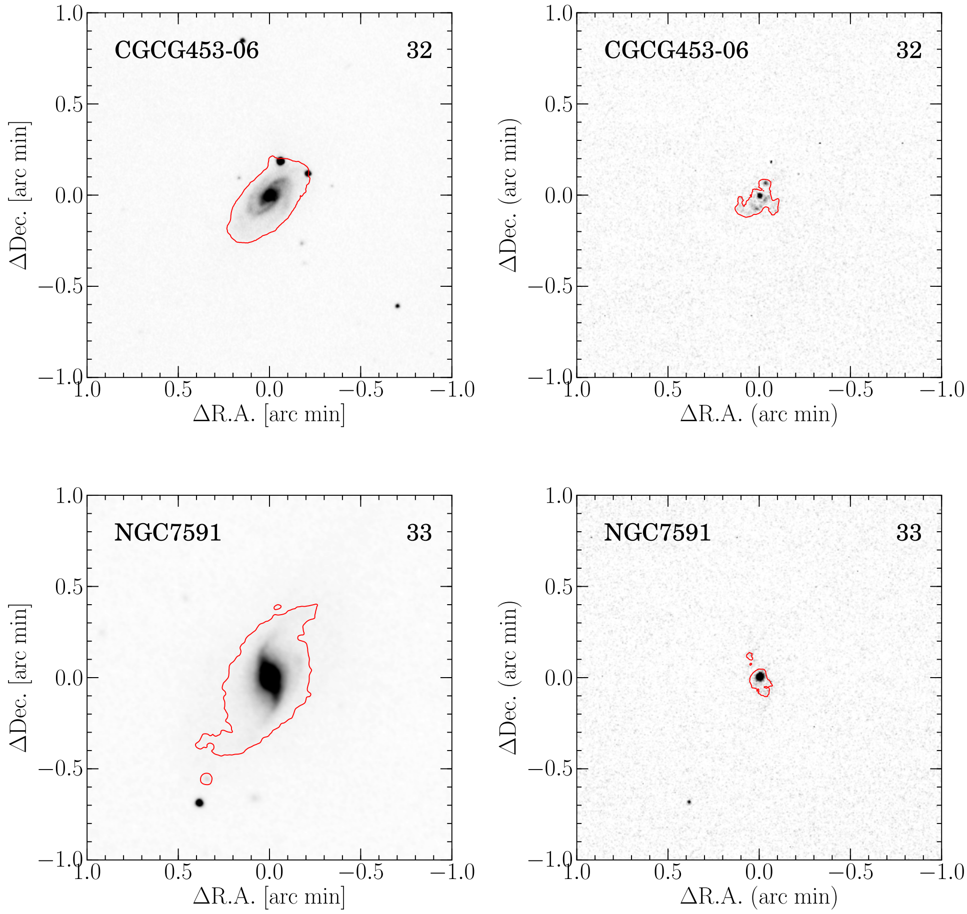

Figure 4.1: Continued

(Alonso-Herrero et al., 2006).

29. IC 5179 (IRAS F22132−3705; AM 2213−370): This is a barred spiral (Sbc; HyperLeda) classified as an HII galaxy (Yuan et al., 2010). Type Ia SN 1999ee and the Type Ib/c SN 1999ex have been discovered in this galaxy (Stritzinger et al., 2002). Paα emission is distributed along the spiral arms as clumpy knots. These HII knots, which are widely spread over the entire galaxy, is not be covered by the field of view of VLT/VIMOS (Rodríguez-Zaurín et al., 2011) and *HST*/NICMOS (Alonso-Herrero et al., 2006) observations.

30. ESO 534-G009 (IRAS F22359−2606): This is a spiral (Sab; HyperLeda) classified as a LINER (Veilleux et al., 1995). There is a strong Paα emission at the central region.

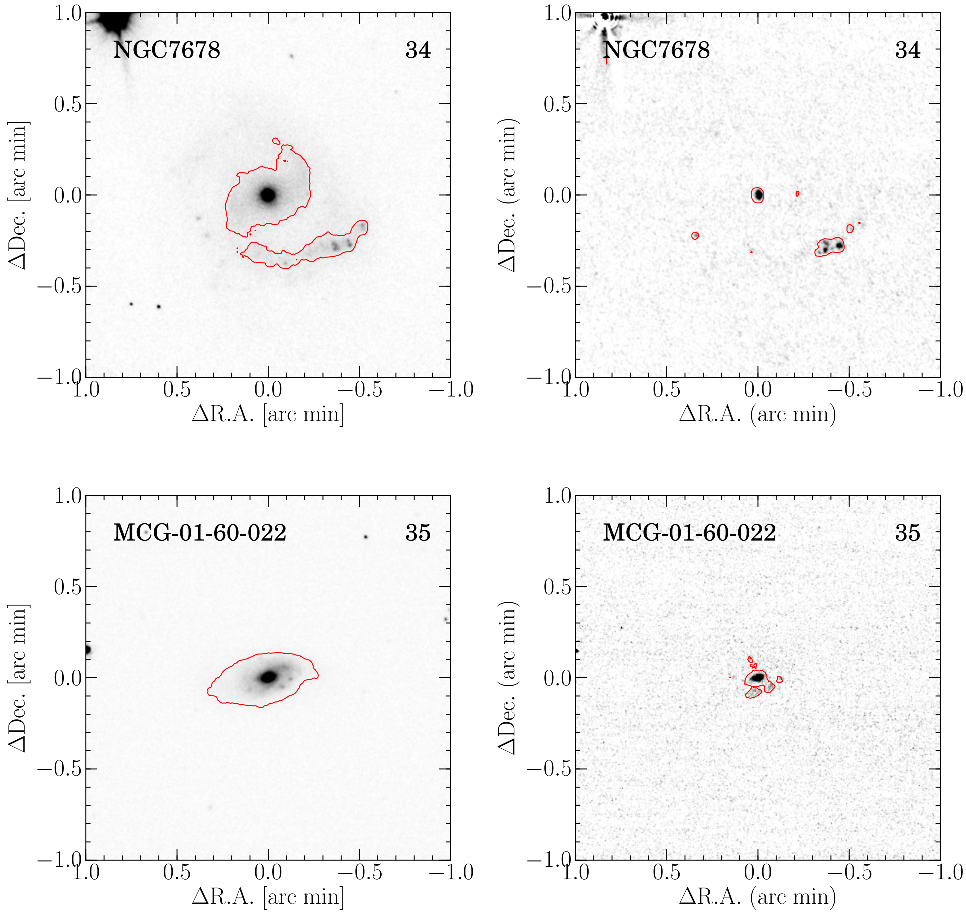

Figure 4.1: Continued

31. NGC 7469 (IRAS F23007+0836; Arp 298; NED 01; Mrk 1514; KPG 575A): This is a spiral (Sa; HyperLeda) classified as a Seyfert 1 (Veilleux et al., 1995). It is known to have a circumnuclear ring with a diameter on scales of $1''.5$–$2''.5$ (Davies et al., 2004), which is observed in the radio (Wilson et al., 1991; Condon et al., 1991; Colina et al., 2001), in the optical (Mauder et al., 1994), in the mid-infrared (Miles et al., 1994; Soifer et al., 2003), and in the near-infrared (Genzel et al., 1995; Lai et al., 1999; Scoville et al., 2000) wavelengths. In Paα image, the ring structure can not be resolved by the seeing size of the ANIR data.

32. CGCG 453-062 (IRAS F23024+1916): This is a spiral (Sab; HyperLeda) classified as a LINER (de Vaucouleurs et al., 1991). In Paα image, it has extended star-forming region distributed not only at the central region but also along the disk.

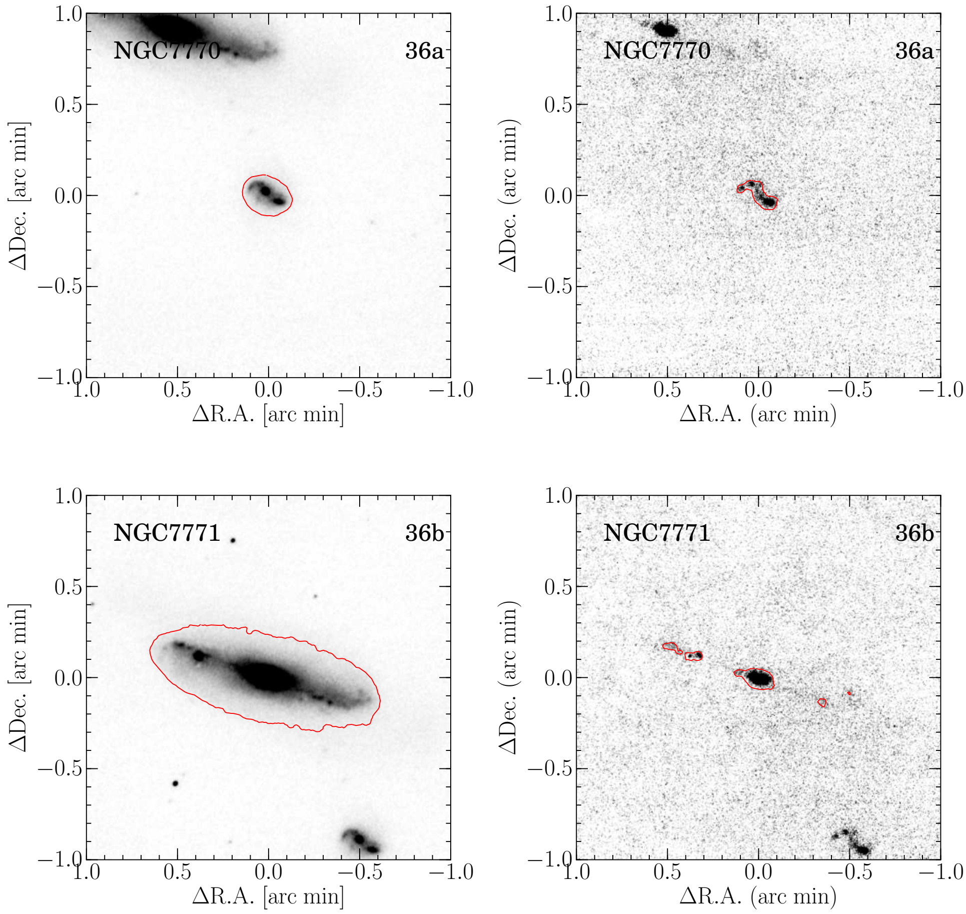

Figure 4.1: Continued

33. NGC 7591 (IRAS F23157+0618): This is an isolated (Yuan et al., 2010) barred spiral (SBbc; HyperLeda) classified as a LINER (Veilleux et al., 1995). In Paα image, a strong emission peak is at the central region, and diffuse emission regions distributed along the spiral arms and the barred structure.

34. NGC 7678 (IRAS F23259+2208; Arp 028; VV 359): This is a barred spiral (Sc; HyperLeda) classified as an HII galaxy (Ann & Kim, 1996). It has a massive spiral arm in the southern part of the galaxy, and is considered to have experienced strong interaction which induced active star formation in the nucleus and in the southern arm (Ann & Kim, 1996). In Paα image, strong emission line regions are at the central region, and at the southern arm. Extended diffuse emission can be seen along the spiral arms.

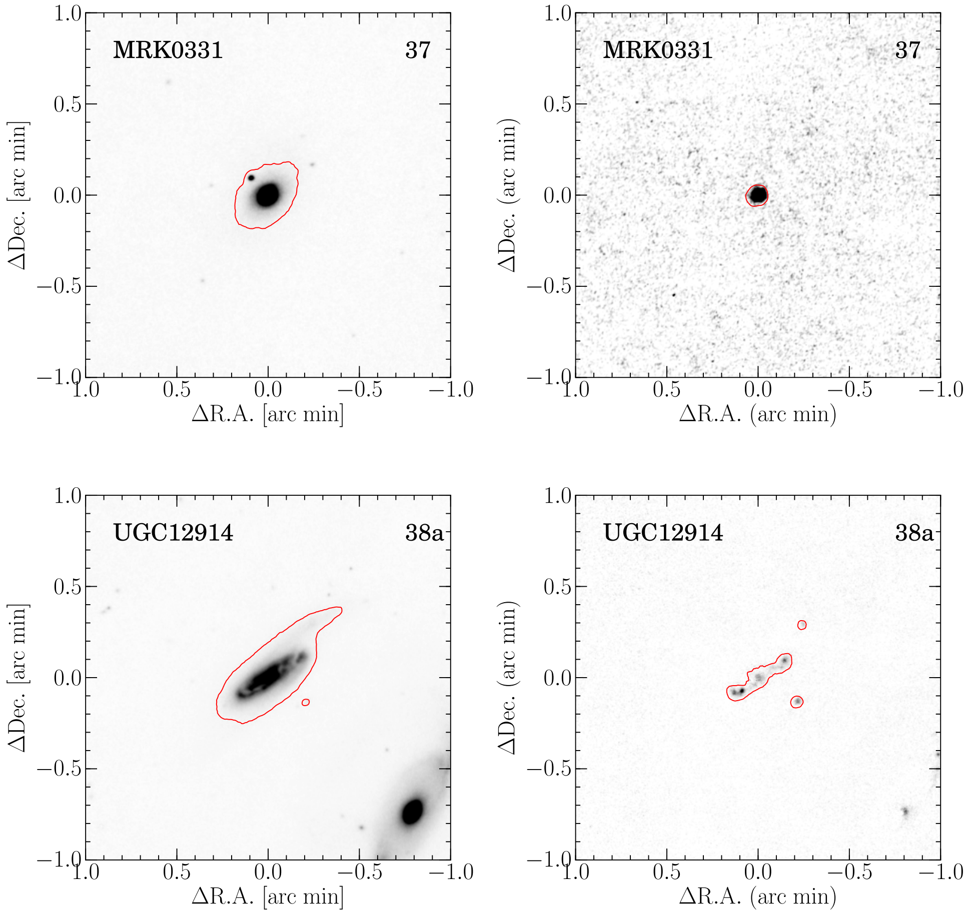

Figure 4.1: Continued

35. MCG −01-60-022 (IRAS F23394−0353; VV 034a; Arp 295B): This is a merging spiral (Sb; HyperLeda) classified as an HII galaxy (Corbett et al., 2003). It is known as an interacting galaxy (Vorontsov-Vel'Yaminov & Arkhipova, 1974; Roche, 2007) paired with MCG −01-60-021, separated by $4'.5$ in the K_s-band image. In Paα image, a strong emission is detected not only at the central region but also along the disk, while a Paα emission can not be detected in the tidal tail between Arp 295A and Arp 295B.

36. NGC 7770/1 (IRAS F23488+19489; Mrk 9006; KPG 592B): This appears to be in the early stage of an interaction with NGC 7770 where a separation between the two galactic nuclei is $1'$ in the K_s-band image. NGC 7770 is a spiral (S0-a; HyperLeda), and NGC 7771 is a barred spiral (Sa; HyperLeda) classified as an HII galaxy (Veilleux et al., 1995). Both NGC 7771 and NGC 7770 show a strong Paα emission. NGC 7770 has strong emission in the spiral arm rather than at the central region, while NGC 7771 has

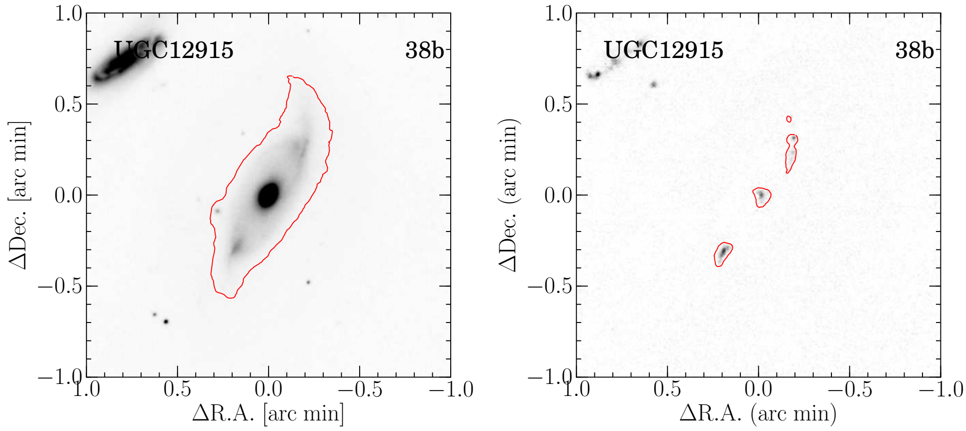

Figure 4.1: Continued

strong emission at the central region rather than in the disk. The morphology of central Paα emission in NGC 7771 seems to be a ring starburst. No Paα emission is detected between these galaxies.

37. Mrk 331 (IRAS F23488+1949; KPG 593B): This is a member of a group of three galaxies; an irregular separated by $1'.4$ and a spiral by $2'$ (Mirabel, 1983). It is a spiral (Sa; HyperLeda) classified as an HII/Seyfert 2 (Soifer et al. 2001). In Paα image, an emission line appears to be concentrated at the central region.

38. UGC 12914/5 (IRAS F23591+2312; VV 254; III Zw 125; KPG 603; TaffyI): These are barred galaxies (SBc; HyperLeda). It is an interacting system with an extended shock-induced synchrotron radio emission connecting the two galaxies (Condon et al., 1993; Peterson et al., 2012). The steepening of the radio spectral index at the bridge indicates a face-on collision which occurred only 20 Myr ago (Condon et al., 1993). There are many HII blobs in a Paα image, and it is considered that many of them are induced by the collision (Komugi et al., 2012).

4.2 Bulge-Disk Decompositions

4.2.1 Identification of Irregular Galaxy

As a first step, we remove irregulars from the sample to evaluate the properties of bulges, because half of LIRGs in the local universe are classified as irregular galaxies (Wang et al., 2006). We determined whether a galaxy is a irregular or not by Gini-coefficient (G) and a second-order moment of a galaxy (M_{20}) which are one of the major nonparametric methods for quantifying galaxy morphology (Lotz et al., 2004). The parameter G is a statistic based on the Lorenz curve of fluxes per pixel in a galaxy and it represents the relative distribution of pixels covering the galaxy, while the other parameter M_{20} is a normalized second-order moment of pixels which is measured to be the brightest 20% of a flux of a galaxy. In Figure 4.2, we show the diagram of M_{20}–G measured in the $K_{\rm s}$ band. In this method, spatial resolution and noise level are critical to measure these parameters. Lotz et al. (2004) find that G and M_{20} are reliable, if the averaged signal-to-noise ratio ($\langle S/N \rangle$) per pixel of the image is larger than 2. Also, they show that M_{20} tends to have systematic offsets greater than $\sim 15\%$ when spatial resolution is worse than 500 pc, as cores of a galaxy become unresolved, while G is relatively stable to decreasing the spatial resolution down to 1000 pc. In our sample, the resolution is 180–400 pc corresponding to typical seeing size of $0\farcs8$ and $\langle S/N \rangle$ is enough high to evaluate their morphology by G and M_{20}. We adopted a criterion defined by Lotz et al. (2004) to distinguish irregulars from the other galaxies on the G–M_{20} diagram, as shown in Figure 4.2. We thus selected 20 non-irregular galaxies out of 38 galaxies for further analysis.

4.2.2 Bulge-Disk Decompositions

To evaluate the properties of bulges for the 20 non-irregular galaxies, we use Sérsic indices of the bulges obtained by two-dimensional bulge-disk decomposition analysis in the $K_{\rm s}$ band images using a software GALFIT (Peng et al., 2002, 2010). We fit each galaxy with a combination of a Sérsic profile as a bulge component and an exponential profile as a disk component,

$$I(r) = I_b \exp\left[-(r/R_b)^{1/n_b}\right] + I_d \exp\left[-(r/R_d)\right], \tag{4.2}$$

where r is a distance from the galaxies center, I_b, R_b, n_b are a central surface brightness, an effective radius, and a Sérsic index of the bulge, respectively, and I_d and R_d are a central surface brightness and a scale length of the disk, respectively. In UV or optical observations, it is difficult to evaluate bulge structure because it is obscured by dust (Fisher & Drory, 2010). Instead, a $K_{\rm s}$ band image is less affected by dust extinction, and is expected to reflect the properties of stellar mass distribution. We assume that the peak in the $K_{\rm s}$ band image is the position of the galaxy center, and use it as an initial input parameter. A PSF is measured by stacking stars detected in the same image.

The results of the bulge-disk decomposition is shown in Figure 4.3. For each galaxy, the left panel shows the $K_{\rm s}$-band image observed by miniTAO/ANIR, the second from the left a model galaxy composed of the best-fit Sérsic and exponential components, and the third from the left the residual image created by subtracting the model galaxy

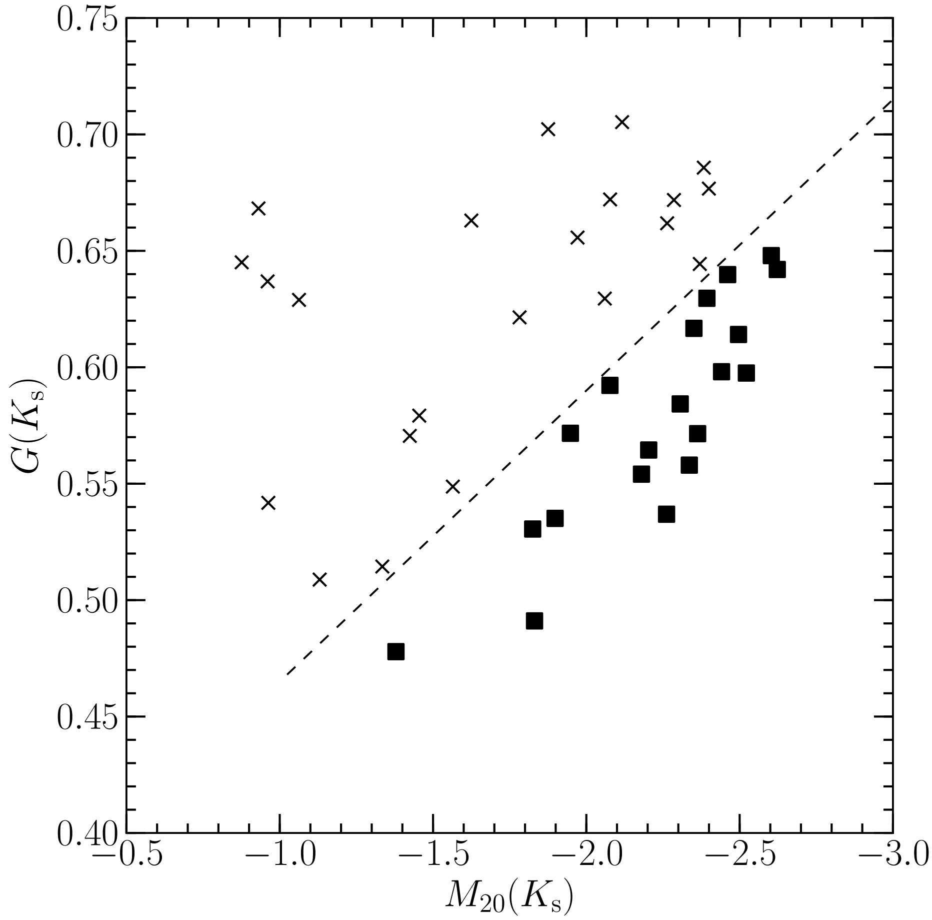

Figure 4.2: Diagram of Gini coefficient (G) and second-order moment of the brightest 20% of the galaxy's flux (M_{20}) measured in the K_s-band image. The dashed line is the threshold of on-going merger or non-merger defined by Lotz et al. (2004). The on-going merger galaxies are removed from our sample because their bulge structure would be evaluated correctly.

from the K_s-band image. The residual structure of spiral arms and bars can be seen in the residual image for most of the sample. The right panel is the radial profile of the surface brightness with model profiles, cut along the major axis of the galaxy.

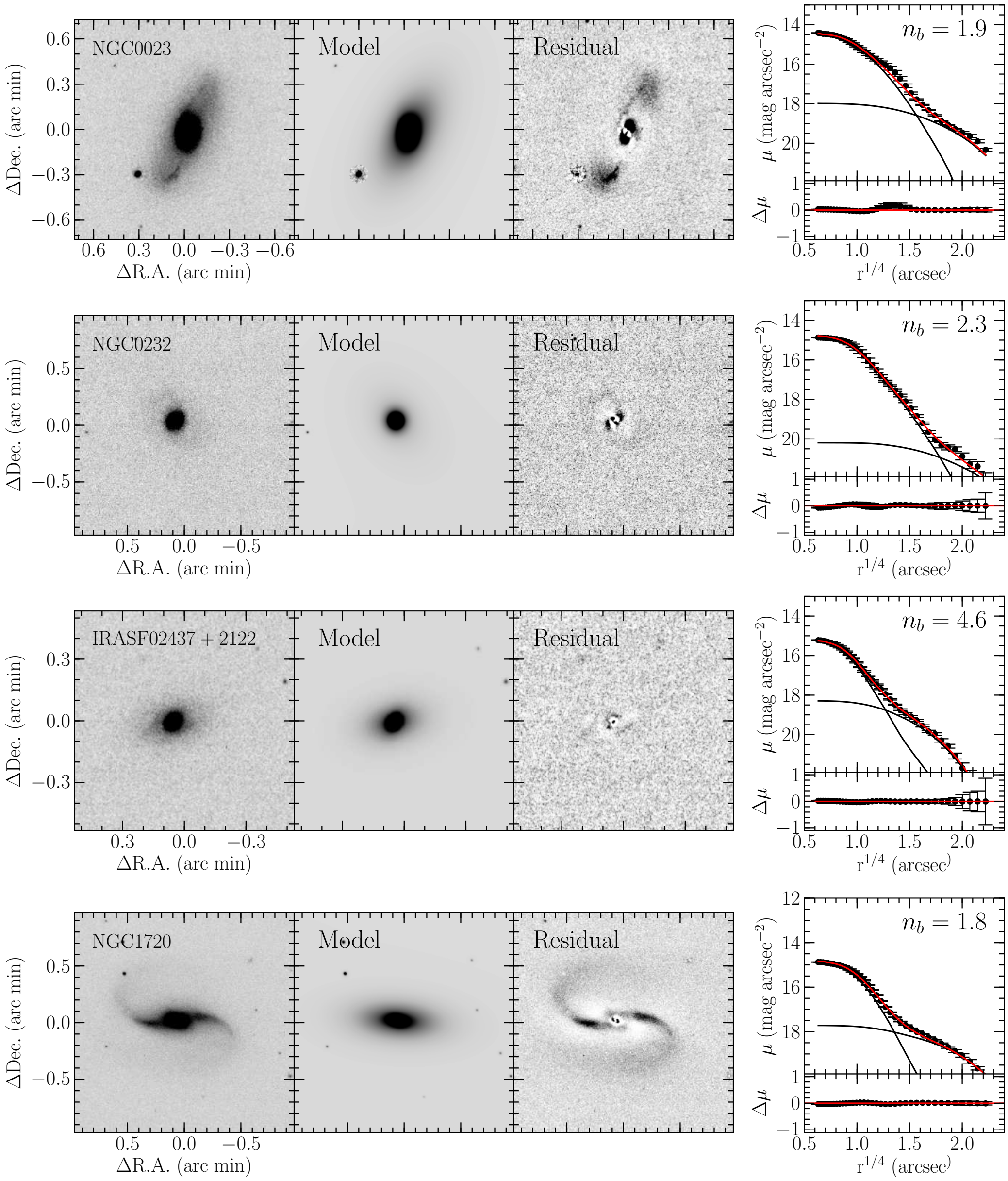

Figure 4.3: Results of bulge-disk decomposition. For the individual galaxies, the K_s band science image, a model image with the best-fit bulge and disk components, the residual image after subtracting the best-fit model image from the science image and one-dimensional luminosity profile of the galaxy are shown, from left to right, respectively.

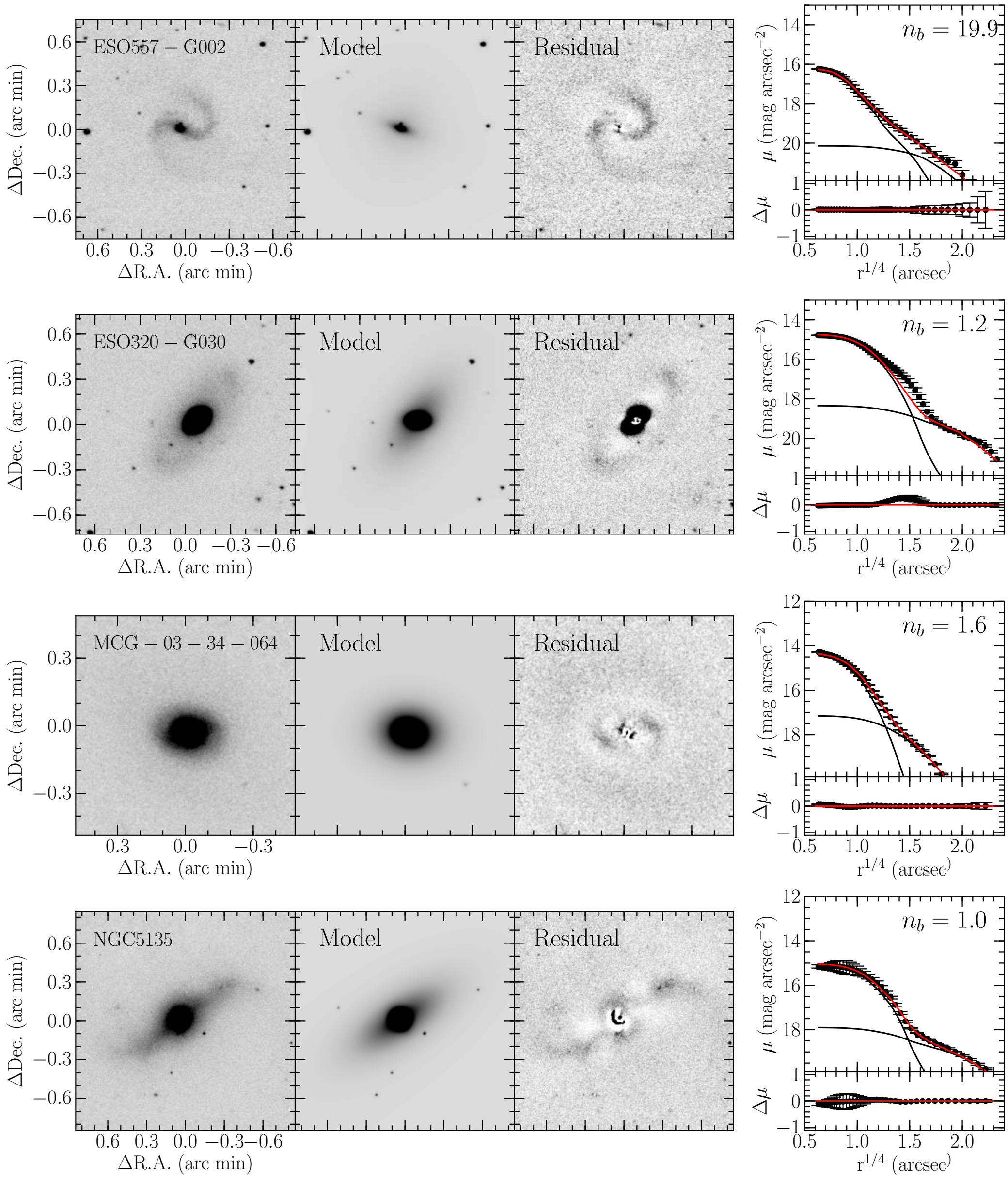

Figure 4.3: Continued

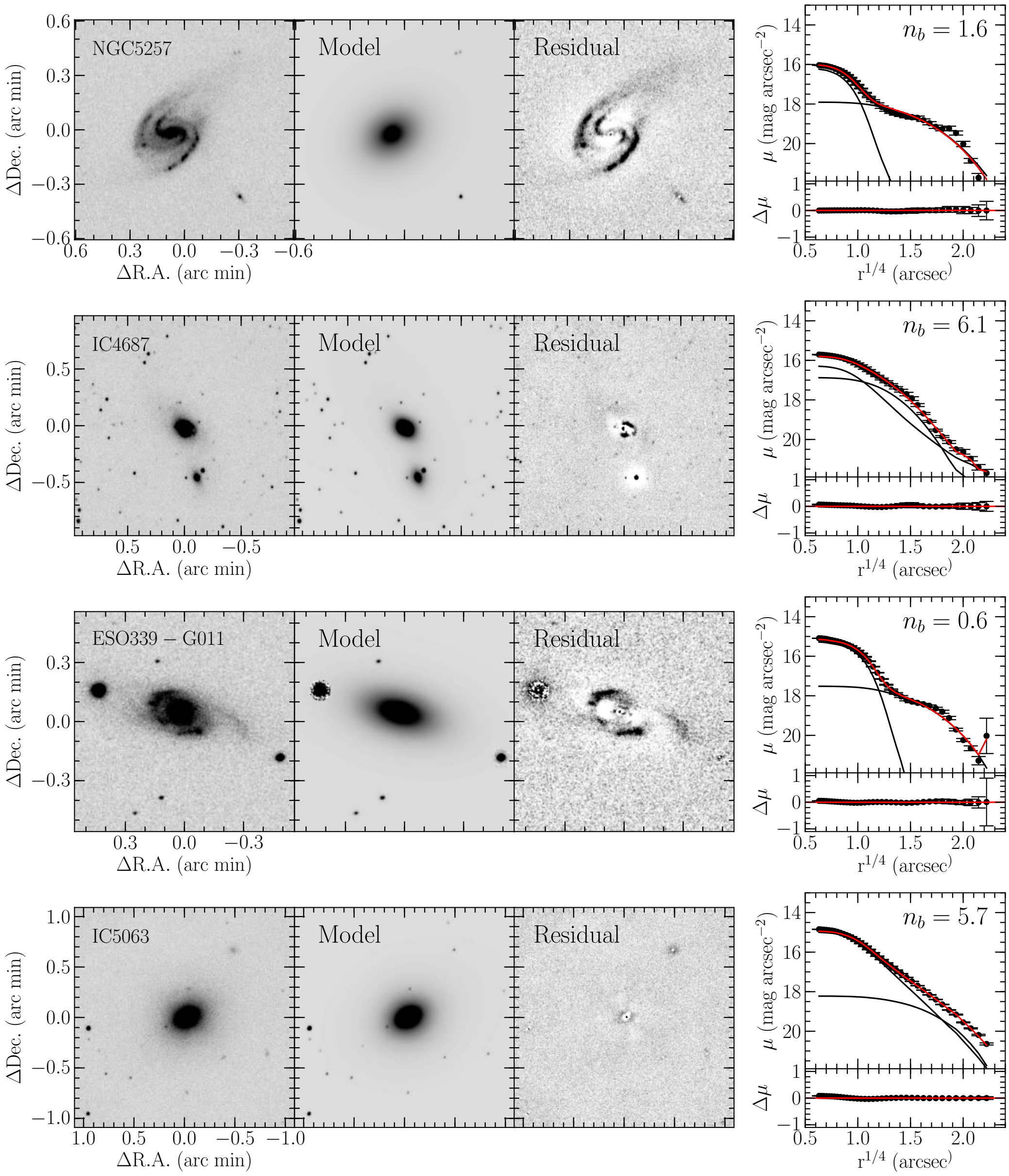

Figure 4.3: Continued

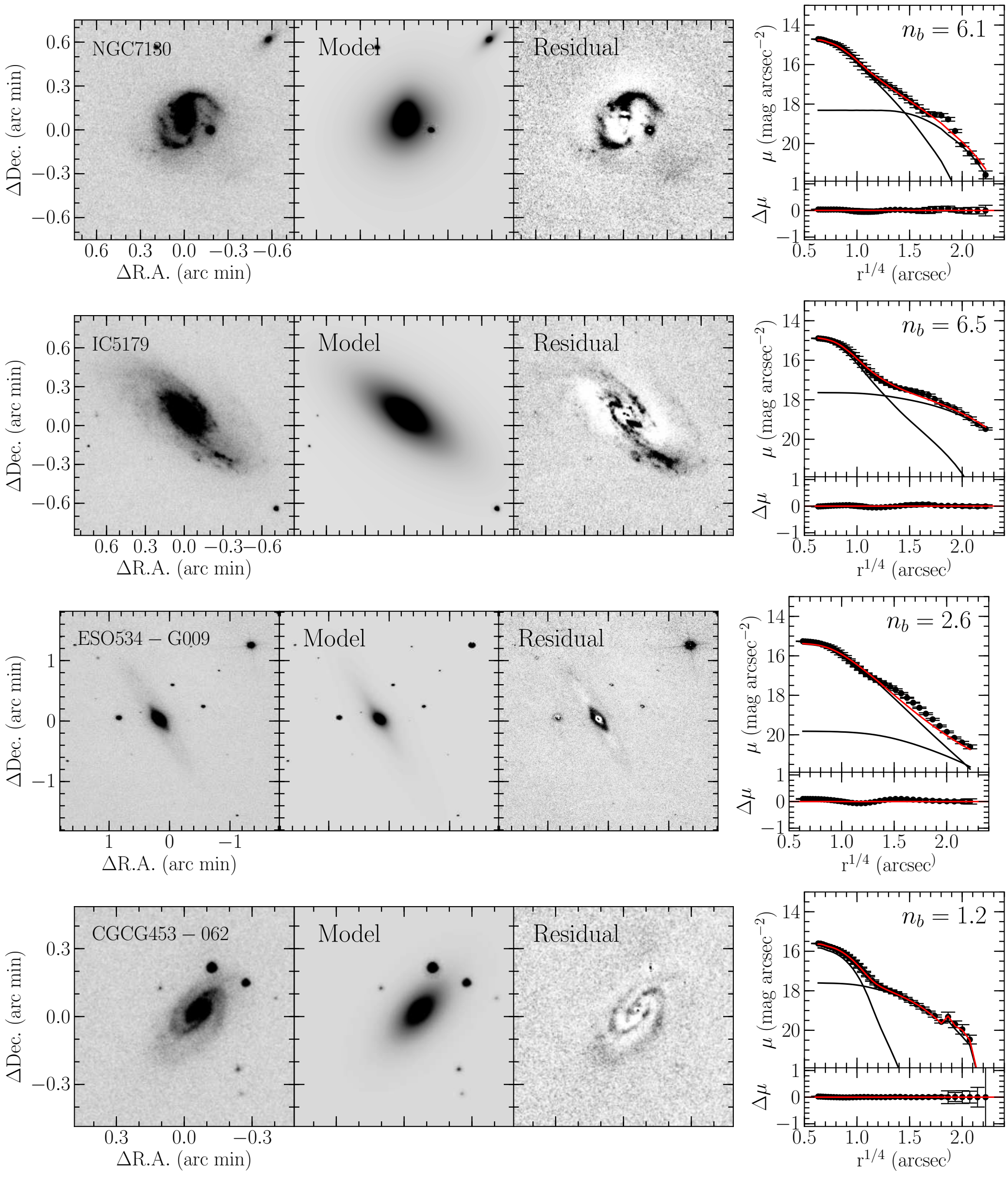

Figure 4.3: Continued

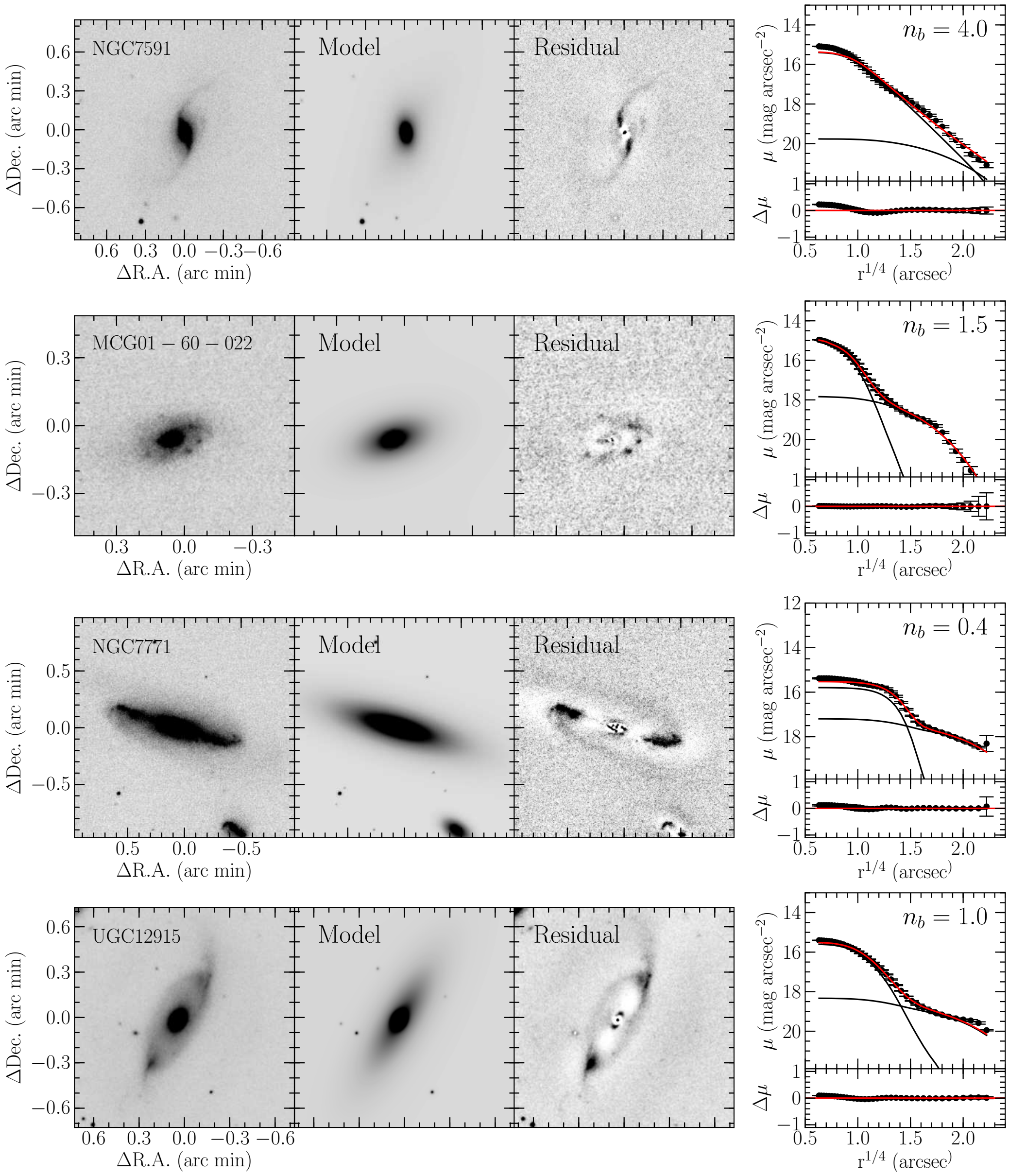

Figure 4.3: Continued

Chapter 5

Discussion

5.1 Star Formation Rates and Surface Densities

5.1.1 The Effect of Dust-extinction for Paα Flux

Even though the Paα emission line is less sensitive against dust extinction, we can not ignore its effect. Typical amount of dust extinction in LIRGs is $A_V \sim 4$ mag (Alonso-Herrero et al. 2006; A06) as derived by the "Balmer Decrement Method" (e.g., Calzetti et al., 2000) using the flux ratio of Hα and Paα. To correct for the dust-extinction in our sample, we adopt the extinction curve of Calzetti et al. (2000) with $R_V = 4.05$, which results in $A_V/A_{\mathrm{Pa}\alpha} = 6.97$, and $A_{\mathrm{H}\alpha}/A_{\mathrm{Pa}\alpha} = 5.68$, meaning that Pa$\alpha$ is typically attenuated by 0.57 mag in LIRGs. In Table 5.1, color excess ($E(B-V)$) derived by the Balmer decrement method using spectroscopically obtained Hα/Hβ taken from Veilleux et al. (1995), Dopita et al. (2002), and Rodríguez-Zaurín et al. (2011) are listed. Note that the intrisic value of Hα/Hβ=2.85 is used, assuming case B condition with electron density of $n_e = 10^4$ cm^{-3} and temperature of $T = 1000$ K.26 galaxies, with Hα and Hβ data in our sample have A_V = 4.25 mag ($E(B-V) = 1.05$) on average, and we adopt this value for the rest of the sample without Hα and Hβ data.

5.1.2 Star Formation Rates

SFRs are derived from Paα luminosity using the following equation, obtained from the SFR-Hα luminosity relation assuming a Kroupa IMF (Kennicutt et al., 2009) and a flux ratio of Hα/Paα = 8.6 ($T = 1000$ K, $n_e = 10^4$ cm^{-3}; Hummer & Storey 1987) in starburst galaxies;

$$SFR(\mathrm{Pa}\alpha)(M_\odot\ \mathrm{yr}^{-1}) \equiv 6.4 \times 10^{-41} L(\mathrm{Pa}\alpha)(\mathrm{erg\ s}^{-1}) \tag{5.1}$$

where $L(\mathrm{Pa}\alpha)$ is the luminosity of Paα. Dust-extinction uncorrected star formation rates ($SFR(\mathrm{Pa}\alpha)$) obtained from $L(\mathrm{Pa}\alpha)$ and those corrected for dust-extinction ($SFR(\mathrm{Pa}\alpha)_{\mathrm{corr}}$) are shown in Table 5.1.

Figure 5.1 shows the comparision between $SFR(\mathrm{Pa}\alpha)_{\mathrm{corr}}$ and SFR derived from the dust-extinction corrected Hα luminosity ($SFR(\mathrm{H}\alpha)_{\mathrm{corr}}$). The dust-extinction corrected

Table 5.1: Paα luminosities and derived star formation rates.

ID (1)	Galaxy Name (2)	R_{90}(Paα) (kpc) (3)	L(Paα) (ergs s^{-1}) (4)	SFR(Paα) ($M_\odot$ yr^{-1}) (5)	SFR(Paα)$_{\rm corr}$ ($M_\odot$ yr^{-1}) (6)	SFR(IR) ($M_\odot$ yr^{-1}) (7)	$E(B-V)$ (8)	Ref. (9)
1	NGC 23	1.9	1.17×10^{41}	7.5	11.2	14.5	0.74	1
2	NGC 34	1.1	3.30×10^{41}	21.1	65.0	35.4	2.08	1
3	NGC 232	0.9	7.98×10^{40}	5.1	10.4	26.5	1.31	1
4	IC 1623A/B	9.8	6.02×10^{41}	38.5	44.3	58.9	0.26	1
5	ESO 244-G012	1.8	4.33×10^{41}	27.7	59.3	32.6	1.41	3
6	UGC 2238	3.3	3.88×10^{41}	24.8	83.8	23.0	2.25	1
7	IRAS F02437+2122	0.5	2.46×10^{40}	1.6	5.0	17.6	2.13	1
8	UGC 2982	4.7	2.67×10^{41}	17.1	47.5	17.0	1.89	1
9	NGC 1614	1.1	5.97×10^{41}	38.2	74.7	49.0	1.24	1,2,3
10	MCG −05-12-006	0.8	1.28×10^{41}	8.2	[14.5]	15.8	[1.05]	–
11	NGC 1720	0.9	3.32×10^{40}	2.1	[3.8]	8.5	[1.05]	–
12	ESO 557-G002	1.2	9.02×10^{40}	5.8	7.3	18.6	0.43	2,3
13	IRAS F06592-6313	0.7	7.39×10^{40}	4.7	9.4	17.0	1.28	3
14	NGC 2342	10.9	1.55×10^{41}	9.9	[17.5]	27.0	[1.05]	–
15	ESO 320-G030	1.5	4.26×10^{40}	2.7	5.1	20.3	1.16	3
16	NGC 4922	1.2	5.50×10^{40}	3.5	[6.2]	22.7	[1.05]	–
17	MCG −03-34-064	0.3	7.45×10^{40}	4.8	[8.4]	20.4	[1.05]	–
18	NGC 5135	1.4	1.72×10^{41}	11.0	14.2	20.0	0.46	3
19	NGC 5257/8	9.5/10.6	$2.65\times10^{41}/1.93\times10^{41}$	16.9/12.4	20.8/15.2	37.5	0.38	1,2
20	IC 4518A/B	0.7/4.6	$4.51\times10^{+40}/2.86\times10^{40}$	2.9/1.8	3.7/2.3	13.4	0.43	2,3
21	IC 4686/87	0.6/2.5	$8.81\times10^{40}/5.41\times10^{41}$	5.6/34.6	8.2/45.6	38.2	0.69	2,3
21c	IC 4689	2.2	1.42×10^{41}	9.1	16.0	–	[1.05]	-
22	IRAS F18293-3413	1.8	6.29×10^{41}	40.3	104.3	70.6	1.76	1
23	ESO 339-G011	1.3	7.37×10^{40}	4.7	[8.3]	14.8	[1.05]	–
24	NGC 6926	24.5	1.16×10^{41}	7.4	14.3	22.2	1.22	1,2
25	IC 5063	0.8	2.64×10^{40}	1.7	[3.0]	7.8	[1.05]	–
26	ESO 286-G035	2.1	1.76×10^{41}	11.3	[19.9]	19.0	[1.05]	–
27	ESO 343-IG013	1.6	7.09×10^{40}	4.5	7.5	13.7	0.93	1,2
28	NGC 7130	1.0	1.35×10^{41}	8.6	14.2	26.5	0.92	1,2,3
29	IC 5179	5.4	1.62×10^{41}	10.4	19.0	17.5	1.11	1,3
30	ESO 534-G009	0.5	6.53×10^{39}	0.4	0.6	5.4	0.63	1
31	NGC 7469	1.0	3.71×10^{41}	23.7	23.7	50.0	0.00	1
32	CGCG 453-062	4.1	1.23×10^{41}	7.9	[13.9]	27.7	[1.05]	–
33	NGC 7591	5.4	6.79×10^{40}	4.3	9.2	13.9	1.39	1
34	NGC 7678	18.8	3.41×10^{40}	2.2	[3.8]	7.4	[1.05]	–
35	MCG −01-60-022	1.3	1.61×10^{41}	10.3	21.9	20.9	1.40	2
36	NGC 7770/1	2.3/3.4	$8.75\times10^{40}/1.77\times10^{+41}$	5.6/11.3	7.8/34.0	28.6	2.03	1
37	Mrk 331	1.6	2.14×10^{41}	13.7	[24.2]	32.4	[1.05]	–
38	UGC 12914/15	6.8/12.2	$6.34\times10^{40}/3.85\times10^{40}$	4.1/2.5	[7.2]/[4.4]	10.5	[1.05]	–

Column (1): Galaxy ID in this paper. Column (2): Galaxy name. Column (3): Size of Paα emission line regions in diameter defined to be an elliptical (major axis) contained 50% flux within the Petrosian radius (Peterson et al., 2012). Column (4): Observed Paα luminosities. Column (5): Paα-derived star formation rates. Column (6): Paα-derived star formation rates with dust extinction correction. Brackets values are dust-extinction corrected SFRs by using assumed $E(B-V) = 1.05$, the average value of all our objects. Column (7): IR-drived star formation rates. Column (8): Amount of dust extinction derived from balmer decrement using the flux ratio of Hα and Hβ. Column (9): References for the dust extinction. 1; Veilleux et al. (1995), 2; Dopita et al. (2002), 3; Rodríguez-Zaurín et al. (2011)

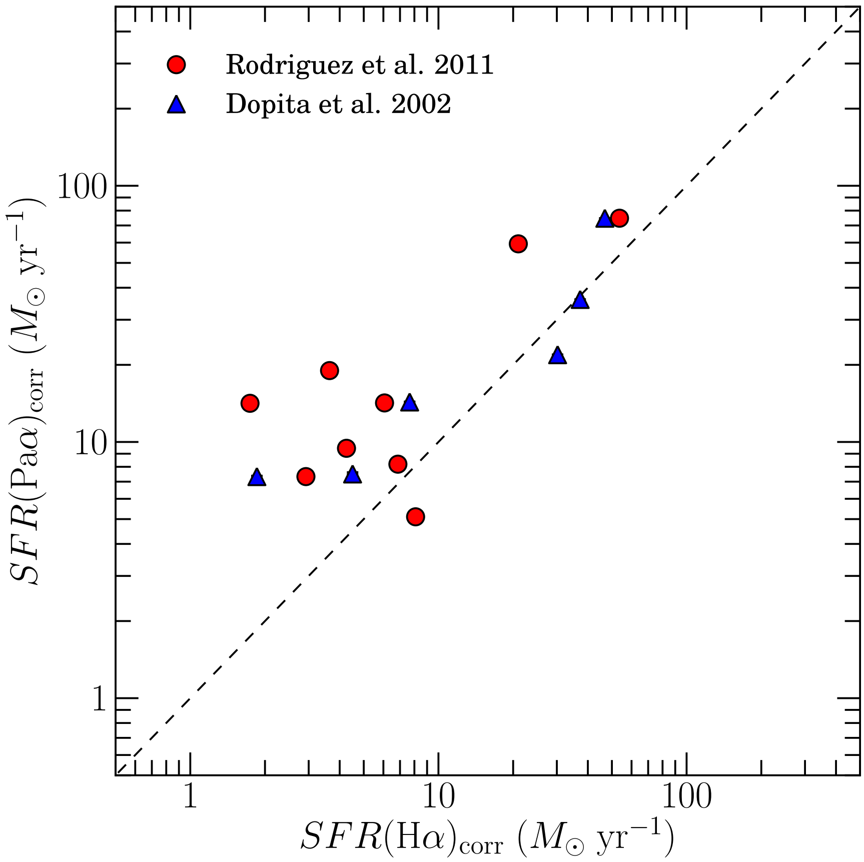

Figure 5.1: Comparison of SFRs derived from Hα and Paα luminosities, both corrected for dust extinction. Hα luminosities are taken from Rodríguez-Zaurín et al. (2011) (circles) and Dopita et al. (2002) (triangles). The dashed line shows the one-to-one relation.

Hα luminosities are taken from Rodríguez-Zaurín et al. (2011) and Dopita et al. (2002), which are obtained by narrow-band imaging or integral field spectroscopy. The correlation between $SFR(\mathrm{Pa}\alpha)_{\mathrm{corr}}$ and $SFR(\mathrm{H}\alpha)_{\mathrm{corr}}$ is generally good, but $SFR(\mathrm{Pa}\alpha)_{\mathrm{corr}}$ is larger than $SFR(\mathrm{H}\alpha)_{\mathrm{corr}}$ systematically. Liu et al. (2013b) have found that correcting dust extinction using Hα/Paβ gives much larger star formation rate than using Hα/Hβ (Balmer decrement) in star-forming regions of M83. Considering this study, the difference between $SFR(\mathrm{Pa}\alpha)_{\mathrm{corr}}$ and $SFR(\mathrm{H}\alpha)_{\mathrm{corr}}$ suggests that Paα can see star-forming activity through a more dusty region than Hα.

FIR and bolometric infrared luminosities are also good indicators for star formation in dusty starburst galaxies (e.g., Kennicutt, 1998; Kewley et al., 2002; Hirashita et al., 2003), because MIR to FIR emission in these galaxies arises from re-radiation of dust-absorbed shorter-wavelength photons. Therefore, we have derived bolometric infrared luminosities

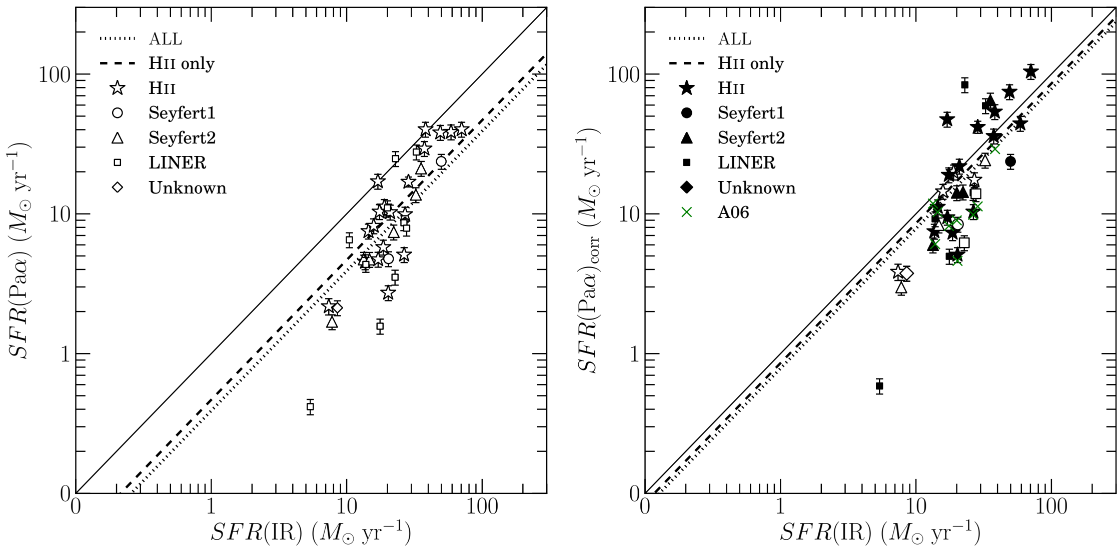

Figure 5.2: Left: Comparison of SFRs derived from bolometric infrared luminosities calculated using *IRAS* ADDSCAN FIR luminosities of 12 μm, 25 μm, 60 μm, and 100 μm, and those derived from Paα luminosities. The dotted line represents the best fit relation for all galaxies assuming a slope of one, that is $\log_{10}(SFR(\mathrm{Pa}\alpha)) = 1.0 \times \log_{10}(SFR(\mathrm{IR})) - 0.4$ while the dashed line represents for the HII galaxies, that is $\log_{10}(SFR(\mathrm{Pa}\alpha)_{\mathrm{corr}}) = 1.0 \times \log_{10}(SFR(\mathrm{IR})) - 0.3$. The solid line shows the one-to-one relation. Stars represent HII galaxies, circles Seyfert Is, triangles Seyfert IIs, squares LINERs, and diamonds galaxies without any classification. The error bars are the total uncertainties in the measurement of the Paα flux (σ_{total}; see text). Right: Same as the left, but plot for SFRs derived from Paα are corrected for dust-extinction. The dotted line represents the best fit relation for all galaxies assuming a slope of one, that is $\log_{10}(SFR(\mathrm{Pa}\alpha)) = 1.0 \times \log_{10}(SFR(\mathrm{IR})) - 0.1$ while the dashed line represents for the HII galaxies, that is $\log_{10}(SFR(\mathrm{Pa}\alpha)_{\mathrm{corr}}) = 1.0 \times \log_{10}(SFR(\mathrm{IR})) - 0.07$. The solid line shows the one-to-one relation. Filled symbols represent galaxies whose extinction is corrected using Balmer decrement method while open symbols assuming $E(B-V)$=1.05. Crosses show galaxies which have Paα data obtained by *HST*/NICMOS and corrected for dust extinction using Balmer decrement method, taken from (A06).

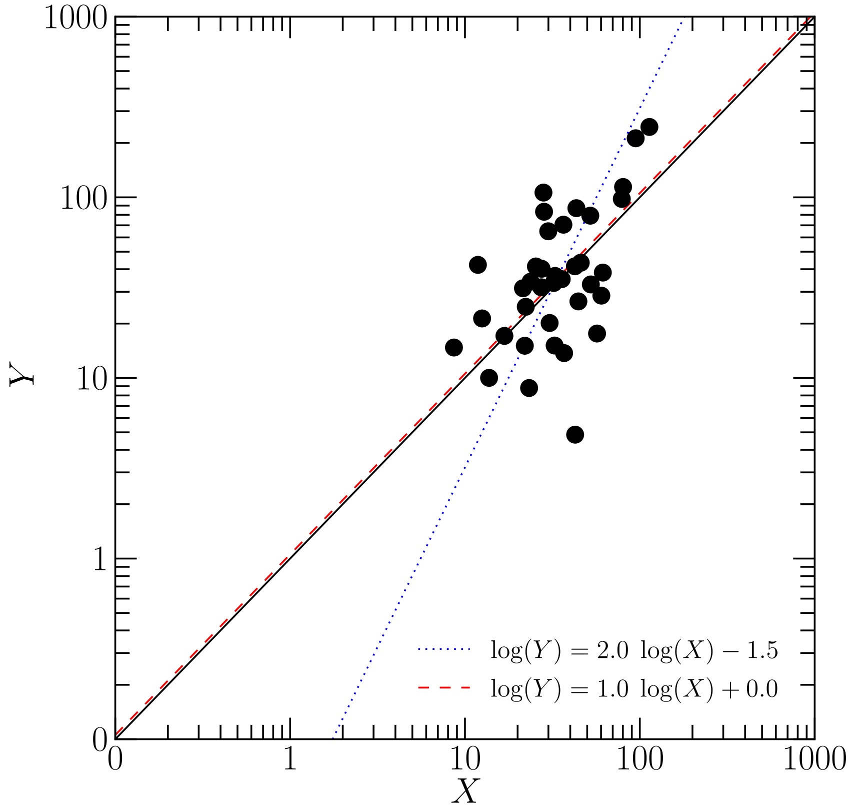

Figure 5.3: An example of Malmquist bias test. The dotted line shows a best-fit relation with 1 free-parameter function ($\log(Y) = \log(X) + b$), and the dashed with two free-parameters function ($\log(Y) = a \times \log(X) + b$). We have carried out the procedure 1000 times (see Sec. Malmquist Bias)

(L(IR)) of our sample using from the *IRAS* ADDSCAN/SCANPI 12 μm, 25 μm, 60 μm, and 100 μm data (Sanders et al., 2003) using the following relation (Sanders & Mirabel, 1996);

$$\begin{aligned} L(\mathrm{IR}) &= 4\pi D_L^2 \times (1.8 \times 10^{-14}(13.48 f_{12} \\ &\quad +5.16 f_{25} + 2.58 f_{60} + f_{100})), \end{aligned} \tag{5.2}$$

where D_L is the luminosity distance in meters and f_{12}, f_{25}, f_{60}, and f_{100} are the IRAS flux densities in Jy at 12, 25, 60, and 100 μm, respectively. Then, SFR(IR) is derived using the following relation (Calzetti , 2013);

$$SFR(\mathrm{IR})\ (M_\odot\ \mathrm{yr}^{-1}) \equiv 2.8 \times 10^{-44}\ L(\mathrm{IR})\ (\mathrm{erg\ s}^{-1}), \tag{5.3}$$

The results are listed in Table 5.1.

Left panel of Figure 5.2 is comparison of SFR(IR) and SFR(Paα). The dotted line represents the best fit relation for all galaxies assuming a slope of one and the dashed line represents the same but using only HII galaxies. Both indicate that SFR(Paα) are systematically offset by -0.3 dex from SFR(IR).

Right panel of Figure 5.2 is comparison of SFR(IR) and $SFR(\mathrm{Pa}\alpha)_{\mathrm{corr}}$. Some samples have no H$\alpha$ data, therefore we correct for dust-extinction assuming $E(B-V) = 1.05$ ($A_V = 4.3$) which is an average value of our sample which has Hα and Hβ spectroscopic data. In this figure, we also plot a sample of galaxies from A06 where SFR(Paα) are derived in the same way as described above, however, we do not use this sample to obtain the best-fit relations. The offset between $SFR(\mathrm{Pa}\alpha)_{\mathrm{corr}}$ and SFR(IR) is -0.07 dex, which is within a scatter of 0.27dex, where the scatter is 1σ assuming Gussian profile and the center is along the best-fit relation.

Malmquist Bias

In Figure 5.2, it seems that the best-fit slopes of the distribution of HII galaxies are larger than one. Actually, the slopes are 1.8 for the best-fit relation of SFR(IR)–SFR(Paα) plot if we fit with two-parameter linear relation, and 2.1 for SFR(IR)–$SFR(\mathrm{Pa}\alpha)_{\mathrm{corr}}$ relation. This may be caused by "Malmquist bias" (Malmquist, 1925), where brightness of a sample falls off quickly until the brightness falls below observational threshold, because the infrared luminosity range of our sample is spread over only 1 order of magnitude. Therefore we have estimated this effect in our sample with the following simple test.

We first create a model set of 38 galaxies with SFR of "X" ($M_\odot$ yr^{-1}) within the same IR luminosity range as our sample. This X for each galaxy is converted into "Y" by adding Gaussian-random "noise" with $\sigma = 0.3$ dex, which is the same value as the dispersion between $\log(SFR(\mathrm{Pa}\alpha)_{\mathrm{corr}})$ and $\log(SFR(\mathrm{IR}))$. Then, a best-fit relation is obtained for the plot of X and Y. In this fitting, two kinds of relations are used; one is 1 free-parameter function ($\log(Y) = \log(X) + b$) and the other is two free-parameters function ($\log(Y) = a \cdot \log(X) + b$). We have carried out the above procedure 1000 times and one of them is shown in Figure 5.3.

In the 2 free-parameter fitting, we find the slope a to be 2.0 ± 0.3, which is larger than the intrinsic value of 1 and consistent with the observed value of $a = 2.1$. In the one free-parameter fitting, we find that the offset is $b = 0 \pm 0.05$. The Large slope of the distributions in right panel of Figure 5.2 come from the Malmquist bias. To remove the Malmquist bias it is necessary to expand the luminosity range.

Comparison Between IR SFR and Paα SFR

Above test shows that the vertical offsets in Figure 5.2 are insensitive to the Malmquist bias. To explain the offset of -0.3 dex in the left panel fo Figure 5.2 by dust-extinction, $A_V = 5.7$ is required. A06 suggested that the dust-extinction derived from flux ratio of Hα and Paα is $A_V = 4.1$ on average, which is almost the same value as our result but slightly smaller. The right panel of Figure 5.2 shows that there is a relatively good coincidence between the $SFR(\mathrm{Pa}\alpha)_{\mathrm{corr}}$ and the SFR(IR) on average.

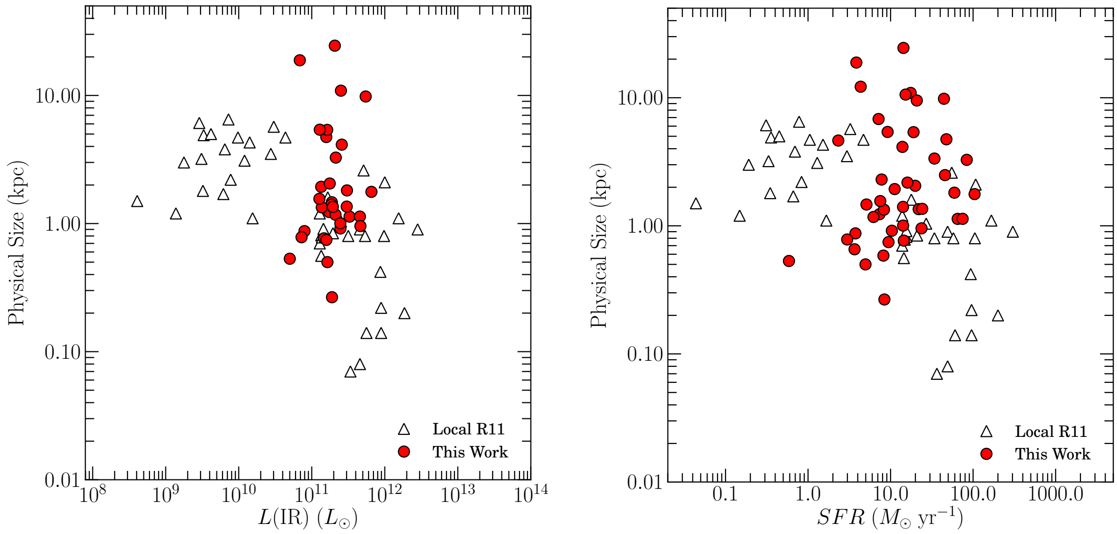

Figure 5.4: Left: Comparison of L(IR) and physical sizes (in diameter) of star-forming regions. To compare with local sample in Rujopakarn et al. (2011), the area of star-forming region is measured in Paα images convolved with a gaussian function with $\sigma = 4$ kpc in physical scale. Triangles represent normal galaxies and U/LIRGs derived from Rujopakarn et al. (2011). Right: Comparison of SFR and physical sizes (in diameter) of star-forming regions. SFRs are derived not only from Paα but also from MIR luminosity in Rujopakarn et al. (2011).

Although our result shows that there is a good coincidence between $SFR(\mathrm{Pa}\alpha)_{\mathrm{corr}}$ and SFR(IR), some of the galaxies have offset from it. For example, ESO 534-G009, having lowest $SFR(\mathrm{Pa}\alpha)_{\mathrm{corr}}$ in our sample, is a late-type spiral (Sab) classified as a LINER, and its Paα emission is emitted from an unresolved compact central region. This galaxy shows an order of magnitude lower $SFR(\mathrm{Pa}\alpha)_{\mathrm{corr}}$ than SFR(IR). Such galaxies with smaller $SFR(\mathrm{Pa}\alpha)_{\mathrm{corr}}$ than SFR(IR) may have larger dust extinction than measured; indeed, Piqueras López et al. (2013) shows that dust-extinction of central region of LIRGs are estimated to be $A_V = 5 \sim 13$ mag by using infrared indicators, larger than the value obtained using optical. Another possibility is contribution to IR luminosity by dust particles heated by more evolved stars, called the "IR cirrus" component (e.g., Kennicutt, 1998; Kennicutt et al., 2009), which may overestimate SFR(IR).

5.1.3 Surface Densities of Infrared Luminosity and Star Formation Rate

The distribution of star-forming regions in LIRGs at high IR luminosity end and in ULIRGs are compact while the normal galaxies show extended star-forming regions over a few kilo-parsecs along the spiral arm (e.g., Soifer et al., 2000; Díaz-Santos et al., 2010; Alonso-Herrero et al., 2012).

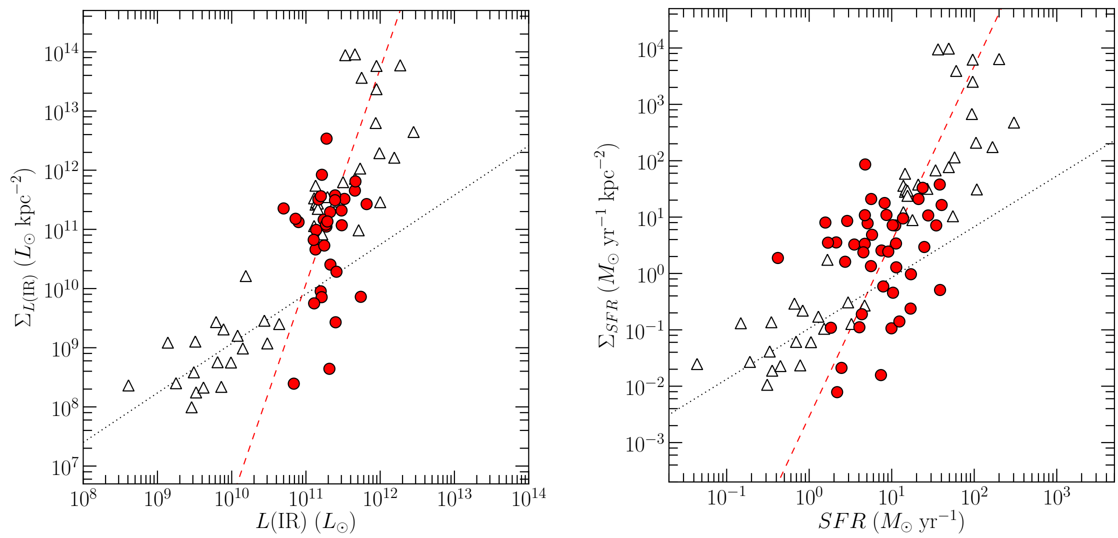

Figure 5.5: Left: Comparison of L(IR) and L(IR) surface densities. The dotted line represent the sequence of normal galaxies (Rujopakarn et al., 2011), while dashed line the sequence of U/LIRGs, which is the best fit relation using the sample from this work and Rujopakarn et al. (2011). Right: Comparison of SFRs derived from Paα luminosities and SFR surface densities. The dotted line represent the sequence of normal galaxies (Rujopakarn et al., 2011), while dashed line the sequence of U/LIRGs, which is the best fit relation using the sample from this work and Rujopakarn et al. (2011).

Rujopakarn et al. (2011) find that the extent of distribution of star-forming regions changes drastically at the LIRG luminosity, suggesting that these differences are caused by strong interaction (Totani et al., 2011). However, there are few sample at the "transition" point. To investigate this relationship between the distribution of star-forming regions and star-forming activity, we measure extent of distribution of star-forming regions in our large sample of LIRGs with Paα emission line images to fill the gap between normal galaxies and ULIRGs in Rujopakarn et al. (2011).

We define the extent of distribution of a star-forming region of a galaxy to be an elliptical diameter (major axis) containing 50% of total Paα flux within a Petrosian radius (Petrosian, 1976) defined in the Paα line image convolved with a Gaussian function with σ = 4 kpc in physical scale as done in Rujopakarn et al. (2011) and list it in column-(3) of Table 5.1. The left panel of Figure 5.4 shows the comparison between the IR luminosities and the sizes of the star-forming regions except for 5 galaxies (NGC 5257/8, IC 4518A/B, IC 4686/7, NGC 7770/1, UGC 12914/5) which are paired galaxies and the extent of distribution of SFR can not be defined. We find that the extent of distribution of the LIRGs in our sample is distributed from 0.3 kpc or less to 25 kpc. Especially, IC 1623A/B, NGC 2342, NGC 7678, NGC 6926 have a large extent of (> 9.5 kpc) star-forming regions along their spiral arms. The right panel of Figure 5.4 shows the comparison between the SFRs derived from Paα and the extent of distribution of the star-forming regions including the 5 galaxies

(NGC 5257/8, IC 4518A/B, IC 4686/7, NGC 7770/1, UGC 12914/5) removed from the left panel of Figure 5.4. Our results fill the blank parameter space between normal galaxies and ULIRGs in Rujopakarn et al. (2011).

The left panel of Figure 5.5 shows a comparison of IR luminosites and surface densities of IR luminosity ($\Sigma_{L(\mathrm{IR})}$) derived by dividing a IR by area of a star-forming region;

$$\Sigma_{L(\mathrm{IR})} \equiv L(\mathrm{IR})/(\pi R_{90}(\mathrm{Pa}\alpha)^2), \tag{5.4}$$

where $R_{90}(\mathrm{Pa}\alpha)$ is the extent of distribution of star-forming regions listed in Table 5.1. In this figure, the dotted line represents the sequence of normal galaxies derived by best fitting of local normal galaxies and high-z star-forming galaxies in Rujopakarn et al. (2011) and Rujopakarn et al. (2013). Rujopakarn et al. (2011) shows that the sequence of local U/LIRGs is different from that of local normal galaxies. Therefore we obtained the sequence of U/LIRGs by fitting sub-LIRGs ($L(\mathrm{IR}) \geq 10^{10}\ L_\odot$) and ULIRGs of both ours and those in Rujopakarn et al. (2011), that is $\log_{10}(\Sigma_{L(\mathrm{IR})}) = 3.6 \times \log_{10}(L(\mathrm{IR})) - 30.0$ shown as dashed line.

The left panel of Figure 5.5 shows that $\Sigma_{L(\mathrm{IR})}$ becomes larger and the extent of distribution of the star-forming regions becomes more compact as $L(\mathrm{IR})$ increase. In this plot, our results fill the blank between the sequence of normal galaxies and U/LIRGs, and the transition point of the sequence from normal galaxies to U/LIRGs is at $L(\mathrm{IR}) = 8 \times 10^{10}\ L_\odot$ ($SFR(\mathrm{IR}) = 8.5\ M_\odot \mathrm{yr}^{-1}$), which confirms the implication of Rujopakarn et al. (2011).

The right panel of Figure 5.5 shows a comparison of $SFR(\mathrm{Pa}\alpha)_{\mathrm{corr}}$ and surface densities of SFR (Σ_{SFR}) derived by dividing $SFR(\mathrm{Pa}\alpha)_{\mathrm{corr}}$ by area of a star-forming region;

$$\Sigma_{SFR} \equiv SFR(\mathrm{Pa}\alpha)_{\mathrm{corr}}/(\pi R_{90}(\mathrm{Pa}\alpha)^2). \tag{5.5}$$

The dashed line is the best fit linear relation for U/LIRGs and sub-LIRGs ($SFR(\mathrm{Pa}\alpha)_{\mathrm{corr}} \geq 1.1\ M_\odot\ \mathrm{yr}^{-1}$) including both ours and those in Rujopakarn et al. (2011), where $\log_{10}(\Sigma_{SFR}) = 3.4 \times \log_{10}(SFR) - 3.2$. In this plot, our results fill the blank between the sequence of normal galaxies and U/LIRGs, and the transition point is at $SFR = 7\ M_\odot\ \mathrm{yr}^{-1}$, which is a consistent value with that in the $\Sigma_{L(\mathrm{IR})}$–$L(\mathrm{IR})$ relation.

We also find that there is a large scatter in both figures, different from those of normal galaxies and U/LIRGs in Rujopakarn et al. (2011). Some simulations of galaxy formation suggest that while merging or interacting galaxies in their early stages have extended star-forming regions along their collision interfaces and disks (Saitoh et al., 2009), late-stage mergers have compact and concentrated star-forming regions at their centers (Barnes & Hernquist, 1996). Our results show that LIRGs have a wide range in the extend of distribution of the star-forming regions from less than 1 kpc to over 10 kpc. Considering the fact that all the ULIRGs are mergers (Soifer et al., 2000), there is a possibility that ULIRGs and LIRGs at high luminosity end with compact star-forming regions are at the late-stage in the merging history. On the other hand, sub-LIRGs and LIRGs at low luminosity end with extended star-forming regions may be at first-stage in merging history.

Table 5.2: Sample of Local Luminous Infrared Galaxies

Galaxy Name (1)	Hubble Type (2)	G (3)	M_{20} (4)	R_e (Paα) (kpc) (5)	R_b (K_s) (kpc) (6)	n_b (K_s) (7)	log(B/T) (8)
NGC 23	1	0.63	–2.39	1.10	1.06	1.9 ± 0.03	–0.4
NGC 232	1	0.59	–2.08	0.49	0.46	2.3 ± 0.03	–0.22
IRAS F02437+2122	–5	0.61	–2.50	0.28	0.98	4.6 ± 0.26	–0.43
NGC 1720	2	0.65	–2.60	0.48	0.39	1.8 ± 0.02	–0.73
ESO 557-G002	4	0.54	–2.26	0.65	9.64	19.9 ± 2.1	–0.2
ESO 320-G030	1	0.54	–1.90	0.79	0.49	1.2 ± 0.02	–0.37
MCG −03-34-064 . .	–2	0.62	–2.35	0.24	0.39	1.6 ± 0.03	–0.43
NGC 5135	2	0.60	–2.52	0.77	0.67	1.0 ± 0.02	–0.45
NGC 5257	3	0.48	–1.38	5.27	0.23	1.6 ± 0.2	–1.39
IC 4687	3	0.57	–1.95	0.34	0.31	6.1 ± 0.31	–0.16
ESO 339-G011	3	0.56	–2.34	0.37	0.39	0.6 ± 0.02	–0.77
IC 5063	0	0.58	–2.31	0.45	4.82	5.7 ± 0.08	–0.19
NGC 7130	1	0.53	–1.82	0.46	2.91	6.1 ± 0.32	–0.52
IC 5179	4	0.49	–1.83	2.83	0.23	6.5 ± 0.43	–0.77
ESO 534-G009	2	0.56	–2.20	0.22	0.61	2.6 ± 0.02	–0.21
CGCG 453-062	2	0.55	–2.18	2.03	0.24	1.2 ± 0.15	–0.97
NGC 7591	4	0.64	–2.46	0.40	3.46	4.0 ± 0.04	–0.26
MCG −01-60-022 . .	7	0.60	–2.44	0.64	0.26	1.5 ± 0.08	–0.71
NGC 7771	1	0.57	–2.36	2.17	0.86	0.4 ± 0.01	–0.91
UGC 12915	5	0.64	–2.62	6.55	0.55	1.0 ± 0.01	–0.66

Column (1): Galaxy names. Column (2): Hubble type obtained by HyperLeda database (http://leda.univ-lyon1.fr). Column (3): Gini coefficient. Column (4): Second-order moment of the brightest 20% of the flux of galaxy. Column (5): Effective radius of the distribution of Paα emission. Column (6): Effective radius of the bulge measured in the K_s-band. Column (7): Sérsic index of bulge measured in the K_s band image. Column (8): The ratio of the bulge and total (bulge + disk) luminosity.

5.2 Properties of Bulge

5.2.1 The Sérsic Indices of Bulges

The left panel of Figure 5.6 is the histogram of Sérsic indecies of the bulges, where we use the sample defined in Chapter 4.2.1. Our result shows the bimodal distribution of the Sérsic indices with a separation of $n_b \sim 2.5$, which is consistent with the separation of classical ($n_b \geq 2.2$) and pseudo-bulges ($n_b < 2.2$) in normal galaxies reported in Fisher & Drory (2008). The vertical dotted line, $n_b = 2.2$, is the criteria between the classical and pseudo-bulges (Fisher & Drory, 2008) in the V-band image. claimed that the Sérsic indices measured in the V-band and in the H-band have almost the same value, suggesting that the criteria can also be used in the K_s band images. These results suggest that the properties of bulges of LIRGs are same as those of normal galaxies. Also, Our sample consists of 45% (9/20) classical bulges and 55% (11/20) pseudobulges, suggesting that the fraction of classical bulges in LIRGs is higher than that in normal galaxies, which is 28.5% (Kormendy

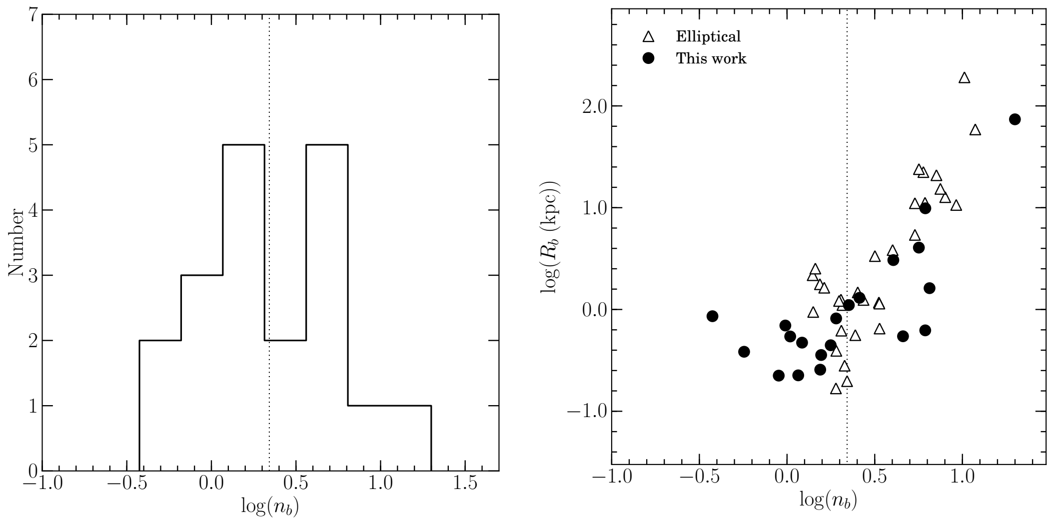

Figure 5.6: Left: Distribution of the Sérsic index of the bulges measured in the K_s-band. The dashed line represents the border of the classical and pseudo-bulge classification shown by V-band study (Fisher & Drory, 2008). Right: Sérsic index and effective radius of the bulges measured in the K_s-band (Circles (triangles) represent pseudo- (classical) bulges). Crosses shows elliptical galaxies taken from Kormendy et al. (2009).

& Kennicutt, 2004). Although the volume of sample is not enough large statistically, our result that LIRGs have larger fraction of classical bulges is consistent with previous works that the classical bulges may be formed through major-merger process (e.g. Kormendy & Kennicutt, 2004; Fisher & Drory, 2008) and that LIRGs may have experienced more major-merger events than normal galaxies (e.g., Sanders & Mirabel, 1996; Wang et al., 2006).

5.2.2 The Size of Bulge

The right panel of Figure 5.6 is a relationship between the Sérsic indices and the sizes of the bulges. The effective radii of the classical bulges increase with increasing Sérsic indices. This is consistent with Fisher & Drory (2008), showing that the properties of bulges of LIRGs are are same as those of normal galaxies.

5.2.3 K_s-band Luminosity

We calculate the bulge-to-total luminosity ratio (B/T) which is obtained from a model profile by the bulge-disk decomposition described in Section 4.2 Chapter 4. Figure 5.7 shows a relationship between the Sérsic indices and B/T ratios, suggesting that the B/T ratios increase with increasing Sérsic indeces. This also suggests that the classical bulges have higher B/T ratios, while the pseudobulges have lower, being consistent with the properties of normal galaxies (Fisher & Drory, 2008).

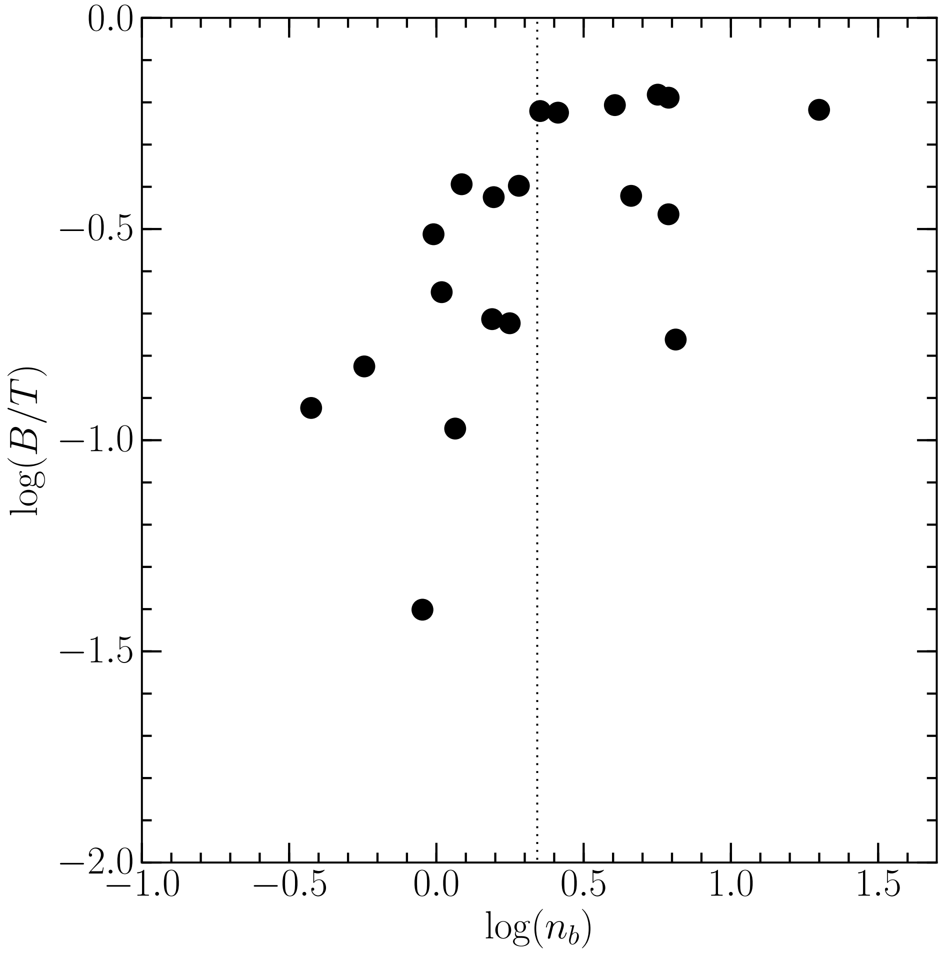

Figure 5.7: Relationship between Sérsic indices and bulge-to-total luminosity ratio (B/T) obtained from a model profile by the bulge-disk decomposition in the K_s-band image. The dotted line represents the border of the classical and pseudo-bulge classification shown by V-band study (Fisher & Drory, 2008).

From these results, it is suggested that the properties of bulges in LIRGs are almost the same as those in normal galaxies except for the fraction of classical and pseudo-bulges.

5.3 Distribution of Star-Forming Region

To understand a relationship between star formation activities and type of bulges, we derive the extent of distribution of star-forming regions in the Paα narrow-band images. The extensions (R_e(Paα)) are defined to be a half light radii in Paα emission line images, where the results are shown in Table 5.2.

In order to understand the extent of distribution of star-forming activities, we normalize the extent of distribution of the star-forming regions by the sizes of bulges (R_e(Paα)$/R_b$). Figure 5.8 shows a relationship between the Sérsic indices of the bulges and R_e(Paα)$/R_b$. We find that the normalized extent of distribution of the star-forming regions decrease with increasing Sérsic indices. Also, we find that the extents of distribution of the star-forming regions become equal to the sizes of the bulges at $n_b \sim 2.2$, which is the point to separate classical and pseudo-bulges defined by Fisher & Drory (2008). These results suggest that galaxies with classical bulges have compact star-forming regions concentrated within the bulges, while those with pseudobulges have extend star-forming regions beyond the bulge, possibly along their spiral arms.

Classical bulges are expected to have experienced major-merging events to lose angular momentum and have similar properties to elliptical galaxies (Kormendy & Kennicutt, 2004). Theoretically, gas tends to be concentrated to the central region of the galaxy after the major-merging events (Naab & Trujillo, 2006). Also, there is a simulation which forms a classical bulge with inflow of cold gas toward a center of a galaxy (Sales et al., 2012), inducing extreme star formation at the central region of the galaxy. Our result, that the star formation is concentrated at the center of the galaxy in the classical bulge, is consistent with such theoretical simulations. On the other hand, pseudobulges are expected to be formed by minor-merging events or secular evolution in which a galaxy evolves over a long time without major-merging or strong-interacting events (e.g. Kormendy & Kennicutt, 2004). In these processes, pseudobulges evolve with outer disks, spiral arms, and barred structures, and starbursts occur along their arms and bar-ends, therefore it is expected that star-forming regions are spread beyond the size of bulge structures. Our result, where the galaxies with pseudobulges have extend star-forming regions beyond their bulges, is consistent with such theoretical predictions. From above discussions, we suggest that classical and pseudo-bulges may have formed by different mechanism as predicted by theoretical models for formation of classical and pseudo-bulges.

In this senario, considering that LIRGs are gas rich galaxies, the classical bulges in LIRGs with compact star-forming regions may be a late-stage merger. Numerical simulations suggest that a merger proceed roughly as follows; (1) Interacting/merging phase; from the phase of pre-merger infall to apocentre/turnaround, (2) Coalesecence phase; from phase of final merger to just after nuclear coalescence, and (3) After Coalescence phase (e.g., Hopkins et al., 2013). In this scenario, late-stage means from final merger phase to after coalescence phase. Lotz et al. (2008) claimed that enhanced star formation peaks after the strong morphological disturbances (phase (1)) and lasts significantly longer than the interacting/merging phase (about 500 Myr after coalesence), during which the star formation is enhanced by more than 10 times (e.g., Lotz et al., 2008; Teyssier et al., 2010). Also, Hopkins et al. (2013) suggests that extent of distribution of star forming regions within a galaxy become small (a few kpc or less). These pictures are consistent with our result that the classical bulges have compact star-forming regions. On the other hand, pseudobulges are isolate galaxies or minor-merger galaxies, where the effect of merger events to growth of bulges (increasing the Sérsic indices) are sufficiently small.

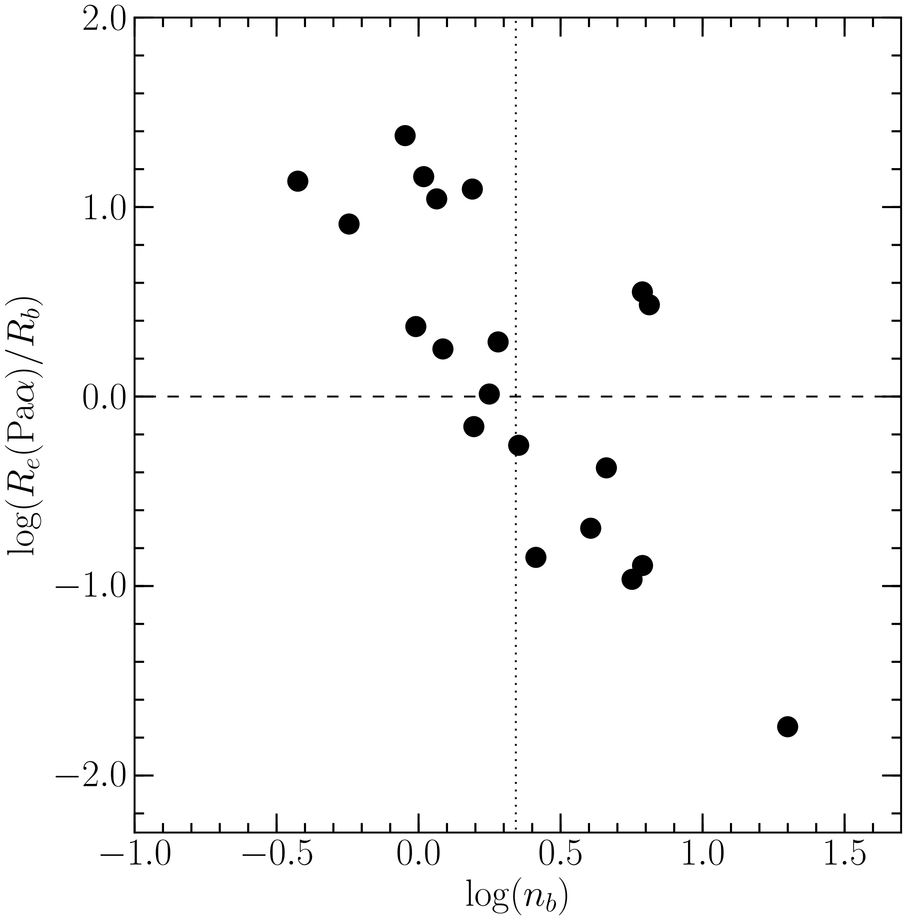

Figure 5.8: Comparision between the Sérsic index of bulge and the distribution measured by which the half light radius of Paα emission line region divided by the effective radius of bulge. The horizontal dashed-line is the value of the distribution is 1.0 which means the effective radius of bulge and the effective radius of star forming region is almost equal. The vertical dashed-line is the threshold ($n_b = 2.2$) of the empirical classification between classical or pseudo-bulge determined by using 77 local normal galaxies (Fisher & Drory, 2008). There is a tendency that high Sérsic index of bulge represents compact star forming region while low Sérsic index of bulge represents extend star forming region.

Chapter 6

Conclusion

6.1 Summary of Results

6.1.1 Star Formation Surface Densities of LIRGs

We have observed 38 galaxy system listed in *IRAS* RBGS catalog in Paα with narrow-band imaging (cz = 2800–8100 km s^{-1}, L(IR) = 4.5×10^{10}–6.5×10^{11} $L_{\odot}$) using ANIR on the miniTAO 1.0 m telescope, installed at the summit of Co. Chajnantor in northern Chile. We have estimated Paα fluxes from narrow-band images with our newly developed flux calibration method, and find that $SFR(\mathrm{Pa}\alpha)_{\mathrm{corr}}$ which is SFR obtained from Paα luminosity corrected for effect of dust extinction with balmer decrement method (Hβ/Hα) shows good agreement with SFR(IR) which is SFR estimated from total infrared luminoisity. This result suggests that Paα with dust-extinction correction is sufficient for estimating SFR of whole the galaxy. However, some galaxies have large differences between the $SFR(\mathrm{Pa}\alpha)_{\mathrm{corr}}$ and the SFR(IR), which may be caused by effect of AGNs, strong dust-extinction, or IR cirrus component. We also obtain surface densities of L(IR) ($\Sigma_{L(\mathrm{IR})}$) and SFR obtained from Paα (Σ_{SFR}) for individual galaxies by measuring extension of distribution of star forming regions within a galaxy with Paα emission line. The range of $SFR(\mathrm{Pa}\alpha)_{\mathrm{corr}}$ in our sample (from 0.6 to 104 $M_{\odot}$ yr^{-1}) fill the blank of the range of SFR in previous works. We find that most of the samples follow a sequence of local U/LIRGs on the $L(\mathrm{IR})$-$\Sigma_{L(\mathrm{IR})}$ and $SFR(\mathrm{Pa}\alpha)_{\mathrm{corr}}$-$\Sigma_{SFR}$ plane. We have found that a transition of the sequence from normal galaxies to U/LIRGs is seen at L(IR) = 8×10^{10}. Also, we find that there is a large scatter in physical size of distribution of star forming regions, different from those of normal galaxies or ULIRGs. Considering the fact that most of U/LIRGs are merging or interacting galaxies, this scatter may be caused by some strong external factors such as interacting/merging or may reflect differences of their merging stage.

6.1.2 Bulge Properies in LIRGs

We present properties of two types of bulges (classical and pseudo- bulges) in 20 LIRGs observed with the Paα survey. To classify the two types of bulges, we remove 18 irregular galaxies from our sample and perform a two-demensional bulge-disk decomposition analysis with a combination of a Sérsic profile as the bulge component and an exponential

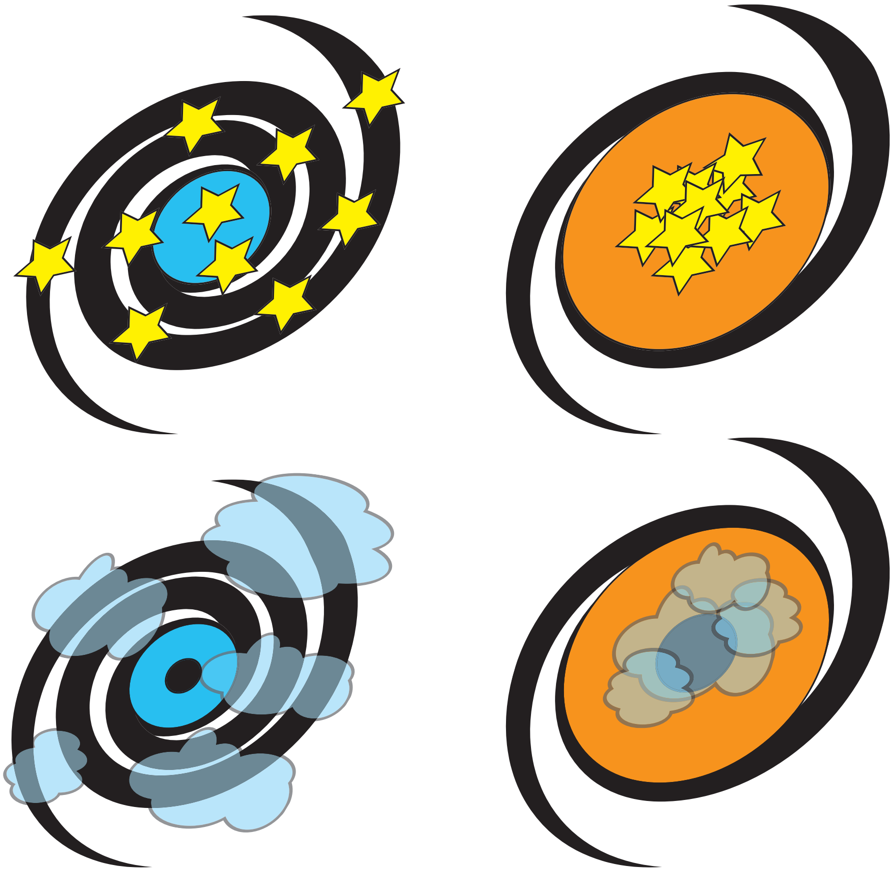

Figure 6.1: Top: Cartoon of galaxies with pseudobulge (left) and classical bulge (right). The stars show the star-forming regions observed by Paα emission line. Our result in Paα survey of LIRG shows that pseudobulges have extended star-forming regions beyond the bulge, and classical bulges have compact star-forming regions concentrated at the center of galaxy. Bottom: Cartoon of pseudobulge (left) and classical bulge (right) with black holes and molecular gas.

profile as the disk component using the K_s-band images. We find a bimodal distribution of the Sérsic indices with a separation of $n_b \sim 2.5$, which is consistent with the separation of classical ($n_b \geq 2.2$) and pseudo-bulges ($n_b < 2.2$) in normal galaxies reported in Fisher & Drory (2008) and the physical sizes and B/T ratios increasing with Sérsic indices. These results suggest that the properties of bulges in LIRGs are same as those of normal galaxies. Also, we measure extent of distribution of star-forming regions in Paα emission line images, and find that the extent normalized by the bulge sizes correlate with Sérsic indices of bulges, suggesting that pseudobulges have extended star-forming regions beyond the bulges, while classical bulges have compact star-forming regions concentrated at the centers of the galaxies (Top illustrations in Figure 6.1). These results suggest that there are different formation scenarios at work in classical and pseudo-bulges. Classical bulges are expected to have experienced major-merging events to lose angular momentum and have similar properties to elliptical galaxies while pseudobulges to be formed by minor-merging events or secular evolution in which a galaxy evolves over a long time without major-merging or strong-interacting events. In this scenario, considering that LIRGs are gas rich galaxies, the classical bulges in LIRGs with compact star-forming regions may be late-stage mergers, and pseudobulges are isolate galaxies or minor-merger galaxies, where the effect of merger events to growth of bulges (increasing the Sérsic indices) are sufficiently small.

6.2 Formation of Bulges and Black Holes

Kormendy et al. (2011) find that the correlation between masses of SMBs ($M_\bullet$) and velocity dispersions of a classical bulges have a tight correlation, while those of pseudobulges do not. These results suggest that growth of the SMBs and the galaxy is controlled by a same global process where large amounts of gas fall into the center of the galaxy via rapid feeding with major-merger process, and the other is that the growth of the black hole is controlled by a local process that feed gas from $\sim 10^2$ pc stochastically, and independent or have a weak connection to the growth of the mass of host galaxies with secular evolution. Therefore, they claim that there are two fundamentally different feeding mechanisms for a black hole. To verify observationally the hypothesis of the two types of formation scenario of SMBs and bulges, it is necessary to observe in the middle of building bulges with molecular gas, because it is considered that the classical bulges have concentrated molecular gas at the centers of the galaxies, while pseudobulges have extended molecular gas beyond bulges (Bottom illustrations in Figure 6.1).

From the Kennicutt–Schmidt (KS) law (Kennicutt, 1998), an empirical power-law relation between surface densities of SFR ($\Sigma_{\rm SFR}$) and molecular gas ($\Sigma_{\rm H2}$), amount of molecular gas is approximately proportional to the star formation rate, suggesting that molecular gas clouds exists around star-forming regions. Therefore, our result, classical bugles have compact star-forming regions concentrated at the centers of the galaxies, suggests that large amounts of molecular gas clouds also exist at their centers, and these molecular gas clouds have potential to feed not only the bulges but also the black hole. Also, our result, pseduobulges have extended star-forming regions beyond the bulges, possibly along their spiral arms, suggests that molecular gas clouds exist mainly beyond the bulges, and these molecular gas clouds may mainly to feed disks and pseudobulge components but not black

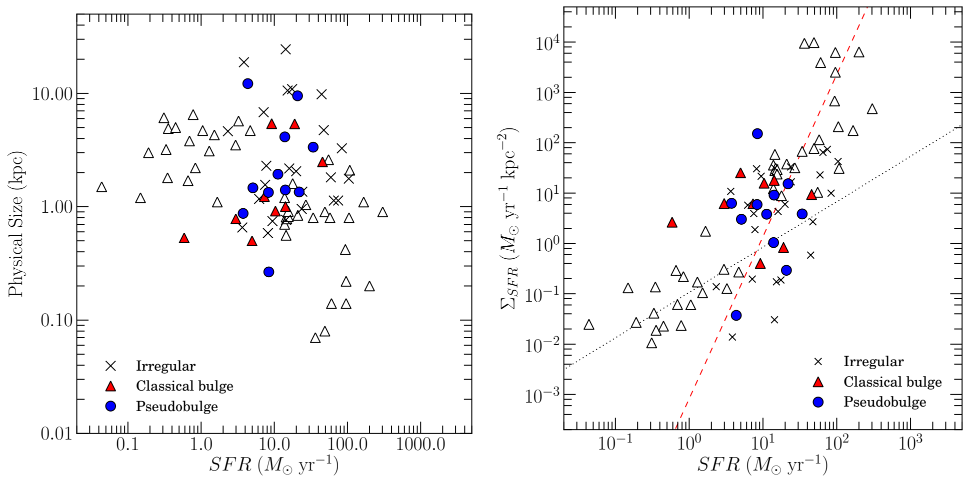

Figure 6.2: Left: Comparison of SFRs derived from Paα luminosities and the extent of distribution of star-forming regions described in Figure 5.4. Blank triangles represent normal galaxies and U/LIRGs derived from Rujopakarn et al. (2011), filled triangles classical bulges and filled circles are pseudobulges, and crosses irregular galaxies. Right: Comparison of SFRs derived from Paα luminosities and SFR surface densities. The dotted line represent the sequence of normal galaxies (Rujopakarn et al., 2011), while dashed line the sequence of U/LIRGs, which is the best fit relation using the sample from this work and Rujopakarn et al. (2011). These are same as Figure 5.5

holes. In this case, the growth of black holes and pseudobulges have a weak connection. These results may support the hypothesis of formation of SMBs and bulges.

6.3 Study of Morphogenesis with LIRGs

In the Hubble-Sandage de Vaucouleurs classifications, the bulge is important component to classify the morphology of galaxies. Therefore the knowledge of the bulge formation is key for understanding to the morphogenesis of galaxies.

To form the clasical bulges, it is necessary to remove their angular momentum from their central region and the mechanism is considered to be strong galactic major-merger and/or interaction. Classical bulges having compact star-forming regions, our results are consistent with the formation scenario of classical bulges with major-merger process. Also, considering that LIRGs are gas rich galaxies, the classical bulges in LIRGs with compact star-forming regions are expected to be a late-stage merger. These properties are similar to local ULIRGs, which are considered to be in the sequence of U/LIRGs (starburst sequence) and have very compact and concentrated at central regions (e.g., Soifer et al., 2000; Díaz-Santos et al., 2010; Rujopakarn et al., 2011; Alonso-Herrero et al., 2012), suggesting that the classical bulges in LIRGs are expected to be in the starburst sequence. On the other hand, pseudobulges having extended star-forming regions beyond the bulges, our results for pseudobulges are also consistent with the formation senario of pseudobulges with secular evolution. These properties are similar to local normal galaxies, which are considered to be in the sequecence of normal galaxies and extended star-forming regions along the spiral arms, suggesting that the pseudobulges in LIRGs are expected to be in the sequecence of normal galaxies.

To check above hypothesis, we re-plot Figure 5.4 and Figure 5.5 with bulge classification. In the right panel of the Figure 6.2, the classical bulges, which is considered to be in the starburst sequence, are expected to be located above the sequence of normal galaxies. However, some of the classical bulges are seem to be on the sequence of normal galaxies, which are caused by either having a weak SFR or extended distribution of star-forming region. The lowest Σ_{SFR} in classical bulges are IC 5179, which has HII clumpy knots at the southern part of its arms, and the next is NGC 7591, which has extended Paα regions, in the right panel of Figure 6.2. They also have the largest extent of Paα regions in the left panel of Figure 6.2. Therefore, these these outliners are mainly prduced by the extent of star-forming regions, which may caused by minor-merger or some additional external factor after establishment of the classical bulges. Also, there is a potential that the SFR of these galaxies goes weak. Lotz et al. (2008) suggest that enhanced star formation lasts about 500 Myr after coalesence and the star-forming activities are weaken rapidly after that. Under this assumption, these galaxies are late-stage merger after coalesence. On the other hand, the pseudobulges, which is considered to be in the sequence of normal galaxies, are expected to be located in the sequence of normal galaxies in the rigth panel of Figure 6.2. However, some of the galaxies are seem to be located above the sequence of normal galaxies. The highest Σ_{SFR} in pseudobulge is MCG −03-34-064, which is the only Sy1 galaxy in the sample where the bulge profile can be estimated, suggesting that the extent of distribution of star-forming regions may be underestimated due to AGN. It is difficult for these results to be explained by a model of secular evolution. These galaxies might be enhanced their star-forming activities by minor-merger process.

Bibliography

Alonso-Herrero, A., Ward, M. J., Aragon-Salamanca, A., & Zamorano, J. 1999, MNRAS 302, 561

Alonso-Herrero, A., Engelbracht, C. W., Rieke, M. J., Rieke, G. H., & Quillen, A. C. 2001, ApJ 546, 952

Alonso-Herrero, A., Rieke, G. H., Rieke, M. J., & Scoville, N. Z. 2002, AJ 124, 166

Alonso-Herrero, A., Rieke, G. H., Rieke, M. J., et al. 2006, ApJ 650, 835 ; A06

Alonso-Herrero, A., García-Marín, M., Monreal-Ibero, A., et al. 2009, A&A 506, 1541

Alonso-Herrero, A., Pereira-Santaella, M., Rieke, G. H., & Rigopoulou, D. 2012, ApJ 744, 2

Ann, H.-B., & Kim, J.-M. 1996, Journal of Korean Astronomical Society, 29, 255

Antonucci, R. R. J., & Miller, J. S. 1985, ApJ 297, 621

Agüero, E. L., Paolantonio, S., Günthardt, G. 2000, AJ 119, 94

Athanassoula, E. 2005, MNRAS 358, 1477

Ballero, S. K., Matteucci, F., Origlia, L., & Rich, R. M. 2007, A&A 467, 123

Barnes, J. E., & Hernquist, L. E. 1991, ApJL 370, L65

Barnes, J. E., & Hernquist, L. 1996, ApJ 471, 115

Becklin, E. E., Frogel, J. A., Kleinmann, D. E., et al. 1971, ApJL 170, L15

Becklin, E. E., & Neugebauer, G. 1972, BAAS 4, 224

Burbidge, G. R., & Stein, W. A. 1970, ApJ 160, 573

Chaboyer, B., & Vader, J. P. 1991, PASP 103, 35

Colina, L., Sparks, W. B., & Macchetto, F. 1991, ApJ 370, 102

Colina, L., Alberdi, A., Torrelles, J. M., Panagia, N., & Wilson, A. S. 2001, ApJL 553, L19

Combes, F. 2009, Galaxy Evolution: Emerging Insights and Future Challenges, 419, 31

Calzetti, D., Armus, L., Bohlin, R. C., et al. 2000, ApJ 533, 682

Calzetti, D., Kennicutt, R. C., Engelbracht, C. W., et al. 2007, ApJ 666, 870

Calzetti, D., 2013, arXiv:1208.2997v1, in press

Cardelli, J. A., Clayton, G. C., & Mathis, J. S. 1989, ApJ 345, 245

Caputi, K. I., Lagache, G., Yan, L., et al. 2007, ApJ 660, 97

Condon, J. J., Huang, Z.-P., Yin, Q. F., & Thuan, T. X. 1991, ApJ 378, 65

Condon, J. J., Helou, G., Sanders, D. B., & Soifer, B. T. 1993, AJ 105, 1730

Corbett, E. A., Kewley, L., Appleton, P. N., et al. 2003, ApJ 583, 670

Cotini, S., Ripamonti, E., Caccianiga, A., et al. 2013, MNRAS 431, 2661

Cutri, R. M., & McAlary, C. W. 1985, ApJ 296, 90

Daddi, E., Elbaz, D., Walter, F., et al. 2010, ApJL 714, L118

Davies, R. I., Tacconi, L. J., & Genzel, R. 2004, ApJ 602, 148

de Vaucouleurs, G., de Vaucouleurs, A., Corwin, H. G., Jr., et al. 1991, S&T 82, 621

Di Matteo, T., Springel, V., & Hernquist, L. 2005, Nature 433, 604

Díaz-Santos, T., Charmandaris, V., Armus, L., et al. 2010, ApJ 723, 993

Dopita, M. A., Pereira, M., Kewley, L. J., & Capaccioli, M. 2002, ApJS 143, 47

Driver, S. P., Allen, P. D., Liske, J., & Graham, A. W. 2007, ApJL 657, L85

Elmegreen, B. G., & Elmegreen, D. M. 2005, ApJ 627, 632

Elmegreen, D. M., Elmegreen, B. G., Ravindranath, S., & Coe, D. A. 2007, ApJ 658, 763

Falcke, H., Rieke, M. J., Rieke, G. H., Simpson, C., & Wilson, A. S. 1998, ApJL 494, L155

Falcón-Barroso, J., Peletier, R. F., & Balcells, M. 2002, MNRAS 335, 741

Fernández, X., van Gorkom, J. H., Schweizer, F., & Barnes, J. E. 2010, AJ 140, 1965

Ferrarese, L., & Merritt, D. 2000, ApJL 539, L9

Fisher, D. B., & Drory, N. 2008, AJ 136, 773

Fisher, D. B., & Drory, N. 2010, ApJ 716, 942

Fisher, D. B., Bolatto, A., Drory, N., et al. 2013, ApJ 764, 174

Förster Schreiber, N. M., Genzel, R., Lehnert, M. D., et al. 2006, ApJ 645, 1062

Gadotti, D. A. 2009, MNRAS 393, 1531

Gebhardt, K., Bender, R., Bower, G., et al. 2000, ApJL 539, L13

Genzel, R., Weitzel, L., Tacconi-Garman, L. E., et al. 1995, ApJ 444, 129

Genzel, R., Tacconi, L. J., Eisenhauer, F., et al. 2006, Nature 442, 786

Graham, A. W. 2001, AJ 121, 820

Guedes, J., Mayer, L., Carollo, M., & Madau, P. 2013, ApJ 772, 36

Gültekin, K., Richstone, D. O., Gebhardt, K., et al. 2009, ApJ 698, 198

Goto, T., Takagi, T., Matsuhara, H., et al. 2010, A&A 514, A6

Grimes, J. P., Heckman, T., Hoopes, C., et al. 2006, ApJ 648, 310

Hill, G. J., Goodrich, R. W., & Depoy, D. L. 1996, ApJ 462, 163

Hirashita, H., Buat, V., & Inoue, A. K. 2003, A&A 410, 83

Hough, J. H., Brindle, C., Axon, D. J., Bailey, J., & Sparks, W. B. 1987, MNRAS 224, 1013

Ho, L. C., Filippenko, A. V., & Sargent, W. L. W. 1997, ApJS 112, 315

Hopkins, A. M., & Beacom, J. F. 2006, ApJ 651, 142

Hopkins, P. F., Hernquist, L., Cox, T. J., et al. 2006, ApJS 163, 1

Hopkins, P. F., Bundy, K., Croton, D., et al. 2010, ApJ 715, 202

Hopkins, P. F., Cox, T. J., Hernquist, L., et al. 2013, MNRAS 430, 1901

Hubble, E. P. 1926, ApJ 64, 321

Hubble, E. P. 1927, The Observatory, 50, 276

Hummer, D. G., & Storey, P. J. 1987, MNRAS 224, 801

Inglis, M. D., Brindle, C., Hough, J. H., et al. 1993, MNRAS 263, 895

Inoue, S., & Saitoh, T. R. 2012, MNRAS 422, 1902

Iono, D., Yun, M. S., & Ho, P. T. P. 2005, ApJS 158, 1

Iono, D., Saito, T., Yun, M. S., et al. 2013, PASJ 65, L7

Jablonka, P., Gorgas, J., & Goudfrooij, P. 2007, A&A 474, 763

Jenkins, L. P., Roberts, T. P., Ward, M. J., & Zezas, A. 2005, MNRAS 357, 109

Joseph, R. D., Meikle, W. P. S., Robertson, N. A., & Wright, G. S. 1984, MNRAS 209, 111

Kennicutt, R. C., Jr. 1998, ARA&A 36, 189

Kennicutt, R. C., Jr., Calzetti, D., Walter, F., et al. 2007, ApJ 671, 333

Kennicutt, R. C., Jr., Hao, C.-N., Calzetti, D., et al. 2009, ApJ 703, 1672

Kewley, L. J., Geller, M. J., Jansen, R. A., & Dopita, M. A. 2002, AJ 124, 3135

Kim, D.-C., Veilleux, S., & Sanders, D. B. 1998, ApJ 508, 627

Kim, D., Im, M., & Kim, M. 2010, ApJ 724, 386

Kleinmann, D. E., & Low, F. J. 1970, ApJL 159, L165

Kleinmann, D. E., & Low, F. J. 1970, ApJL 161, L203

Kormendy, J., & Gebhardt, K. 2001, 20th Texas Symposium on relativistic astrophysics, 586, 363

Kormendy, J., & Kennicutt, R. C., Jr. 2004, ARA&A 42, 603

Kormendy, J., & Fisher, D. B. 2005, Revista Mexicana de Astronomia y Astrofisica Conference Series, 23, 101

Kormendy, J., Fisher, D. B., Cornell, M. E., & Bender, R. 2009, ApJS 182, 216

Kormendy, J., Bender, R., & Cornell, M. E. 2011, Nature 469, 374

Komugi, S., Sofue, Y., Nakanishi, H., Onodera, S., & Egusa, F. 2005, PASJ 57, 733

Komugi, S., Tateuchi, K., Motohara, K., et al. 2012, ApJ 757, 138

Konishi, M., Motohara, K., Tateuchi, K., et al. 2013, PASJ, accepted

Koss, M., Mushotzky, R., Veilleux, S., & Winter, L. 2010, ApJL 716, L125

Koss, M., Mushotzky, R., Baumgartner, W., et al. 2013, ApJL 765, L26

Lada, C. J., Forbrich, J., Lombardi, M., & Alves, J. F. 2012, ApJ 745, 190

Lai, O., Rouan, D., & Alloin, D. 1999, European Southern Observatory Conference and Workshop Proceedings, 56, 555

Lauberts, A. 1982, Garching: European Southern Observatory (ESO), 1982,

Lecureur, A., Hill, V., Zoccali, M., et al. 2007, A&A 465, 799

Levenson, N. A., Weaver, K. A., Heckman, T. M., Awaki, H., & Terashima, Y. 2005, ApJ 618, 167

Liu, G., Calzetti, D., Kennicutt, R. C., Jr., et al. 2013, ApJ 772, 27

Liu, G., Calzetti, D., Hong, S., et al. 2013, ApJL 778, LL41

Lord, S. D. 1992, NASA Technical Memorandum, 103957

Lonsdale, C. J., Persson, S. E., & Matthews, K. 1984, ApJ 287, 95

Lotz, J. M., Primack, J., & Madau, P. 2004, AJ 128, 163

Lotz, J. M., Jonsson, P., Cox, T. J., & Primack, J. R. 2008, MNRAS 391, 1137

Lumsden, S. L., Heisler, C. A., Bailey, J. A., Hough, J. H., & Young, S. 2001, MNRAS 327, 459

Lutz, D. 1991, Dynamics of Galaxies and Their Molecular Cloud Distributions, 146, 312

Magorrian, J., Tremaine, S., Richstone, D., et al. 1998, AJ 115, 2285

Malmquist, K. G. 1925, The Observatory, 48, 142

Mauder, W., Weigelt, G., Appenzeller, I., & Wagner, S. J. 1994, A&A 285, 44

McWilliam, A., Matteucci, F., Ballero, S., et al. 2008, AJ 136, 367

Miles, J. W., Houck, J. R., & Hayward, T. L. 1994, ApJL 425, L37

Mirabel, I. F. 1983, ApJL 270, L35

Minezaki, T., Kato, D., Sako, S., et al. 2010, Proc. SPIE 7733,

Moorthy, B. K., & Holtzman, J. A. 2006, MNRAS 371, 583

Morganti, R., Oosterloo, T., & Tsvetanov, Z. 1998, AJ 115, 915

Morganti, R., Holt, J., Saripalli, L., Oosterloo, T. A., & Tadhunter, C. N. 2007, A&A 476, 735

Motohara, K., Aoki, T., Sako, S., et al. 2008, Proc. SPIE 7012,

Motohara, K., Mitani, N., Sako, S., et al. 2008, Proc. SPIE 7014,

Motohara, K., Konishi, M., Toshikawa, K., et al. 2010, Proc. SPIE 7735,

Motohara, K. M., Aoki, T., Asano, K., et al. 2011, Revista Mexicana de Astronomia y Astrofisica Conference Series, 41, 83

Murphy, T. W., Jr., Soifer, B. T., Matthews, K., Kiger, J. R., & Armus, L. 1999, ApJL 525, L85

Naab, T., & Trujillo, I. 2006, MNRAS 369, 625

Naim, A., Lahav, O., Buta, R. J., et al. 1995, MNRAS 274, 1107

Noguchi, M. 1999, ApJ 514, 77

Okamoto, T. 2013, MNRAS 428, 718

Olsson, E., Aalto, S., Thomasson, M., & Beswick, R. 2010, A&A 513, A11

Paturel G., Petit C., Prugniel P., Theureau G., Rousseau J., Brouty M., Dubois P., Cambrésy L., 2003, A&A, 412, 45

Peterson, B. W., Appleton, P. N., Helou, G., et al. 2012, ApJ 751, 11

Peng, C. Y., Ho, L. C., Impey, C. D., & Rix, H.-W. 2002, AJ 124, 266

Peng, C. Y., Ho, L. C., Impey, C. D., & Rix, H.-W. 2010, AJ 139, 2097

Petrosian, V. 1976, ApJL 209, L1

Piqueras López, J., Colina, L., Arribas, S., & Alonso-Herrero, A. 2013, arXiv:1304.0894

Rees, M. J., Silk, J. I., Werner, M. W., & Wickramasinghe, N. C. 1969, Nature 223, 788

Richter, O.-G., Sackett, P. D., & Sparke, L. S. 1994, AJ 107, 99

Rieke, G. H., & Low, F. J. 1972, ApJL 176, L95

Rieke, G. H., Alonso-Herrero, A., Weiner, B. J., et al. 2009, ApJ 692, 556

Roche, N. D. 2007, RMXAA, 43, 179

Rodríguez-Zaurín, J., Arribas, S., Monreal-Ibero, A., et al. 2011, A&A 527, A60

Rothberg, B., & Joseph, R. D. 2004, AJ 128, 2098

Rujopakarn, W., Eisenstein, D. J., Rieke, G. H., et al. 2010, ApJ 718, 1171

Rujopakarn, W., Rieke, G. H., Eisenstein, D. J., & Juneau, S. 2011, ApJ 726, 93

Rujopakarn, W., Rieke, G. H., Weiner, B. J., et al. 2013, ApJ 767, 73

Rush, B., Malkan, M. A., & Spinoglio, L. 1993, ApJS 89, 1

Saito, T., Iono, D., Yun, M., et al. 2013, Astronomical Society of the Pacific Conference Series, 476, 287

Saitoh, T. R., Daisaka, H., Kokubo, E., et al. 2009, PASJ 61, 481

Sales, L. V., Navarro, J. F., Theuns, T., et al. 2012, MNRAS 423, 1544

Sanders, D. B., & Mirabel, I. F. 1996, ARA&A 34, 749

Sanders, D. B., Soifer, B. T., Elias, J. H., et al. 1988, ApJ 325, 74

Sanders, D. B., Mazzarella, J. M., Kim, D.-C., Surace, J. A., & Soifer, B. T. 2003, AJ 126, 1607

Scoville, N. Z., Evans, A. S., Thompson, R., et al. 2000, AJ 119, 991

Scoville, N. Z., Polletta, M., Ewald, S., et al. 2001, AJ 122, 3017

Schweizer, F., & Seitzer, P. 2007, AJ 133, 2132

Sheen, Y.-K., Jeong, H., Yi, S. K., et al. 2009, AJ 138, 1911

Skrutskie, M. F., Cutri, R. M., Stiening, R., et al. 2006, AJ 131, 1163

Stritzinger, M., Hamuy, M., Suntzeff, N. B., et al. 2002, AJ 124, 2100

Soifer, B. T., Neugebauer, G., & Houck, J. R. 1987, ARA&A 25, 187

Soifer, B. T., & Neugebauer, G. 1991, AJ 101, 354

Soifer, B. T., Neugebauer, G., Matthews, K., et al. 2000, AJ 119, 509

Soifer, B. T., Neugebauer, G., Matthews, K., et al. 2001, AJ 122, 1213

Soifer, B. T., Bock, J. J., Marsh, K., et al. 2003, AJ 126, 143

Spinoglio, L., Malkan, M. A., Rush, B., Carrasco, L., & Recillas-Cruz, E. 1995, ApJ 453, 616

Spergel, D. N., Verde, L., Peiris, H. V., et al. 2003, ApJS 148, 175

Springel, V., & Hernquist, L. 2005, ApJL 622, L9

Tacconi, L. J., Genzel, R., Neri, R., et al. 2010, Nature 463, 781

Tanabé, T., Motohara, K., Tateuchi, K., et al. 2013, PASJ 65, 55

Tateuchi, K., Motohara, K., Konishi, M., et al. 2012a, Publication of Korean Astronomical Society, 27, 297

Tateuchi, K., Motohara, K., Konishi, M., et al. 2012b, Proc. SPIE 8446,

Tateuchi, K., Motohara, K., Konishi, M., et al. 2013, Astronomical Society of the Pacific Conference Series, 476, 301

Tateuchi, K., Motohara, K., Konishi, M., et al. 2015, accepted for publication in ApJS.

Teyssier, R., Chapon, D., & Bournaud, F. 2010, ApJL 720, L149

Thomas, H. C., Alexander, P., Clemens, M. S., et al. 2004, MNRAS 351, 362

Thomas, D., & Davies, R. L. 2006, MNRAS 366, 510

Toomre, A., & Toomre, J. 1972, ApJ 178, 623

Toomre, A. 1977, Evolution of Galaxies and Stellar Populations, 401

Totani, T., Takeuchi, T. T., Nagashima, M., Kobayashi, M. A. R., & Makiya, R. 2011, PASJ 63, 1181

Tran, H. D. 2001, ApJL 554, L19

Tremaine, S., Gebhardt, K., Bender, R., et al. 2002, ApJ 574, 740

Treyer, M., Schiminovich, D., Johnson, B. D., et al. 2010, ApJ 719, 1191

van den Broek, A. C., van Driel, W., de Jong, T., et al. 1991, A&AS 91, 61

Väisänen, P., Rajpaul, V., Zijlstra, A. A., Reunanen, J., & Kotilainen, J. 2012, MNRAS 420, 2209

Veilleux, S., Kim, D.-C., Sanders, D. B., Mazzarella, J. M., & Soifer, B. T. 1995, ApJS 98, 171

Véron-Cetty, M.-P., & Véron, P. 2006, A&A 455, 773

Vorontsov-Vel'Yaminov, B. A., & Arkhipova, V. P. 1974, Morphological catalogue of galaxies., 5 (1974), 0

Wang, J. L., Xia, X. Y., Mao, S., et al. 2006, ApJ 649, 722

Wilson, A. S., Helfer, T. T., Haniff, C. A., & Ward, M. J. 1991, ApJ 381, 79

West, R. M. 1976, A&A 46, 327

Yoshii, Y., Doi, M., Handa, T., et al. 2002, 8th Asian-Pacific Regional Meeting, Volume II, 35

Yoshii, Y., Aoki, T., Doi, M., et al. 2010, Proc. SPIE 7733,

Yuan, T.-T., Kewley, L. J., & Sanders, D. B. 2010, ApJ 709, 884

Zoccali, M., Lecureur, A., Barbuy, B., et al. 2006, A&A 457, L1

Appendix A

Transmittance

Paα emission lines, convolved with atmospheric transmittance curve, are shown with the thick solid line. The solid-thin line represents the atmospheric transmittance calculated by ATRAN. The dashed line represents an intrinsic Paα line profile without atmospheric absorption. The σ of the intrinsic profile is assumed to be 150 (km s^{-1}).

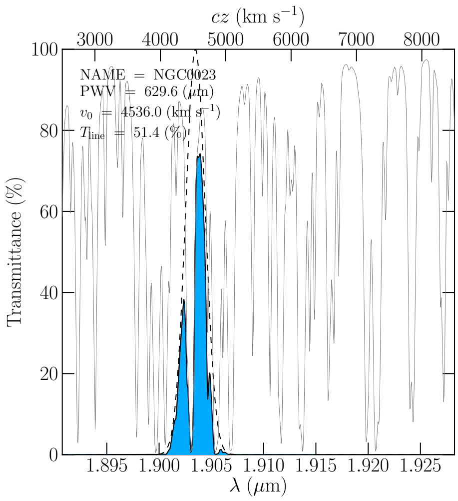

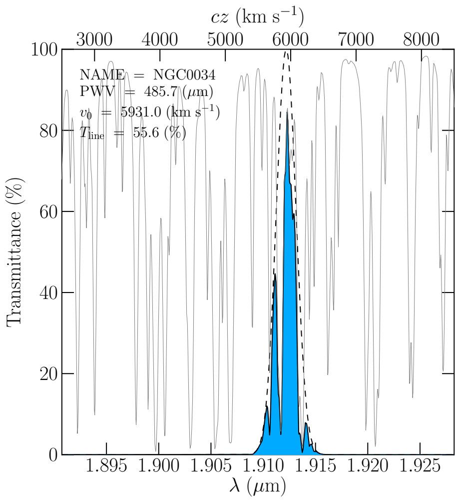

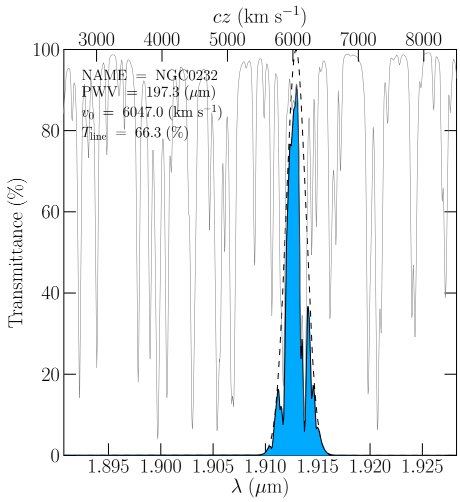

cz (km s^{-1})
NAME = NGC0232
PWV = 197.3 (μm)
v_0 = 6047.0 (km s^{-1})
$T_{\rm line}$ = 66.3 (%)
Transmittance (%)
λ (μm)

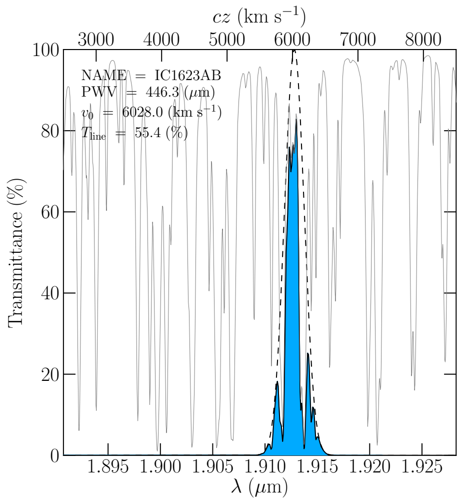

cz (km s^{-1})
NAME = IC1623AB
PWV = 446.3 (μm)
v_0 = 6028.0 (km s^{-1})
$T_{\rm line}$ = 55.4 (%)
Transmittance (%)
λ (μm)

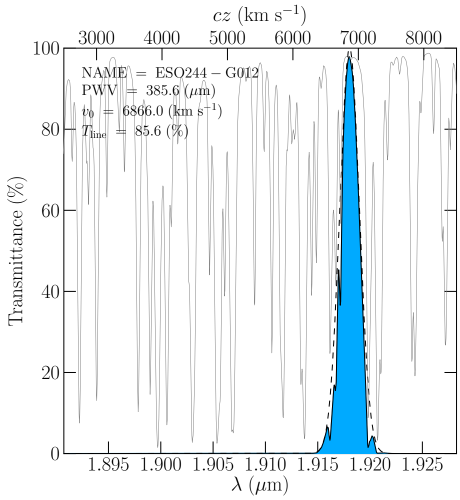

cz (km s^{-1})
NAME = ESO244 − G012
PWV = 385.6 (μm)
v_0 = 6866.0 (km s^{-1})
$T_{\rm line}$ = 85.6 (%)
Transmittance (%)
λ (μm)

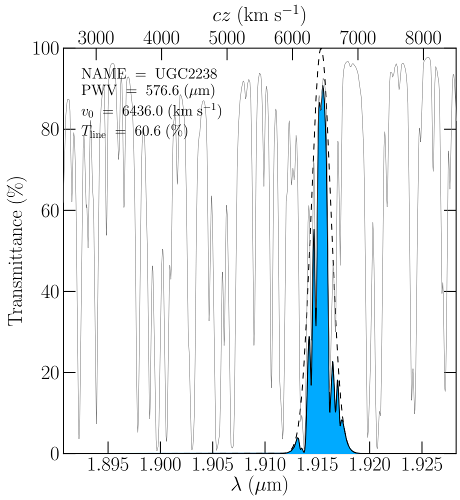

cz (km s^{-1})
NAME = UGC2238
PWV = 576.6 (μm)
v_0 = 6436.0 (km s^{-1})
$T_{\rm line}$ = 60.6 (%)
Transmittance (%)
λ (μm)

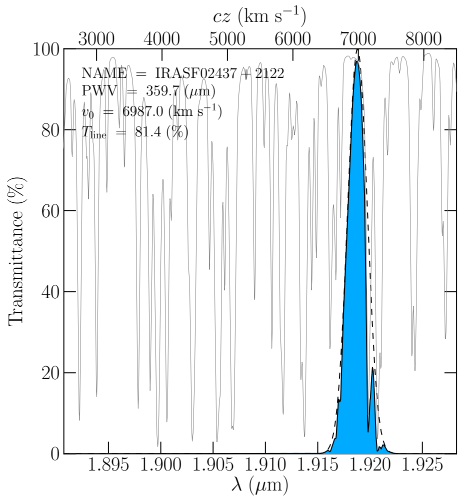

cz (km s^{-1})
NAME = IRASF02437 + 2122
PWV = 359.7 (μm)
v_0 = 6987.0 (km s^{-1})
$T_{\rm line}$ = 81.4 (%)
Transmittance (%)
λ (μm)

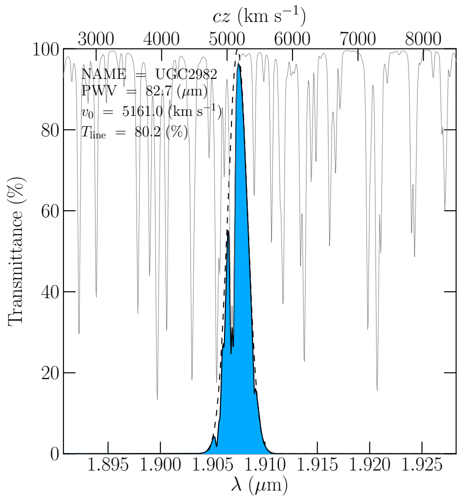

cz (km s^{-1})
NAME = UGC2982
PWV = 82.7 (μm)
v_0 = 5161.0 (km s^{-1})
$T_{\rm line}$ = 80.2 (%)
Transmittance (%)
λ (μm)

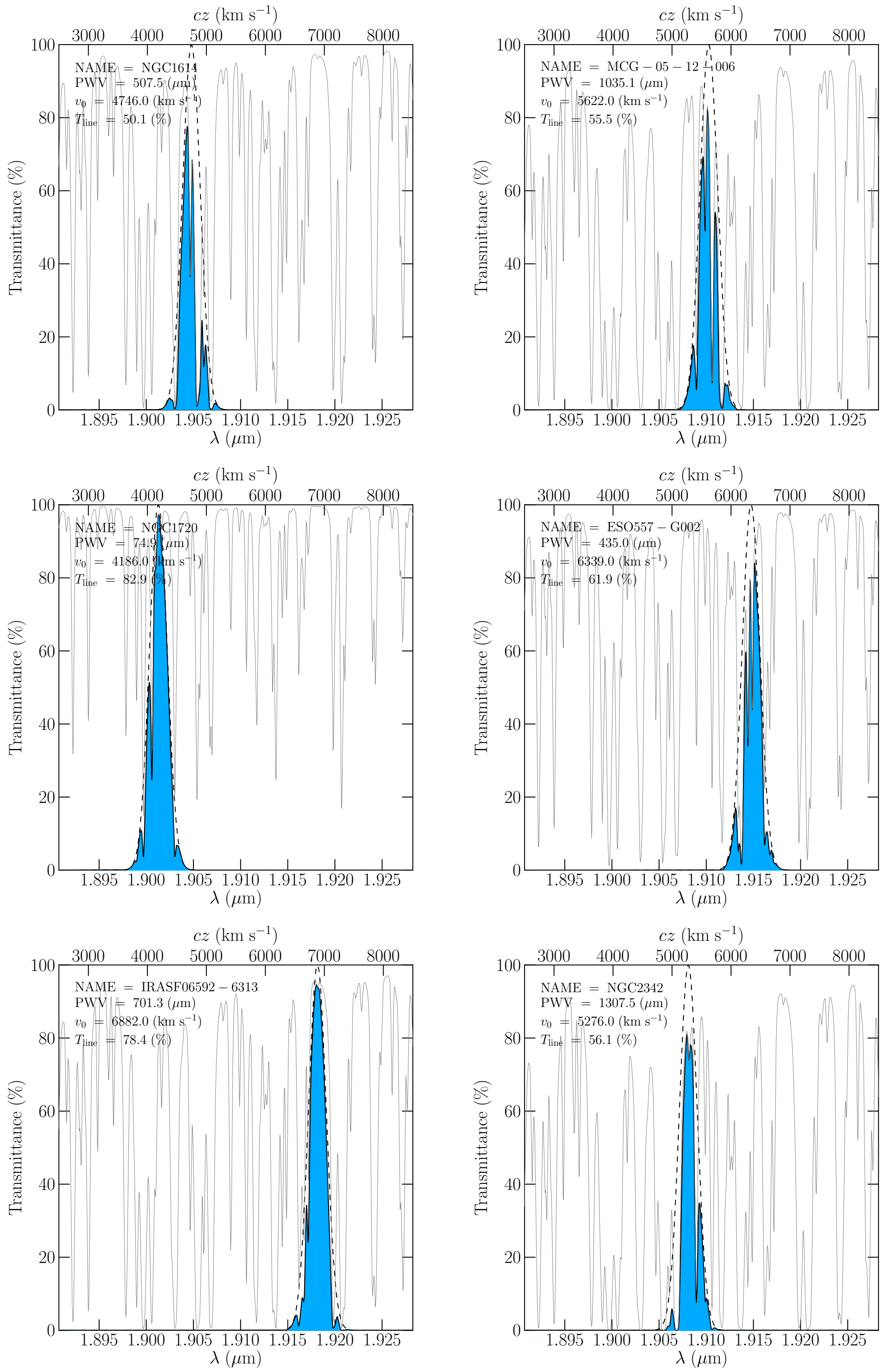
NAME = NGC1614
PWV = 507.5 (μm)
v0 = 4746.0 (km s−1)
Tline = 50.1 (%)
NAME = MCG − 05 − 12 − 006
PWV = 1035.1 (μm)
v0 = 5622.0 (km s−1)
Tline = 55.5 (%)
NAME = NGC1720
PWV = 74.9 (μm)
v0 = 4186.0 (km s−1)
Tline = 82.9 (%)
NAME = ESO557 − G002
PWV = 435.0 (μm)
v0 = 6339.0 (km s−1)
Tline = 61.9 (%)
NAME = IRASF06592 − 6313
PWV = 701.3 (μm)
v0 = 6882.0 (km s−1)
Tline = 78.4 (%)
NAME = NGC2342
PWV = 1307.5 (μm)
v0 = 5276.0 (km s−1)
Tline = 56.1 (%)
cz (km s−1)
Transmittance (%)
λ (μm)

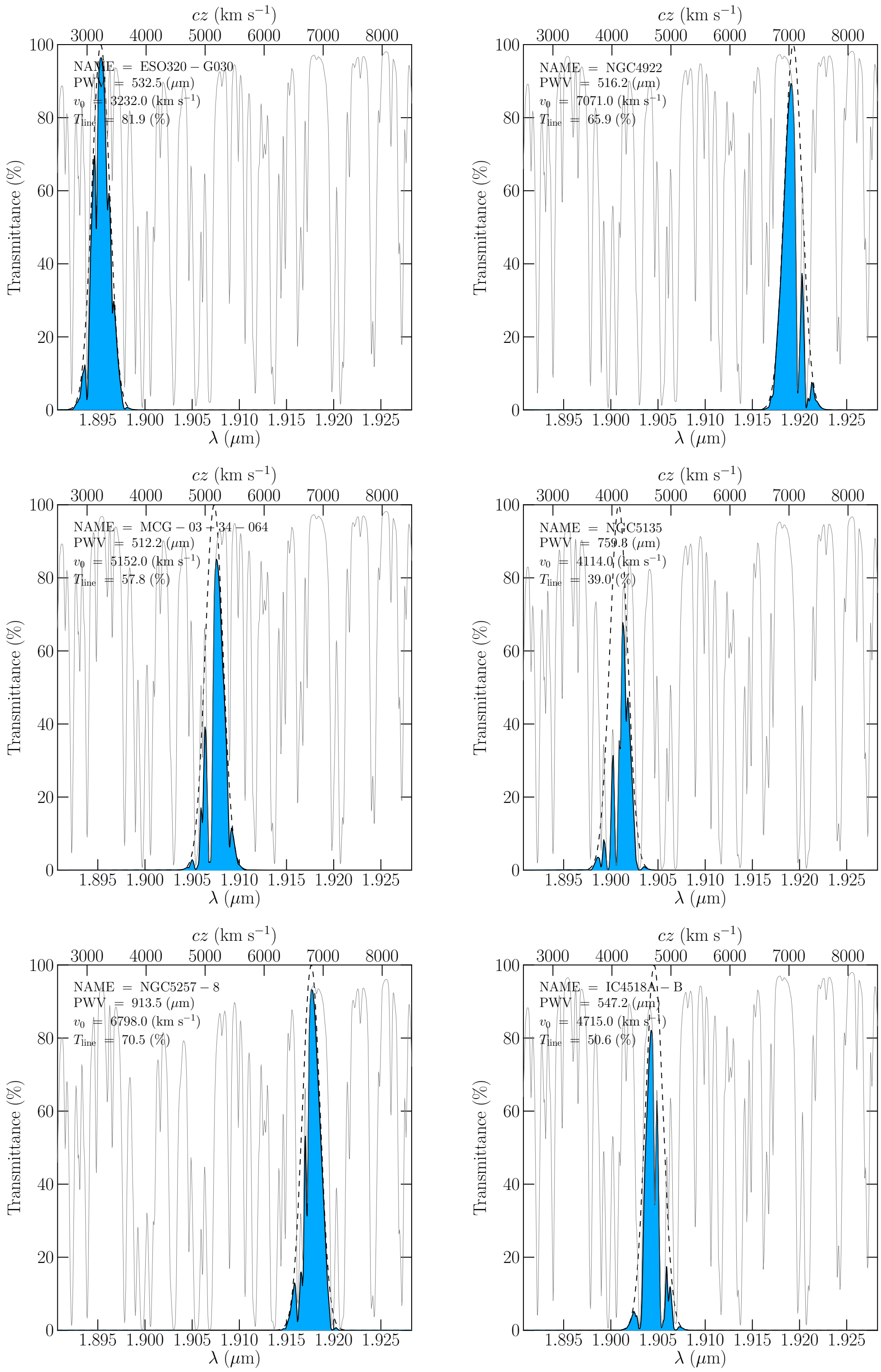

NAME = ESO320 − G030
PWV = 532.5 (μm)
v_0 = 3232.0 (km s^{-1})
$T_{\rm line}$ = 81.9 (%)
NAME = NGC4922
PWV = 516.2 (μm)
v_0 = 7071.0 (km s^{-1})
$T_{\rm line}$ = 65.9 (%)
NAME = MCG − 03 + 34 − 064
PWV = 512.2 (μm)
v_0 = 5152.0 (km s^{-1})
$T_{\rm line}$ = 57.8 (%)
NAME = NGC5135
PWV = 759.8 (μm)
v_0 = 4114.0 (km s^{-1})
$T_{\rm line}$ = 39.0 (%)
NAME = NGC5257 − 8
PWV = 913.5 (μm)
v_0 = 6798.0 (km s^{-1})
$T_{\rm line}$ = 70.5 (%)
NAME = IC4518A − B
PWV = 547.2 (μm)
v_0 = 4715.0 (km s^{-1})
$T_{\rm line}$ = 50.6 (%)
cz (km s^{-1})
Transmittance (%)
λ (μm)

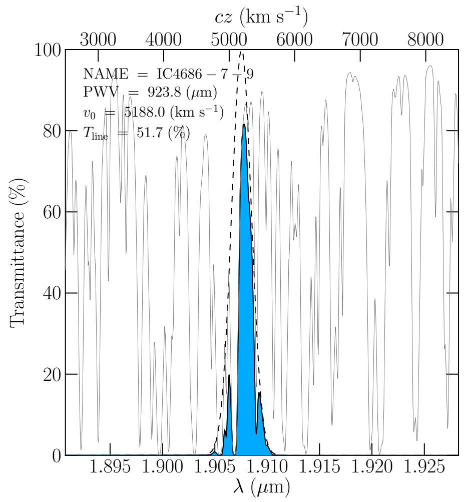
NAME = IC4686 − 7 − 9
PWV = 923.8 (μm)
v_0 = 5188.0 (km s^{-1})
$T_{\rm line}$ = 51.7 (%)
Transmittance (%)
λ (μm)
cz (km s^{-1})

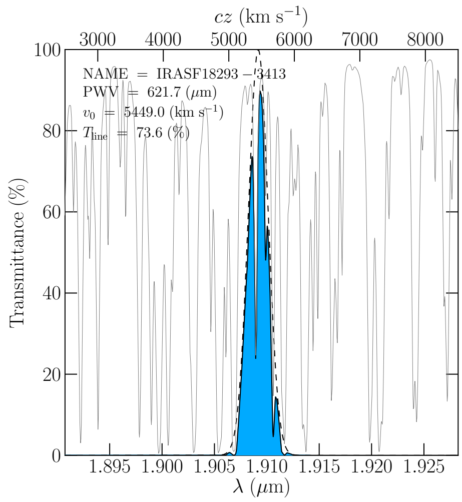
NAME = IRASF18293 − 3413
PWV = 621.7 (μm)
v_0 = 5449.0 (km s^{-1})
$T_{\rm line}$ = 73.6 (%)
Transmittance (%)
λ (μm)
cz (km s^{-1})

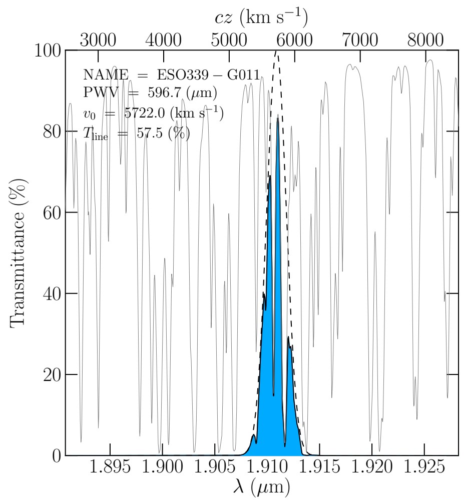
NAME = ESO339 − G011
PWV = 596.7 (μm)
v_0 = 5722.0 (km s^{-1})
$T_{\rm line}$ = 57.5 (%)
Transmittance (%)
λ (μm)
cz (km s^{-1})

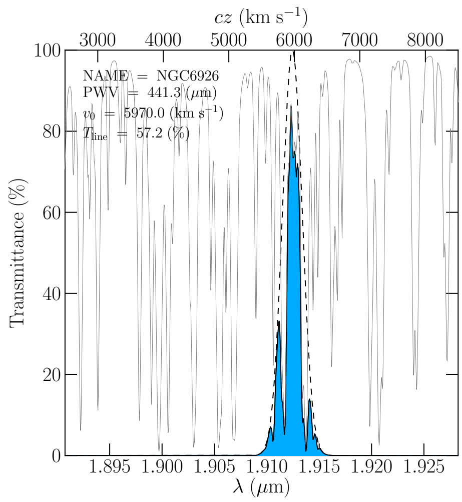
NAME = NGC6926
PWV = 441.3 (μm)
v_0 = 5970.0 (km s^{-1})
$T_{\rm line}$ = 57.2 (%)
Transmittance (%)
λ (μm)
cz (km s^{-1})

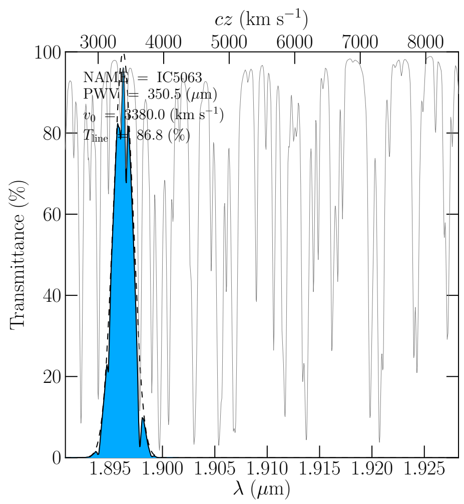
NAME = IC5063
PWV = 350.5 (μm)
v_0 = 3380.0 (km s^{-1})
$T_{\rm line}$ = 86.8 (%)
Transmittance (%)
λ (μm)
cz (km s^{-1})

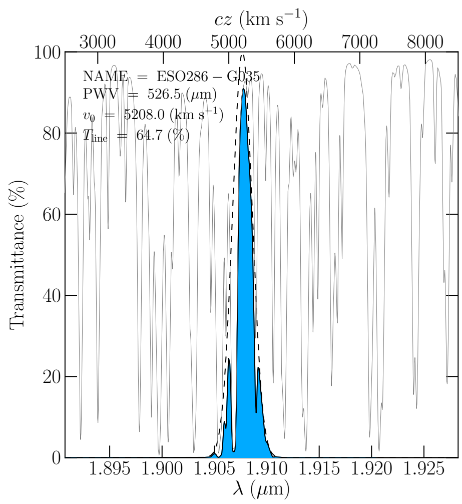
NAME = ESO286 − G035
PWV = 526.5 (μm)
v_0 = 5208.0 (km s^{-1})
$T_{\rm line}$ = 64.7 (%)
Transmittance (%)
λ (μm)
cz (km s^{-1})

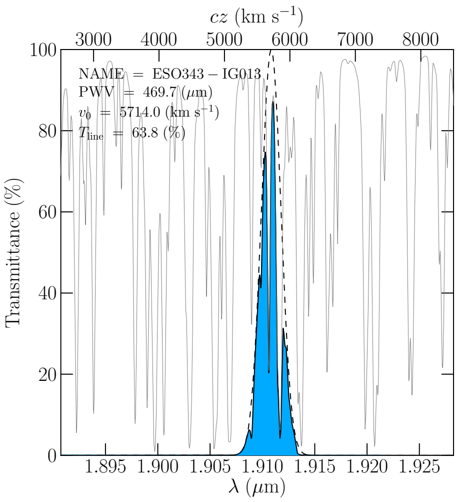

cz (km s−1)
NAME = ESO343 − IG013
PWV = 469.7 (μm)
v0 = 5714.0 (km s−1)
Tline = 63.8 (%)
Transmittance (%)
λ (μm)

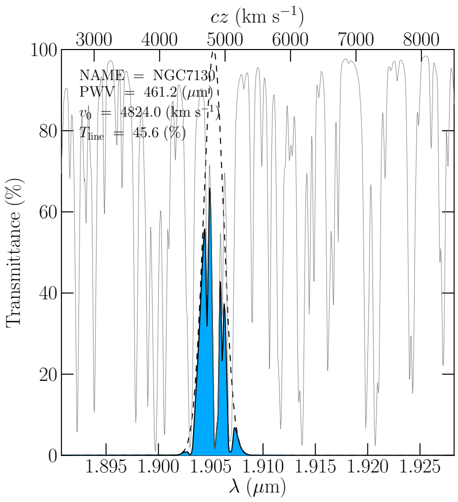

cz (km s−1)
NAME = NGC7130
PWV = 461.2 (μm)
v0 = 4824.0 (km s−1)
Tline = 45.6 (%)
Transmittance (%)
λ (μm)

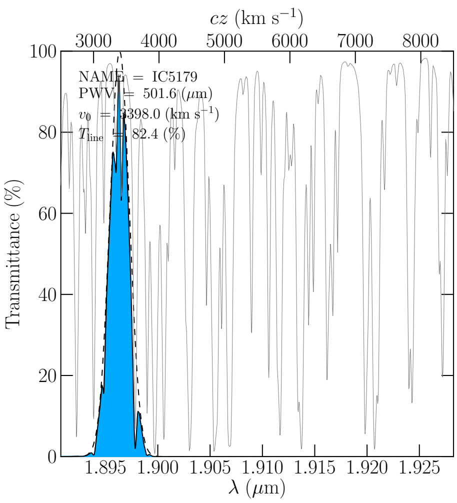

cz (km s−1)
NAME = IC5179
PWV = 501.6 (μm)
v0 = 3398.0 (km s−1)
Tline = 82.4 (%)
Transmittance (%)
λ (μm)

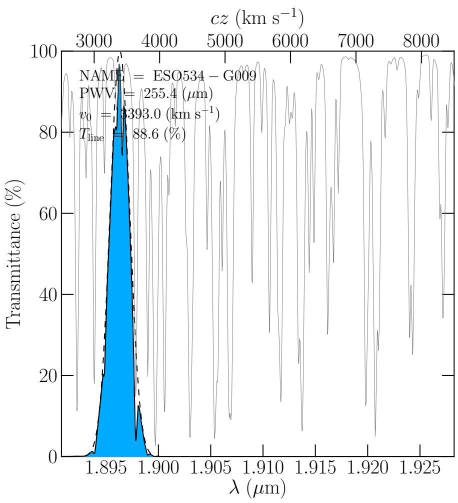

cz (km s−1)
NAME = ESO534 − G009
PWV = 255.4 (μm)
v0 = 3393.0 (km s−1)
Tline = 88.6 (%)
Transmittance (%)
λ (μm)

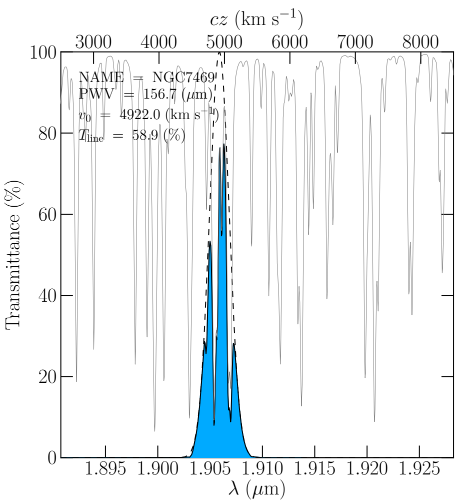

cz (km s−1)
NAME = NGC7469
PWV = 156.7 (μm)
v0 = 4922.0 (km s−1)
Tline = 58.9 (%)
Transmittance (%)
λ (μm)

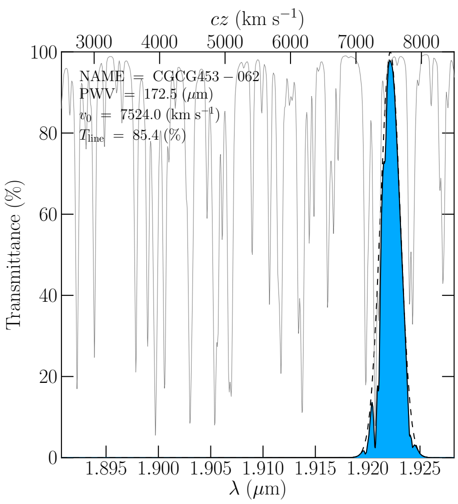

cz (km s−1)
NAME = CGCG453 − 062
PWV = 172.5 (μm)
v0 = 7524.0 (km s−1)
Tline = 85.4 (%)
Transmittance (%)
λ (μm)

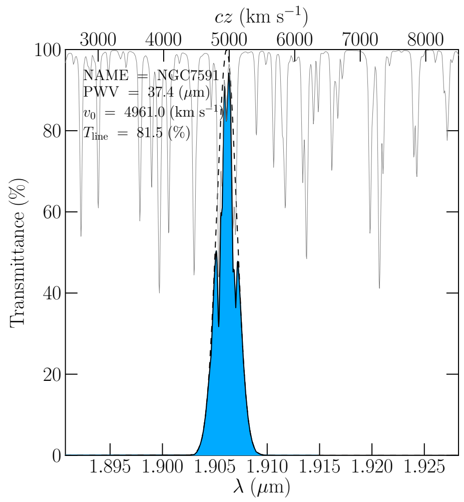
NAME = NGC7591
PWV = 37.4 (μm)
v0 = 4961.0 (km s−1)
Tline = 81.5 (%)
cz (km s−1)
Transmittance (%)
λ (μm)

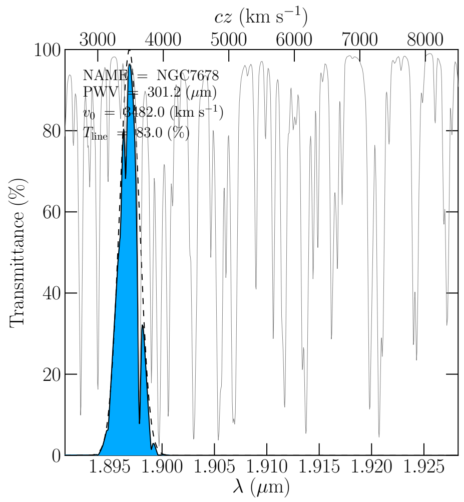
NAME = NGC7678
PWV = 301.2 (μm)
Tline = 83.0 (%)
cz (km s−1)
Transmittance (%)
λ (μm)

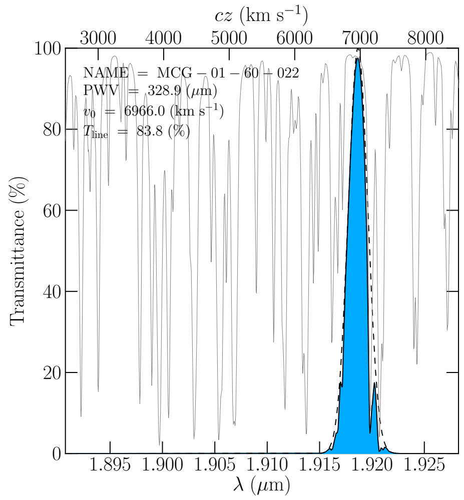
NAME = MCG − 01 − 60 − 022
PWV = 328.9 (μm)
v0 = 6966.0 (km s−1)
Tline = 83.8 (%)
cz (km s−1)
Transmittance (%)
λ (μm)

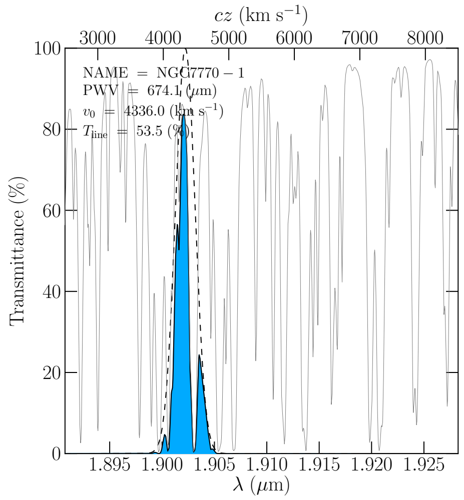
NAME = NGC7770 − 1
PWV = 674.1 (μm)
v0 = 4336.0 (km s−1)
Tline = 53.5 (%)
cz (km s−1)
Transmittance (%)
λ (μm)

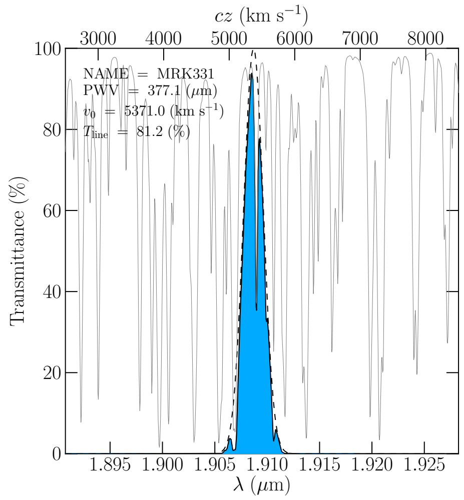
NAME = MRK331
PWV = 377.1 (μm)
v0 = 5371.0 (km s−1)
Tline = 81.2 (%)
cz (km s−1)
Transmittance (%)
λ (μm)

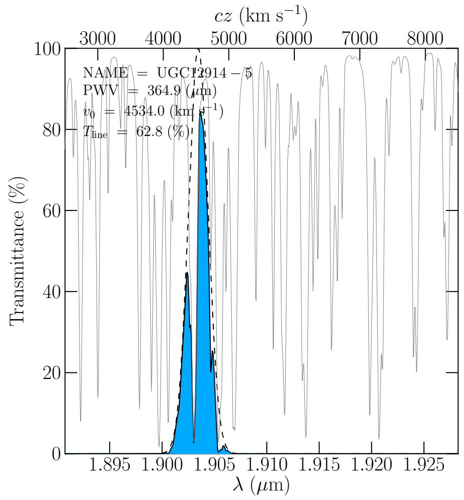
NAME = UGC12914 − 5
PWV = 364.9 (μm)
v0 = 4534.0 (km s−1)
Tline = 62.8 (%)
cz (km s−1)
Transmittance (%)
λ (μm)

Appendix B

Anir Redcution tool for Imaging data Analysis -ARIA-

B.1 Introduction

B.1.1 What is ARIA

ARIA (Anir Redcution tool for Imaging data Analysis) is a imaging data reduction pipeline for optical and near infrared observation, and this package is developed for ANIR (Atacama Near InfraRed camera) which is installed on the University of Tokyo Atacama Observatory (TAO) 1m telescope at the summit of Co. Chajnantor in northern Chile. This package is written by Python scripts, and based on PyRAF. Because ARIA is a simple reduction package and has standerd reduction tools, not only ANIR imaging data, but also other imaging data can be reduced with ARIA.

B.1.2 License

ARIA is developed for analysis of ANIR imaging data and are both free ; Permission is hereby granted, free of charge, to any person obtaining a copy of this software and associated documentation files, to deal in the Software without restriction, including without limitation the rights to use, copy, modify, merge, publish, distribute, sublicense, and/or sell copies of the Software, and to permit persons to whom the Software is furnished to do so, subject to the following conditions: The above copyright notice and this permission notice shall be included in all copies or substantial portions of the Software.

B.1.3 Installing the software

To install from the source archive, you must first uncompress and unarchive the archive:

```
> gzip -dc AireAqua.tar.gz
> tar -xvf AireAqua.tar
```

In addition to the above, following softwares are necessary to run the program;

(1) Python (except Ver.3.0)
We just check Python ver. 2.6.

(2) Numerical Python (http://www.numpy.org/)

(3) PyRAF (http://www.stsci.edu/institute/software_hardware/pyraf/current/download)
These softwares are necessary to install PyRAF; Python (2.6+), Numpy (1.6+), Tcl/Tk (8.4+), ipython (0.12+, optional), matplotlib (1.1+, optional), pip (1.3.1+, optional), readline (5.2+, optional), urwid (1.1.1, optional), PyObjC if on OSX (optional), see the homepage for detailed.

(4) MSCRED (optional)

(5) Sextractor (optional: http://www.astromatic.net/software/sextractor)

(6) OPM (optional: http://stella.astron.s.u-tokyo.ac.jp/nmatsuna/Japanese/software/OPM.html)
Sorry in Japanese

You can check whether these packages have been installed or not by typing as follows;

```
> python
>>> import numpy
>>> import pyraf
...
```

B.2 Sample Script

This is an sample script based on a standerd reduction of near infrared imaging data with self-sky calibration and WCS setting.

```
################################################################################
##                      ANIR Data Reduction Sample
##                              Ken Tateuchi & Masahiro Konishi
##                              ver.0.1         update:20130718
##                              ver.1.0         update:20140107
##                              ver.2.0         update:20140108
##                              ver.2.1         update:20140226
##                              ver.3.0         update:20140301
##
################################################################################
#___ Import check ______________________________________________________________
import ARIA # import ARIA.py
import os

#___ Set rcParameter ___________________________________________________________
ARIA.rcParams['DATA_DIR'] = '/data/rokkaku/anir/1211atacama/uni/20121117'
ARIA.rcParams['OUTPUT_DIR'] = '/data/kousyu/anir/S12B/t001i05'
ARIA.rcParams['DARK'] = './calibdata/sflat_ks_s13b.fits'
ARIA.rcParams['FLAT'] = './calibdata/sflat_ks_s13b.fits'
ARIA.rcParams['DIST'] = './calibdata/sflat_ks_s13b.fits'
ARIA.rcParams['SKY'] = './calibdata/sflat_ks_s13b.fits'
ARIA.rcParams['BPM'] = './calibdata/badpix_S13B.pl'
OUTPUT_NAME = 'irasf05405_paaoff'

#___ Set ImageGroup ____________________________________________________________
"""Input file number list
   from first number to end number + 1"""
objlst = range(39999,40008)
imagegroup = ARIA.ImageGroup(objlst)

#___ Subtract Dark Frame _______________________________________________________
"""For ANIR optical channel
   If dark frame dose not exist, an error is occured.
   Output file : df'filename'.fits"""
#imagegroup.sub_dark()

#___ Divided by Flat Frame _____________________________________________________
"""Run pro_flat() in this function
   If flat file is no set, self-sky flat is produced
   Output file : ff'filename'.fits"""
imagegroup.div_flat()
#overwrite=None

#___ Remove cosmic ray _________________________________________________________
"""Output file : co'ssmcdcffdffilename'.fits
        [**, ff, mcff, ssmcff, cossmcff]"""
imagegroup.cos_remove()
#imagegroup.cos_clean()

#___ Correct Distortion ________________________________________________________
"""For ANIR optical channel
   If distorsion map dose not exist, and error is occured
   Output file : dc'filename'.fits"""
#imagegroup.cor_dist()

#___ Set Bad Pixel Masks with Fixpix ___________________________________________
"""Output file : 'filename'.fits"""
imagegroup.add_head(head_name='bpm', head_state=None)

#___ Make Uniform with Median Flux of Frames ____________________________________
"""Output file : mc'filename'.fits"""
imagegroup.med_image()

#___ Make Object Masks _________________________________________________________
"""Output file : objmask'filename'.pl"""
```

```
imagegroup.pro_objmask(sub_sky=True, nsky=3)

#___ Set Object Mask ____________________________________________________________
"""Output file : 'filename'.fits"""
imagegroup.add_head(head_name='initobjmask', head_state=None)
# [**, ff, mcff]


#___ Loop Section _______________________________________________________________
for i in range(1,0,-1):
        """make object masks again"""
        if i == 1:
                imagegroup.get_history()

        #___ Sky Frame Subtraction ________________________________________________
        """Output file : ss'mcdcffdffilename'.fits
            [**, ff, mcff, ssmcff]"""
        imagegroup.sub_sky(nsky=2,selfsky=True,Clean=False)

        #___ Get 2MASS Catalog ____________________________________________________
        """Output file : tmass'filename'.fits"""
        #imagegroup.get_catalog(outfile='aaa', boxsize=300)
        imagegroup.get_catalog(outfile=OUTPUT_NAME,boxsize=300)

        #___ Add WCS for Each Frames _____________________________________________
        """Tentative wcs mapping with OPM
           Output file : wc'ssmcdcffdffilename'.fits"""
        imagegroup.map_wcs_opm(OUTPUT_NAME,match_band='K',mag_thrs=17.5,clean='no')
        #imagegroup.map_wcs_center(OUTPUT_NAME, match_band='K', init_wcs='no')
        #imagegroup.map_wcs_manual(OUTPUT_NAME, match_band='K', set_tmpwcs='yes',clean='no')
        # [**, ff, mcff, ssmcff, wcssmcff, wcwcssmcff]

        #___ Correct Sub-pixel Shift _____________________________________________
        imagegroup.pro_register()

        #___ Stacking Images _____________________________________________________
        imagegroup.com_image(OUTPUT_NAME)
        #os.system('rm %s/*.pl' % ARIA.rcParams['OUTPUT_DIR'])
        #imagegroup.get_history()

        if i > 1:
                #___ Make Master Object Mask _____________________________________
                imagegroup.pro_masterobjmask(OUTPUT_NAME)
                hist = imagegroup.get_history()
                k = 0
                for i in range(len(hist)):
                        if list(hist[i])[0] == 'r':
                                del_num = i
                                break
                for i in range(len(hist)-del_num):
                        imagegroup.del_history(-1)
                imagegroup.pro_dithobjmask(OUTPUT_NAME)
                for i in range(len(hist)):
                        if list(hist[i])[0] == 's':
                                del_num = i
                                break
                for i in range(len(hist)-del_num):
                        imagegroup.del_history(-1)
                #imagegroup.get_history()
                #exit()
                # [**, ff, mcff]

                #___ Set Object Mask _____________________________________________
                imagegroup.add_head(head_name='momsk', head_state=None)
                #imagegroup.get_history()
                #exit()
                # [**, ff, mcff]
                #hist = imagegroup.get_history()

#___ Flux Calibration using Reference Data ______________________________________
imagegroup.calc_sys(OUTPUT_NAME,filter_band='Paaoff',apert=9,unit='ADU',mag_thrsh=10.0, mag_thrsl=14)
imagegroup.calc_sys(OUTPUT_NAME,infile_name=OUTPUT_NAME,filter_band='Paaoff',apert=9,unit='ADU',mag_thrsh=10.0, mag_thrsl=14)
```

B.3 Source Code of ARIA

Here is the source code of ARIA.py

```
################################################################################
##                      Anir Imaging data REduction tool  --ARIA--
##                              Ken Tateuchi & Masahiro Konishi
##                              ver.0.1         update:20130718
##                              ver.1.0         update:20140107
##                              ver.2.0         update:20140108
##                              ver.2.1         update:20140123
##                              ver.2.2         update:20140226
##                              ver.2.3         update:20140228
##                              ver.3.0         update:20140301
##                              ver.3.1         update:20140303
##
################################################################################
#___ import check _____________________________________________________________
import os, sys, logging, urllib
import numpy as np
from pyraf import iraf


#___ Logging __________________________________________________________________
# create logger
LOG_FILENAME = 'ariaprocess.log'
if os.path.exists(LOG_FILENAME):
                os.remove(LOG_FILENAME)
logging.basicConfig()
logger = logging.getLogger('ARIA')
logger.setLevel(logging.DEBUG)
# create console handler and set level to debug
ch = logging.StreamHandler()
ch.setLevel(logging.DEBUG)
# create file handler and set level to debug
fh = logging.FileHandler(LOG_FILENAME)
fh.setLevel(logging.DEBUG)
# create formatter
formatter = logging.Formatter("%(asctime)s - %(name)s - %(levelname)s - %(message)s")
ch.setFormatter(formatter)
fh.setFormatter(formatter)
# add ch & fh to logger
logger.addHandler(ch)
logger.addHandler(fh)
del ch, fh, formatter


#___ Parameter set ____________________________________________________________
rcParams = {}
isSEXTRACexists = False

def _remove(infiles, verbose=True):
        def remove(infile, verbose=True):
                if os.path.exists(infile):
                        os.remove(infile)
                        if verbose:
                                logger.debug("Deleted file: {0:s}.".format(infile))
                return

        if isinstance(infiles, str):
                remove(infiles, verbose)
        elif isinstance(infiles, list) or isinstance(infiles, tuple):
                for infile in infiles:
                        remove(infile, verbose)
        else:
                msg = "Invalid value: {0}".format(infiles)
                logger.error(msg)
                raise ValueError(msg)
        return

def _error(ErrorType, msg):
```

```
        logger.error(msg)
        raise ErrorType(msg)


#___ ImageGroup Class __________________________________________________________
class ImageGroup(object):

        #___ Initialization _____________________________________________________
        def __init__(self,filelist):
                self.setup(filelist)
                return

        #___ Setup ______________________________________________________________
        def setup(self,infiles):
                self.imarray = []
                for infile in infiles:
                        self.imarray.append( Image(infile) )
                infiles = self.imarray
                for infile in infiles:
                        infile.cp_image()
                return

        #___ Sub_dark ___________________________________________________________
        def sub_dark(self, dark_frame=None):
                infiles = self.imarray
                for infile in infiles:
                        infile.sub_dark(dark_frame)
                return

        #___ Div_flat ___________________________________________________________
        def div_flat(self, flat_frame=None, overwrite=True):
                infiles = self.imarray
                for infile in infiles:
                        infile.div_flat(flat_frame, overwrite)
                return

        #___ Calc_sys ___________________________________________________________
        def calc_sys(self, tmass_data,infile_name=None,filter_band='Ks',mag_thrsh=12.0, \
        mag_thrsl=17.5,apert=10,unit='ADU',display=True):
                if infile_name is None:
                        infiles = self.imarray
                        for infile in infiles:
                                infile.calc_sys(tmass_data,infile_name=infile_name,filter_band=filter_band, \
             mag_thrsh=mag_thrsh,mag_thrsl=mag_thrsl,apert=apert,unit=unit,display=display)
                else:
                        infiles = self.imarray
                        for infile in infiles:
                                infile.calc_sys(tmass_data,infile_name=infile_name,filter_band=filter_band, \
             mag_thrsh=mag_thrsh,mag_thrsl=mag_thrsl,apert=apert,unit=unit,display=display)
                                break

        #___ Cor_dist ___________________________________________________________
        def cor_dist(self, dist_map=None):
                infiles = self.imarray
                for infile in infiles:
                        infile.cor_dist(dist_map)
                return

        #___ Cos_clean __________________________________________________________
        def cos_clean(self):
                infiles = self.imarray
                for infile in infiles:
                        infile.cos_clean()
                return

        #___ Cos_remve __________________________________________________________
        def cos_remove(self):
                infiles = self.imarray
                for infile in infiles:
                        infile.cos_remove()
                return

        #___ Com_image __________________________________________________________
        def com_image(self, outfile):
                infiles = []
                outfiles = []
```

```
        if os.path.exists('%s/%scomb.lst' % (rcParams['OUTPUT_DIR'],outfile)):
            os.system('rm %s/%scomb.lst' % (rcParams['OUTPUT_DIR'],outfile))
        for img in self.imarray:
            infile = img._get_infilename()
            infiles.append(infile)
        file = open('%s/%scomb.lst' % (rcParams['OUTPUT_DIR'],outfile),"w")
        for i in range(len(infiles)):
            file.write("%s\n" % (infiles[i]))
        file.close()
        #comb_frame = ','.join(infiles)
        if os.path.exists('%s/%s.fits' % (rcParams['OUTPUT_DIR'],outfile)):
            os.system('rm %s/%s.fits' % (rcParams['OUTPUT_DIR'],outfile))
        imcomlog = iraf.imcombine('@%s/%scomb.lst' % (rcParams['OUTPUT_DIR'],outfile), \
  '%s/%s.fits' % (rcParams['OUTPUT_DIR'],outfile), combine='average', \
   offsets='wcs' , hthreshold=1e7, lthreshold=-1e7, reject='avsigclip', Stdout=-1)

        return

    #___ Med_image ____________________________________________________________
    def med_image(self):
        infiles = []
        outfiles = []
        med_arr = []
        for img in self.imarray:
            infile = img._get_infilename()
            infiles.append(infile)
            outfile = img._get_outfilename(rcParams["MC"])
            outfiles.append(outfile)
            med = iraf.imstatistics(infile, nclip='10', fields='mean', Stdout=-1)
            med_arr.append(float(med[1]))
        med_arr = np.asarray(med_arr)
        ave = med_arr.mean()
        val_arr = med_arr - ave
        for img, infile, outfile, val in zip(self.imarray, infiles, outfiles, val_arr):
            img._remove("%s.fits" % outfile)
            iraf.imarith(infile, "-", val, outfile)
            logger.debug("'{0:s}' median correction with '{1:f}'.".format(outfile,val))
            img._add_history(os.path.basename(outfile))
        return

    #___ Make_sky _____________________________________________________________
    def make_sky(self, outfile):
        infiles = []
        outfiles = []
        if os.path.exists('%s/%scomb.lst' % (rcParams['OUTPUT_DIR'],outfile)):
            os.system('rm %s/%scomb.lst' % (rcParams['OUTPUT_DIR'],outfile))
        for img in self.imarray:
            infile = img._get_infilename()
            infiles.append(infile)
        file = open('%s/%scomb.lst' % (rcParams['OUTPUT_DIR'],outfile),"w")
        for i in range(len(infiles)):
            file.write("%s\n" % (infiles[i]))
        file.close()
        #comb_frame = ','.join(infiles)
        if os.path.exists('%s/%s.fits' % (rcParams['OUTPUT_DIR'],outfile)):
            os.system('rm %s/%s.fits' % (rcParams['OUTPUT_DIR'],outfile))
        imcomlog = iraf.imcombine('@%s/%scomb.lst' % (rcParams['OUTPUT_DIR'],outfile), \
   '%s/%s.fits' % (rcParams['OUTPUT_DIR'],outfile),combine='median', \
   masktype='!OBJMASK',maskvalue=0, reject='avsigclip', Stdout=-1)
        return


    #___ Pro_objmask __________________________________________________________
    def pro_objmask(self, sub_sky=False, nsky=4):
        infiles = self.imarray
        if sub_sky == True:
            self.sub_sky(nsky)
        for infile in infiles:
            if isSEXTRACexists == True:
                infile.run_sextractor()
            else:
                infile.run_objmask()
        if sub_sky == True:
```

```
				self.del_history(-1)
				#self.del_history(-1)
			return

	#___ Pro_register ____________________________________________________________
	def pro_register(self):
			infiles = self.imarray
			for infile in infiles:
				infile.pro_register()
			return

	#___ Pro_masterobjmask _______________________________________________________
	def pro_masterobjmask(self, masterfile):
			#___ Make master object mask
			if os.path.exists('%s/%s.pl' % (rcParams['OUTPUT_DIR'],masterfile)):
				os.system('rm %s/%s.pl' % (rcParams['OUTPUT_DIR'],masterfile))
			if os.path.exists('%s/maskmaster.fits' % rcParams['OUTPUT_DIR']):
				os.system('rm %s/maskmaster.fits' % rcParams['OUTPUT_DIR'])
			iraf.noao.nproto(Stdout=-1)
			iraf.objmasks('%s/%s.fits' % (rcParams['OUTPUT_DIR'],masterfile), \
	'%s/%s.pl' % (rcParams['OUTPUT_DIR'],masterfile), omtype='boolean', hsigma=5)
			iraf.imcopy('%s/%s.pl' % (rcParams['OUTPUT_DIR'],masterfile), \
	'%s/maskmaster.fits' % rcParams['OUTPUT_DIR'])
			iraf.chpixtype('%s/maskmaster.fits' % rcParams['OUTPUT_DIR'], \
	'%s/maskmaster.fits' % rcParams['OUTPUT_DIR'],'real')
			return

	#___ Pro_dithobjmask _________________________________________________________
	def pro_dithobjmask(self, masterfile):
			#___ Create dithered object masks
			infiles = []
			for img in self.imarray:
				infile = img._get_infilename()
				print infile
				if os.path.exists('%smomsk.fits' % infile):
					os.system('rm %smomsk.fits' % infile)
				if os.path.exists('%smomsk.pl' % infile):
					os.system('rm %smomsk.pl' % infile)
				iraf.skymap('%s/%s.fits' % (rcParams['OUTPUT_DIR'],masterfile), \
	  infile, '%sgrid.tran' % infile, inter='No')
				iraf.geotran('%s/maskmaster.fits' % rcParams['OUTPUT_DIR'], \
	  '%smomsk.fits' % infile, '%sgrid.tran' % infile,'%s/%s.fits' % (rcParams['OUTPUT_DIR'],masterfile))
				iraf.imreplace('%smomsk.fits' % infile, 1, lower=0.00001)
				iraf.chpixtype('%smomsk.fits' % infile,'%smomsk.fits' % infile, 'int')
				iraf.imcopy('%smomsk.fits' % infile, '%smomsk.pl' % infile)

				if os.path.exists('%smomsk.fits' % infile):
					os.system('rm %smomsk.fits' % infile)
			return

	#___ Sub_sky _________________________________________________________________
	def sub_sky(self, nsky=2, selfsky=True, imsurf=False, Clean=True):
			if nsky*2 > len(self.imarray):
				logger.error("Need more files.")
				raise ValueError("Need more files.")
				#nsky = -1

			infiles = [img._get_infilename() for img in self.imarray]
			for i, (img, infile) in enumerate(zip(self.imarray, infiles)):
				skyfiles = []
				if nsky == -1:
					for skyfile in infiles:
						if infile != skyfile:
							skyfiles.append(skyfile)
				else:
					indices = np.fabs(np.arange(0, len(infiles)) - i)
					j = 1
					while len(skyfiles) < nsky*2:
						skyfiles += [infiles[k] for k in np.where(indices==j)[0]]
						j += 1
				#print "###______________________________"
```

```
                        #print infile, skyfiles
                        img.sub_sky(infile, skyfile=skyfiles, selfsky=selfsky, imsurf=imsurf, clean=Clean)
                return

        #___ Add_head ______________________________________________________________
        def add_head(self, head_name=None, head_state=None):
                infiles = self.imarray
                for infile in infiles:
                        infile.add_head(head_name, head_state)
                self.del_history(-2)
                return

        #___ Map_wcs_center ________________________________________________________
        def map_wcs_center(self, tmass_file,match_band='K',init_wcs='yes'):
                infiles = self.imarray
                for infile in infiles:
                        infile.map_wcs_center(tmass_file, match_band=match_band, init_wcs=init_wcs)
                return

        #___ Map_wcs_opm ___________________________________________________________
        def map_wcs_opm(self, tmass_file,match_band='K',mag_thrs=17.5,clean='yes'):
                infiles = self.imarray
                for infile in infiles:
                        infile.map_wcs_opm(tmass_file,match_band=match_band,mag_thrs=mag_thrs,clean=clean)
                return

    #___ Map_wcs_manual ____________________________________________________________
        def map_wcs_manual(self,tmass_file,match_band='K',clean='yes',set_tmpwcs='yes'):
                infiles = self.imarray
                for infile in infiles:
                        infile.map_wcs_manual(tmass_file,match_band=match_band,clean=clean,set_tmpwcs=set_tmpwcs)
                return

    #___ Run OPM ___________________________________________________________________
        def run_OPM(self, infiles=None):
                """
                if infiles is None:
                        infiles = self.images
                for infile in infiles:
                        infile.run_OPM()
                        #self.isAllOPMdone *= !(infile.isOPMdone)
                        self.isOPMdone.append(infile.isOPMdone)
                """
                return

        #___ Get_history ___________________________________________________________
        def get_history(self):
                ghis = []
                infiles = self.imarray
                for infile in infiles:
                        ghis.append(infile.get_history())
                print ghis[1]
                return ghis[1]

        #___ Del_history ___________________________________________________________
        def del_history(self, histnum):
                ghis = []
                infiles = self.imarray
                for infile in infiles:
                        ghis.append(infile._del_history(histnum))
                print ghis[1]
                return

        #___ Get_catalog ___________________________________________________________
        def get_catalog(self, outfile=None, boxsize=300):
                infiles = self.imarray
                infiles[0].get_catalog(outfile,boxsize)
                return


#___ Image Class ___________________________________________________________________
class Image(object):

        #___ initialization ________________________________________________________
        def __init__(self,infile):
```

```

                if type(infile) == type(int()):
                        infile = "ANIA{0:08d}".format(infile)
                        #print infile
                else:
                        logger.error("Invalid infile: {0:s}".format(str(infile)))
                        raise ValueError("Invalid infile: {0:s}".format(str(infile)))

                self.filename = infile
                self.isOBJMASKexists = False
                self.hasCatalog = False
                self.isOPMdone = False
                self.__history = []
                self._add_history(self.filename)

                rcParams['DC'] = 'dc'
                rcParams['DF'] = 'df'
                rcParams['FF'] = 'ff'
                rcParams['MC'] = 'mc'
                rcParams['SS'] = 'ss'
                rcParams['WC'] = 'wc'
                rcParams['RE'] = 're'
                rcParams['CO'] = 'co'
                rcParams['CAL'] = 'cal_'
                rcParams['OBJMASK'] = 'objmask'
                return

        def __str__(self):
                return "Image class for '{0}.fits'".format(self.filename)

        #___ add_head ______________________________________________________________
        def add_head(self, head_name=None, head_state=None):
                """add header to the data.

                This function add headers and their states. You can set header name and
                state which you want to add and/or change.

                Args:
                        head_name: a FITS header name to be used (string).
                        head_state: a file of header state to be used (string).

                Returns:
                        None

                Intermediate files:
                        None

                Raises:
                        logger.error: An error occurred when no dark frame found."""
                if head_name is 'bpm':
                        if "BPM" in rcParams:
                                head_state = rcParams["BPM"]
                        head_name_val = head_name
                if head_name is 'objmask':
                        head_state = rcParams["OUTPUT_DIR"] + "/" + rcParams["OBJMASK"] \
          + self.__history[-1] + ".pl"
                        head_name_val = 'bpm'
                if head_name is 'initobjmask':
                        head_state = rcParams["OUTPUT_DIR"] + "/" + rcParams["OBJMASK"] \
          + rcParams["SS"] + self.__history[-1] + ".pl"
                        head_name_val = 'objmask'
                if head_name is 'momsk':
                        head_state = rcParams["OUTPUT_DIR"] + "/" + "wcss" + self.__history[-1] + "momsk.pl"
                        head_name = 'objmask'
                        head_name_val = 'objmask'
                if head_name is None:
                        logger.error("No head name found.")
                        raise ValueError("No head name found.")

                infile = self._get_infilename()
                iraf.hedit(infile, fields=head_name_val, value=head_state, add='Yes', verify='No')
                if head_name is 'bpm':
                        iraf.fixpix(infile, 'BPM')
                logger.debug("'{0:s}' add header.".format(infile))
                self._add_history(os.path.basename(infile))
                return

```

```
    #___ add_histroy ___________________________________________________________
    def _add_history(self, infile):
        self.__history.append(infile)
        logger.debug("'{0:s}' added to history.".format(infile))
        return

    #___ delete_history ________________________________________________________
    def _del_history(self, histnum=-1):
        filename = self.__history[histnum]
        del self.__history[histnum]
        logger.debug("'{0:s}' deleted from history".format(filename))
        return filename

    #___ clean_history _________________________________________________________
    def clean_history(self):
        self.__history = []
        logger.debug("clean history.")
        return

    #___ get_history ___________________________________________________________
    def get_history(self):
        logger.debug("get history.")
        return self.__history

    #___ undo __________________________________________________________________
    def undo(self):
        filename = self._del_history()
        os.remove(rcParams["OUTPUT_DIR"] + "/" + filename + ".fits")
        logger.debug("Undo!! '{0:s}' deleted.".format(filename))
        return

    #___ get_infilename ________________________________________________________
    def _get_infilename(self):
        return rcParams["OUTPUT_DIR"] + "/" + self.__history[-1]

    #___ get_outfilename _______________________________________________________
    def _get_outfilename(self, prefix):
        return rcParams["OUTPUT_DIR"] + "/" + prefix + self.__history[-1]

    #___ remove ________________________________________________________________
    def _remove(self, infile, verbose=True):
        if os.path.exists("%s" % infile):
            #raise ARIAError
            logger.debug("Deleted file: {0:s}.".format(infile))
            os.remove("%s" % infile)
        return

    #___ map_wcs_center ________________________________________________________
    def map_wcs_center(self, tmass_file, match_band='K', mag_thrs=18, init_wcs='yes'):
        """map wcs to data using iraf.center().
        Args:
            head_name: a FITS header name to be used (string).
            head_state: a file of header state to be used (string).
        Returns:
            None
        Intermediate files:
            None
                Raises:
            logger.error: An error occurred when no dark frame found."""
        #if head_name is None:
        #       logger.error("No head name found.")
        #       raise ValueError("No head name found.")

        infile = self._get_infilename()
        outfile = self._get_outfilename(rcParams["WC"])
        tmass_ra, tmass_dec = [], []
        tmass_ra2, tmass_dec2 = [], []
        tmass_ra_sel, tmass_dec_sel, tmass_mag_sel= [], [], []
        tmass_mag, tmass_magj, tmass_magh, tmass_magk = [], [], [], []
        tmass_flag_phqual, tmass_flag_rdflg, tmass_flag_blflg, tmass_flag_ccflg = [], [], [], []
        center_x, center_y, center_flg = [], [], []

        #___ set tempolary wcs
        if init_wcs == 'yes':
```

```
                iraf.hedit(infile, 'CD1_1', 8.28922276933383E-5, verify='No' )
                iraf.hedit(infile, 'CD1_2', -1.5897419834518E-6, verify='No' )
                iraf.hedit(infile, 'CD2_1', -1.6019556673250E-6, verify='No' )
                iraf.hedit(infile, 'CD2_2', -8.2661883090236E-5, verify='No' )
                iraf.hedit(infile, 'WCSDIM', 2, add='Yes', verify='No' )
                iraf.hedit(infile, 'LTM1_1', 1, add='Yes', verify='No' )
                iraf.hedit(infile, 'LTM2_2', 1, add='Yes', verify='No' )
                iraf.hedit(infile, 'WAT0_001', 'system=image', add='Yes', verify='No' )
                iraf.hedit(infile, 'WAT1_001', 'wtype=tan axtype=ra', add='Yes', verify='No' )
                iraf.hedit(infile, 'WAT2_001', 'wtype=tan axtype=dec', add='Yes', verify='No' )
                iraf.hedit(infile, 'CRPIX1', 539, verify='No' )
                iraf.hedit(infile, 'CRPIX2', 464, verify='No' )

        i = 0
        for line in open('./2mass/%s.tbl' % tmass_file, 'r'):
                if i > 100 and line.split(' ')[0] != '\\' and line.split(' ')[0] != '|':
                        tmass_data = line.split(' ')
                        while tmass_data.count('') > 0:
                                tmass_data.remove('')
                        tmass_ra.append(tmass_data[0])
                        tmass_dec.append(tmass_data[1])
                        tmass_magj.append(float(tmass_data[8])+0.893845) #ABmag-J
                        tmass_magh.append(float(tmass_data[12])+1.37432) #ABmag-H
                        tmass_magk.append(float(tmass_data[16])+1.84024) #ABmag-K
                        tmass_flag_phqual.append(tmass_data[20])
                        tmass_flag_rdflg.append(tmass_data[21])
                        tmass_flag_blflg.append(tmass_data[22])
                        tmass_flag_ccflg.append(tmass_data[23])
                i += 1
        #match_band = 'K'
        #mag_thrs = 15
        if match_band == 'J':
                tmass_mag = tmass_magj
        elif match_band == 'H':
                tmass_mag = tmass_magh
        elif match_band == 'K':
                tmass_mag = tmass_magk
        else:
                print 'Cannot input %s as match_band parameter' % match_band
                exit()
        if match_band == 'J':
                match_num = 0
        elif match_band == 'H':
                match_num = 1
        elif match_band == 'K':
                match_num = 2
        else:
                print 'Input match_band parameter'
                exit()
        file = open('%s/%s.coo' % (rcParams['OUTPUT_DIR'],tmass_file),"w")
        for i in range(len(tmass_ra)):
                if list(tmass_flag_ccflg[i])[match_num].isdigit(): # Contamination check
                        if list(tmass_flag_phqual[i])[match_num]=='A' or \
        list(tmass_flag_phqual[i])[match_num]=='B' or \
        list(tmass_flag_phqual[i])[match_num]=='C' or \
        list(tmass_flag_phqual[i])[match_num]=='D' or \
        list(tmass_flag_phqual[i])[match_num]=='E': # Quality check
                                if float(list(tmass_flag_blflg[i])[match_num])==1: # Blend flag
                                        if tmass_mag[i] < mag_thrs:
                                                file.write("%s %s\n" % (tmass_ra[i],tmass_dec[i]))
                                                tmass_ra_sel.append(tmass_ra[i])
                                                tmass_dec_sel.append(tmass_dec[i])
                                                tmass_mag_sel.append(tmass_mag[i])
        file.close()
        file = open('%stmass.reg' % infile,"w")
        file.write('global color=cyan font=\"helvetica 10 normal\" \
select=1 edit=1 move=1 delete=1 include=1 fixed=0 source\n')
        for i in range(len(tmass_ra_sel)):
                rah = float(tmass_ra_sel[i])/360.*24
                ram = (rah-int(rah))*60
                ras = (ram-int(ram))*60
                ded = float(tmass_dec_sel[i])
```

```
                    if ded < 0:
                            dec = - ded
                    else:
                            dec = ded
                    dem = (dec-int(dec))*60
                    des = (dem-int(dem))*60
                    file.write("fk5;circle(%s:%s:%s,%s:%s:%s,0.0005)\n" \
      % (int(rah),int(ram),ras,int(ded),int(dem),des))
            file.close()

            #___ serch center
            if os.path.exists('%s.star' % infile):
                    os.system('rm %s.star' % infile)
            iraf.noao(Stdout=-1)
            iraf.digiphot(Stdout=-1)
            iraf.apphot(Stdout=-1)
            imstat=iraf.imstatistics(infile,nclip=10,Stdout=-1)[1].split(' ')
            while imstat.count('') > 0:
                    imstat.remove('')
            sig = float(imstat[3])*1
            iraf.center(infile, output='%s.star' % infile, \
   coords='%s/%s.coo' % (rcParams['OUTPUT_DIR'],tmass_file), \
   wcsin='world', cbox=50, maxshift=50, cthreshold=sig, minsnratio=3, verify='No', inter='No')
            i = 0
            for line in open('%s.star' % infile,"r"):
                    i += 1
                    if i > 43:
                            center_data = line.split(' ')
                            while center_data.count('') > 0:
                                    center_data.remove('')
                            if center_data[0].replace(".","").replace("-","").isdigit():
                                    center_x.append(center_data[0])
                                    center_y.append(center_data[1])
                                    center_flg.append(center_data[7])
            #print len(center_x), len(tmass_ra_sel)
            #exit()
            file = open('%s.match' % outfile,"w")
            for i in range(len(center_x)):
                    if not center_flg[i]=='OffImage':
                            file.write("%s %s %s %s\n" % (center_x[i],center_y[i],tmass_ra_sel[i],tmass_dec_sel[i]))
            file.close()
            file = open('%s.reg' % infile,"w")
            file.write('global color=green font=\"helvetica 10 normal\" \
   select=1 edit=1 move=1 delete=1 include=1 fixed=0 source\n')
            for i in range(len(center_x)):
                    if not center_flg[i]=='OffImage':
                            file.write("image;circle(%s,%s,10)\n" % (center_x[i],center_y[i]))
            file.close()

            #___ wcs mapping
            if os.path.exists('%s.fits' % outfile):
                    os.system('rm %s.fits' % outfile)
            iraf.imcopy(infile, outfile)
            file = open('%s.plt' % outfile,"w")
            file.write('f\n')
            file.write(': .snap eps\n')
            file.write('q\n')
            file.close()
            if os.path.exists('%s.ccmap' % outfile):
                    os.system('rm %s.ccmap' % outfile)
            iraf.ccmap('%s.match' % outfile, '%s.db' % outfile,xcolumn=1,\
   ycolumn=2,lngcolumn=3,latcolumn=4,lngunit='degrees',latunits='degrees',\
   projection='tnx', xxorder=2, xyorder=2, yxorder=2, yyorder=2,\
   results='%s.ccmap' % outfile, maxiter=3, reject=3, interactive='no', cursor='%s.plt' % outfile)
            iraf.ccsetwcs(outfile, '%s.db' % outfile, '%s.match' % outfile)

            logger.debug("'{0:s}' map wcs using ccmap.".format(outfile))
            self._add_history(os.path.basename(outfile))
            return


#___ map_wcs_manual _______________________________________________________
    def map_wcs_manual(self, tmass_file, match_band='K', mag_thrs=17.5, set_tmpwcs='yes',clean='yes'):
            """map wcs to data using iraf.center().
```

```
    Args:
                head_name: a FITS header name to be used (string).
                head_state: a file of header state to be used (string).
    Returns:
                None
    Intermediate files:
                None
    Raises:
                logger.error: An error occurred when no dark frame found."""
        infile = self._get_infilename()
        outfile = self._get_outfilename(rcParams["WC"])
        tmass_ra, tmass_dec = [], []
        tmass_ra2, tmass_dec2 = [], []
        tmass_ra_sel, tmass_dec_sel, tmass_mag_sel= [], [], []
        tmass_mag, tmass_magj, tmass_magh, tmass_magk = [], [], [], []
        tmass_flag_phqual, tmass_flag_rdflg, tmass_flag_blflg, tmass_flag_ccflg = [], [], [], []
        center_x, center_y, center_flg = [], [], []

        #___ set tempolary wcs
        if set_tmpwcs == 'yes':
                iraf.hedit(infile, 'CD1_1', 8.28922276933383E-5, verify='No' )
                iraf.hedit(infile, 'CD1_2', -1.5897419834518E-6, verify='No' )
                iraf.hedit(infile, 'CD2_1', -1.6019556673250E-6, verify='No' )
                iraf.hedit(infile, 'CD2_2', -8.2661883090236E-5, verify='No' )
                iraf.hedit(infile, 'WCSDIM', 2, add='Yes', verify='No' )
                iraf.hedit(infile, 'LTM1_1', 1, add='Yes', verify='No' )
                iraf.hedit(infile, 'LTM2_2', 1, add='Yes', verify='No' )
                iraf.hedit(infile, 'WAT0_001', 'system=image', add='Yes', verify='No' )
                iraf.hedit(infile, 'WAT1_001', 'wtype=tan axtype=ra', add='Yes', verify='No' )
                iraf.hedit(infile, 'WAT2_001', 'wtype=tan axtype=dec', add='Yes', verify='No' )
                iraf.hedit(infile, 'CRPIX1', 539, verify='No' )
                iraf.hedit(infile, 'CRPIX2', 464, verify='No' )

        i = 0
        for line in open('./2mass/%s.tbl' % tmass_file, 'r'):
                if i > 100 and line.split(' ')[0] != '\\' and line.split(' ')[0] != '|':
                        tmass_data = line.split(' ')
                        while tmass_data.count('') > 0:
                                tmass_data.remove('')
                        tmass_ra.append(tmass_data[0])
                        tmass_dec.append(tmass_data[1])
                        tmass_magj.append(float(tmass_data[8])+0.893845) #ABmag-J
                        tmass_magh.append(float(tmass_data[12])+1.37432) #ABmag-H
                        tmass_magk.append(float(tmass_data[16])+1.84024) #ABmag-K
                        tmass_flag_phqual.append(tmass_data[20])
                        tmass_flag_rdflg.append(tmass_data[21])
                        tmass_flag_blflg.append(tmass_data[22])
                        tmass_flag_ccflg.append(tmass_data[23])
                i += 1
        if match_band == 'J':
                tmass_mag = tmass_magj
        elif match_band == 'H':
                tmass_mag = tmass_magh
        elif match_band == 'K':
                tmass_mag = tmass_magk
        else:
                print 'Cannot input %s as match_band parameter' % match_band
                exit()
        if match_band == 'J':
                match_num = 0
        elif match_band == 'H':
                match_num = 1
        elif match_band == 'K':
                match_num = 2
        else:
                print 'Input match_band parameter'
                exit()
        file = open('%s/%s.coo' % (rcParams['OUTPUT_DIR'],tmass_file),"w")
        for i in range(len(tmass_ra)):
                if list(tmass_flag_ccflg[i])[match_num].isdigit(): # Contamination check
                        if list(tmass_flag_phqual[i])[match_num]=='A' or \
        list(tmass_flag_phqual[i])[match_num]=='B' or \
```

```
         list(tmass_flag_phqual[i])[match_num]=='C' or \
         list(tmass_flag_phqual[i])[match_num]=='D' or \
         list(tmass_flag_phqual[i])[match_num]=='E': # Quality check
                                 if float(list(tmass_flag_blflg[i])[match_num])==1: # Blend flag
                                         if tmass_mag[i] < mag_thrs:
                                                 file.write("%s %s\n" % (tmass_ra[i],tmass_dec[i]))
                                                 tmass_ra_sel.append(tmass_ra[i])
                                                 tmass_dec_sel.append(tmass_dec[i])
                                                 tmass_mag_sel.append(tmass_mag[i])
         file.close()
         file = open('%stmass.reg' % infile,"w")
         file.write('global color=cyan font=\"helvetica 10 normal\" \
select=1 edit=1 move=1 delete=1 include=1 fixed=0 source\n')
         for i in range(len(tmass_ra_sel)):
                 rah = float(tmass_ra_sel[i])/360.*24
                 ram = (rah-int(rah))*60
                 ras = (ram-int(ram))*60
                 ded = float(tmass_dec_sel[i])
                 if ded < 0:
                         dec = - ded
                 else:
                         dec = ded
                 dem = (dec-int(dec))*60
                 des = (dem-int(dem))*60
                 file.write("fk5;circle(%s:%s:%s,%s:%s:%s,0.0005)\n" \
   % (int(rah),int(ram),ras,int(ded),int(dem),des))
         file.close()

 #___ make ***.match file yourself
         if not os.path.exists('%s.lst' % outfile):
                 print "----------< Warning >----------"
                 print "Make %s.lst file !!" % outfile
                 print "fomat: ANIR_X ANIR_Y 2mass_X 2mass_Y"
                 print "unit : logical logical logical logical"
                 exit()

         tran_data,tran_x1,tran_x2,tran_y1,tran_y2=[],[],[],[],[]
         i = 0
         for line in open('%s.lst' % outfile, 'r'):
                 i += 1
                 tran_data = line.split(' ')
                 while tran_data.count('') > 0:
                         tran_data.remove('')
                 tran_x1.append(tran_data[0])
                 tran_y1.append(tran_data[1])
                 tran_x2.append(tran_data[2])
                 tran_y2.append(tran_data[3])

         file = open('%s.tmp' % outfile,"w")
         for i in range(len(tran_x2)):
                 file.write("%s %s" % (tran_x2[i],tran_y2[i]))
         file.close()

         if os.path.exists('%s.tmp2'%outfile):
                 os.system('rm %s.tmp2'%outfile)
         iraf.skyctran('%s.tmp'%outfile,'%s.tmp2'%outfile, \
'\"%s logical\"'%rcParams['REFIMG'],'fk5')

         tran_data3,tran_x3,tran_y3=[],[],[]
         i = 0
         for line in open('%s.tmp2' % outfile, 'r'):
                 i += 1
                 if i > 9:
                         tran_data3 = line.split(' ')
                         while tran_data3.count('') > 0:
                                 tran_data3.remove('')
                         tran_xh = tran_data3[2].split(':')[0]
                         tran_xm = tran_data3[2].split(':')[1]
                         tran_xs = tran_data3[2].split(':')[2]
                         tran_yd = tran_data3[3].split(':')[0]
                         tran_ym = tran_data3[3].split(':')[1]
                         tran_ys = tran_data3[3].split(':')[2]
                         tran_ra = float(tran_xh) + float(tran_xm)/60. + float(tran_xs)/3600.
                         if float(tran_yd) >= 0:
```

```
                                        tran_de = float(tran_yd) + float(tran_ym)/60. + float(tran_ys)/3600.
                                else:
                                        tran_de = float(tran_yd) - float(tran_ym)/60. - float(tran_ys)/3600.
                                tran_x3.append(tran_ra)
                                tran_y3.append(tran_de)

                file = open('%s.match' % outfile,"w")
                for i in range(len(tran_x1)):
                        file.write("%s %s %s %s\n" % (tran_x1[i],tran_y1[i],tran_x3[i],tran_y3[i]))
                file.close()

                file = open('%s.reg' % infile,"w")
                file.write('global color=green font=\"helvetica 10 normal\" \
         select=1 edit=1 move=1 delete=1 include=1 fixed=0 source\n')
                for i in range(len(center_x)):
                        if not center_flg[i]=='OffImage':
                                file.write("image;circle(%s,%s,10)\n" % (center_x[i],center_y[i]))
                file.close()

                #___ wcs mapping
                if os.path.exists('%s.fits' % outfile):
                        os.system('rm %s.fits' % outfile)
                iraf.imcopy(infile, outfile)
                file = open('%s.plt' % outfile,"w")
                file.write('f\n')
                file.write(': .snap eps\n')
                file.write('q\n')
                file.close()
                if os.path.exists('%s.ccmap' % outfile):
                        os.system('rm %s.ccmap' % outfile)
                iraf.ccmap('%s.match' % outfile, '%s.db' % outfile,xcolumn=1,ycolumn=2,\
        lngcolumn=3,latcolumn=4,lngunit='hours',latunits='degrees', projection='tnx',\
        xxorder=2, xyorder=2, yxorder=2, yyorder=2, results='%s.ccmap' % outfile, \
        maxiter=3, reject=3, interactive='no', cursor='%s.plt' % outfile)
                iraf.ccsetwcs(outfile, '%s.db' % outfile, '%s.match' % outfile)

                if clean == 'yes':
                        os.system('rm %sopm.param' % infile)
                        os.system('rm %stmpdata.par' % infile)
                        os.system('rm %stmpcenter.par' % infile)
                        os.system('rm %stmpfitsky.par' % infile)
                        os.system('rm %stmpphot.par' % infile)
                        os.system('rm %sdao.coo' % infile)
                        os.system('rm %s.phot' % infile)
                        os.system('rm %s.cent' % infile)
                        os.system('rm %slocal.cent' % infile)
                        os.system('rm %sopm.coo' % infile)
                        os.system('rm %sphot.dat' % infile)
                        os.system('rm %sopmout.dat' % outfile)
                        os.system('rm %sopmsf.dat' % outfile)
                        os.system('rm %sopmsf_wcs.dat' % outfile)
                        #os.system('rm %s.match' % outfile)
                        #os.system('rm %s.ccmap' % outfile)
                        #os.system('rm %s.db' % outfile)
                        #os.system('rm %s.plt' % outfile)

                logger.debug("'{0:s}' map wcs using ccmap.".format(outfile))
                self._add_history(os.path.basename(outfile))
                return


        #___ map_wcs_opm ___________________________________________________________
        def map_wcs_opm(self, tmass_file, match_band='K', mag_thrs=17.5, clean='yes'):
                """map wcs to the data using OPM.

                This function add wcs to data.

                Args:
                        head_name: a FITS header name to be used (string).
                        head_state: a file of header state to be used (string).

                Returns:
```

```
                None

        Intermediate files:
                None

        Raises:
                logger.error: An error occurred when no dark frame found."""
        infile = self._get_infilename()
        outfile = self._get_outfilename(rcParams["WC"])
        tmass_ra,tmass_dec=[],[]
        tmass_ra_sel,tmass_dec_sel,tmass_mag_sel=[],[],[]
        tmass_flag_phqual,tmass_flag_rdflg,tmass_flag_blflg,tmass_flag_ccflg=[],[],[],[]
        tmass_mag,tmass_magj,tmass_magh,tmass_magk,tmass_flag=[],[],[],[],[]
        imcent_x_wcs,imcent_y_wcs=[],[]
        apdata_x,apdata_y,apdata_mag=[],[],[]
        opmdata_x1,opmdata_x2,opmdata_y1,opmdata_y2,opmdata_ra,opmdata_de=[],[],[],[],[],[]
        daofind_x,daofind_y=[],[]
        imcent_x,imcent_y,size=500,500,1000

        #___ Photometry initial parameters
        APERTURE=8
        ANNULUS=18
        CENTER="centroid"
        ZMAG=20
        Halfsize = 150

        #___ set tempolary wcs
        if int(rcParams['DATA_DIR'].split('/')[4].split('atacama')[0]) <= 906:
                iraf.hedit(infile, 'CD1_1', -8.27E-5, verify='No' )
                iraf.hedit(infile, 'CD1_2', 1.24E-6, verify='No' )
                iraf.hedit(infile, 'CD2_1', 1.198E-6, verify='No' )
                iraf.hedit(infile, 'CD2_2', 8.26E-5, verify='No' )
                iraf.hedit(infile, 'WCSDIM', 2, add='Yes', verify='No' )
                iraf.hedit(infile, 'LTM1_1', 1, add='Yes', verify='No' )
                iraf.hedit(infile, 'LTM2_2', 1, add='Yes', verify='No' )
                iraf.hedit(infile, 'WAT0_001', 'system=image', add='Yes', verify='No' )
                iraf.hedit(infile, 'WAT1_001', 'wtype=tan axtype=ra', add='Yes', verify='No' )
                iraf.hedit(infile, 'WAT2_001', 'wtype=tan axtype=dec', add='Yes',verify='No' )
                iraf.hedit(infile, 'CRPIX1', 640, verify='No' )
                iraf.hedit(infile, 'CRPIX2', 642, verify='No' )
        else:
                iraf.hedit(infile, 'CD1_1', 8.28922276933383E-5, verify='No' )
                iraf.hedit(infile, 'CD1_2', -1.5897419834518E-6, verify='No' )
                iraf.hedit(infile, 'CD2_1', -1.6019556673250E-6, verify='No' )
                iraf.hedit(infile, 'CD2_2', -8.2661883090236E-5, verify='No' )
                iraf.hedit(infile, 'WCSDIM', 2, add='Yes', verify='No' )
                iraf.hedit(infile, 'LTM1_1', 1, add='Yes', verify='No' )
                iraf.hedit(infile, 'LTM2_2', 1, add='Yes', verify='No' )
                iraf.hedit(infile, 'WAT0_001', 'system=image', add='Yes', verify='No' )
                iraf.hedit(infile, 'WAT1_001', 'wtype=tan axtype=ra', add='Yes', verify='No' )
                iraf.hedit(infile, 'WAT2_001', 'wtype=tan axtype=dec', add='Yes',verify='No' )
                iraf.hedit(infile, 'CRPIX1', 539, verify='No' )
                iraf.hedit(infile, 'CRPIX2', 464, verify='No' )

        #___ 'opm.param' parameter file setting
        file = open('%sopm.param' % infile ,"w")
        file.write('MIRROR     ON\n')
        file.write('MAGNIFY    0.295\n')
        file.write('ANGLE      UNDEF\n')
        file.write('XCENTER    0\n')
        file.write('YCENTER    0\n')
        file.write('HALFSIZE   %s\n' % Halfsize)
        file.write('MAG_CUT1   UNDEF\n')
        file.write('MAG_CUT2   UNDEF\n')
        file.write('NSET       50\n')
        file.write('NVERIFY    -1\n')
        file.write('PV_LIMIT   0.025\n')
        file.write('EPSILON    0.02\n')
        file.write('TOLERANCE  0.5\n')
        file.write('MATCHING   0.01\n')
        file.write('NITER      3\n')
        file.close()

        #___ 'datapars' parameter file setting
        file = open('%stmpdata.par' % infile ,"w")
```

```
file.write('scale,r,h,1.,0.\n')
file.write('fwhmpsfls,r,h,4.7,0.\n')
file.write('emission,b,h,yes\n')
file.write('sigma,r,h,INDEF\n')
file.write('datamin,r,h,INDEF\n')
file.write('datamax,r,h,INDEF\n')
file.write('noise,s,h,"poisson"\n')
file.write('ccdread,s,h,""\n')
file.write('gain,s,h,GAIN\n')
file.write('readnoise,r,h,10\n')
file.write('epadu,r,h,1\n')
file.write('exposure,s,h,"EXPTIME"\n')
file.write('airmass,s,h,"AIRMASS"\n')
file.write('filter,s,h,"FILTER01"\n')
file.write('obstime,s,h,""\n')
file.write('itime,r,h,1.\n')
file.write('xairmass,r,h,INDEF\n')
file.write('ifilter,s,h,INDEF\n')
file.write('otime,s,h,INDEF\n')
file.close()

#___ 'centerpars' parameter file setting
file = open('%stmpcenter.par' % infile ,"w")
file.write('calgorithm,s,h,"%s"\n' % CENTER)
file.write('cthreshold,r,h,0\n')
file.write('minsnratio,r,h,1.,0\n')
file.write('cmaxiter,i,h,10\n')
file.write('maxshift,r,h,1\n')
file.write('clean,b,h,no\n')
file.write('rclean,r,h,1\n')
file.write('rclip,r,h,2.\n')
file.write('kclean,r,h,3\n')
file.write('mkcenter,b,h,no\n')
file.close()

#___ 'fitskypars' parameter file setting
file = open('%stmpfitsky.par' % infile ,"w")
file.write('salgorithm,s,h,"ofilter"\n')
file.write('annulus,r,h,%s\n' % ANNULUS)
file.write('dannulus,r,h,5\n')
file.write('skyvalue,r,h,INDEF\n')
file.write('smaxiter,i,h,10\n')
file.write('sloclip,r,h,0.\n')
file.write('shiclip,r,h,0.\n')
file.write('snreject,i,h,10\n')
file.write('sloreject,r,h,3.\n')
file.write('shireject,r,h,3.\n')
file.write('khist,r,h,3.\n')
file.write('binsize,r,h,0.1\n')
file.write('smooth,b,h,yes\n')
file.write('rgrow,r,h,1\n')
file.write('mksky,b,h,no\n')
file.close()

#___ 'photpars' parameter file setting
file = open('%stmpphot.par' % infile ,"w")
file.write('weighting,s,h,"constant"\n')
file.write('apertures,s,h,%s\n' % APERTURE)
file.write('zmag,r,h,"%s"\n' % ZMAG)
file.write('mkapert,b,h,no\n')
file.close()

#___ daofind star detection with 3 sigma
if os.path.exists('%sdao.coo' % infile):
        os.system('rm %sdao.coo' % infile)
if os.path.exists('%s.phot' % infile):
        os.system('rm %s.phot' % infile)
iraf.noao(Stdout=-1)
iraf.digiphot(Stdout=-1)
iraf.apphot(Stdout=-1)
imstat=iraf.imstatistics(infile,nclip=10,Stdout=-1)[1].split(' ')
while imstat.count('') > 0:
```

```
            imstat.remove('')
        sig = float(imstat[3])*3 # 1.5
        iraf.daofind(infile, output='%sdao.coo' % infile,fwhmpsf=8, \
  verify='No',sigma=sig,sharplo=0.1,sharphi=5,roundlo=-1,roundhi=1)
        i=0
        for line in open('%sdao.coo' % infile, 'r'):
            i += 1
            if i > 41 and line.split(' ')[0] != '#':
                daofind_data = line.split(' ')
                while daofind_data.count('') > 0:
                    daofind_data.remove('')
                daofind_x.append(daofind_data[0])
                daofind_y.append(daofind_data[1])
        file = open('%sdao.reg' % infile,"w")
        file.write('global color=red font=\"helvetica 10 normal\" \
  select=1 edit=1 move=1 delete=1 include=1 fixed=0 source\n')
        for i in range(len(daofind_x)):
            file.write("image;circle(%s,%s,10)\n" % (daofind_x[i],daofind_y[i]))
        file.close()

        #___ daophot star photometry
        iraf.phot(infile, coords='%sdao.coo' % infile,output='%s.phot' % infile, \
 fitskyp='%stmpfitsky.par' % infile, photpars='%stmpphot.par' % infile, \
 datapars='%stmpdata.par' % infile,centerpars='%stmpcenter.par' % infile, \
 interac='No',verify='No')
        i = 0
        for line in open('%s.phot' % infile, 'r'):
            i += 1
            if i > 75 and line.split(' ')[0] != '#':
                apphot_data = line.split(' ')
                while apphot_data.count('') > 0:
                    apphot_data.remove('')
                if i % 5 == 2:
                    apdata_x.append(float(apphot_data[0]))
                    apdata_y.append(float(apphot_data[1]))
                elif i % 5 == 0:
                    apdata_mag.append(apphot_data[4])
        file = open('%sphot.dat' % infile,"w")
        for i in range(len(apdata_x)):
            file.write("%s %s %s\n" % (apdata_x[i],apdata_y[i],apdata_mag[i]))
        file.close()

        #___ make 2mass database
        i = 0
        for line in open('./2mass/%s.tbl' % tmass_file, 'r'):
            if i > 100 and line.split(' ')[0] != '\\' and line.split(' ')[0] != '|':
                tmass_data = line.split(' ')
                while tmass_data.count('') > 0:
                    tmass_data.remove('')
                tmass_ra.append(tmass_data[0])
                tmass_dec.append(tmass_data[1])
                tmass_magj.append(float(tmass_data[8])+0.893845) #ABmag-J
                tmass_magh.append(float(tmass_data[12])+1.37432) #ABmag-H
                tmass_magk.append(float(tmass_data[16])+1.84024) #ABmag-K
                tmass_flag_phqual.append(tmass_data[20])
                tmass_flag_rdflg.append(tmass_data[21])
                tmass_flag_blflg.append(tmass_data[22])
                tmass_flag_ccflg.append(tmass_data[23])
            i += 1
        #match_band = 'K'
        #mag_thrs = 17.5
        if match_band == 'J':
            tmass_mag = tmass_magj
        elif match_band == 'H':
            tmass_mag = tmass_magh
        elif match_band == 'K':
            tmass_mag = tmass_magk
        else:
            print 'Cannot input %s as match_band parameter' % match_band
            exit()
        if match_band == 'J':
            match_num = 0
        elif match_band == 'H':
```

```
                match_num = 1
        elif match_band == 'K':
                match_num = 2
        else:
                print 'Input match_band parameter'
                exit()

        file = open('%s.cent' %infile ,"w")
        file.write("%s %s\n" % (imcent_x,imcent_y))
        file.close()
        if os.path.exists('%slocal.cent' % infile):
                os.system('rm %slocal.cent' % infile)
        iraf.wcsctran('%s.cent' % infile, '%slocal.cent' % infile, infile, \
'logical', 'world', columns="1 2", formats="%.6f %.6f")
        file = open('%s/%s.coo' % (rcParams['OUTPUT_DIR'],tmass_file),"w")
        for i in range(len(tmass_ra)):
                if list(tmass_flag_ccflg[i])[match_num].isdigit(): # Contamination check
                        if list(tmass_flag_phqual[i])[match_num]=='A' or \
        list(tmass_flag_phqual[i])[match_num]=='B' or \
        list(tmass_flag_phqual[i])[match_num]=='C' or \
        list(tmass_flag_phqual[i])[match_num]=='D' or \
        list(tmass_flag_phqual[i])[match_num]=='E': # Quality check
                                if float(list(tmass_flag_blflg[i])[match_num])==1: # Blend flag
                                        if tmass_mag[i] < mag_thrs:
                                                file.write("%s %s %s\n" % (tmass_ra[i],tmass_dec[i],tmass_mag[i]))
                                                tmass_ra_sel.append(tmass_ra[i])
                                                tmass_dec_sel.append(tmass_dec[i])
                                                tmass_mag_sel.append(tmass_mag[i])
        file.close()
        file = open('%stmass.reg' % infile,"w")
        file.write('global color=cyan font=\"helvetica 10 normal\" \
select=1 edit=1 move=1 delete=1 include=1 fixed=0 source\n')
        for i in range(len(tmass_ra_sel)):
                rah = float(tmass_ra_sel[i])/360.*24
                ram = (rah-int(rah))*60
                ras = (ram-int(ram))*60
                ded = float(tmass_dec_sel[i])
                if ded < 0:
                        dec = - ded
                else:
                        dec = ded
                dem = (dec-int(dec))*60
                des = (dem-int(dem))*60
                file.write("fk5;circle(%s:%s:%s,%s:%s:%s,0.0005)\n" \
   % (int(rah),int(ram),ras,int(ded),int(dem),des))
        file.close()

        i = 0
        for line in open('%slocal.cent' % infile,"r"):
                i += 1
                if i >3:
                        center_data = line.split(' ')
                        imcent_x_wcs=float(center_data[0])
                        imcent_y_wcs=float(center_data[1])
        os.system('./OPM/local_coordinate_degree %s/%s.coo %sopm.coo %s %s %s' \
% (rcParams['OUTPUT_DIR'],tmass_file,infile,imcent_x_wcs,imcent_y_wcs,size))
        opmcoo_data = []
        opmcoo_x1 = []
        opmcoo_y1 = []
        i = 0
        for line in open('%sopm.coo' % infile, 'r'):
                i += 1
                opmcoo_data = line.split(' ')
                while opmcoo_data.count('') > 0:
                        opmcoo_data.remove('')
                opmcoo_x1.append(opmcoo_data[0])
                opmcoo_y1.append(opmcoo_data[1])


        #___ OPM
        if os.path.exists('%sopmout.dat' % infile):
                os.system('rm %sopmout.dat' % infile)
        os.system('./OPM/opm %sphot.dat %sopm.coo %sopmout.dat %sopm.param' % (infile,infile,outfile,infile))
        self._remove("%s.fits" % outfile)
```

```
        iraf.imcopy(infile, outfile)
        i = 0
        for line in open('%sopmout.dat' % outfile, 'r'):
            i += 1
            if line.split(' ')[0] != '#':
                opmout_data = line.split(' ')
                while opmout_data.count('') > 0:
                    opmout_data.remove('')
                opmdata_x1.append(opmout_data[1])
                opmdata_y1.append(opmout_data[2])
                opmdata_x2.append(opmout_data[7])
                opmdata_y2.append(opmout_data[8])
                n = 0
                for k in range(len(tmass_ra_sel)):
                    n += 1
                    if float(opmout_data[6]) == n:
                        rah = float(tmass_ra_sel[k])/360.*24
                        ram = (rah-int  (rah))*60
                        ras = (ram-int(ram))*60
                        ded = float(tmass_dec_sel[k])
                        if ded < 0:
                            dec = - ded
                        else:
                            dec = ded
                        dem = (dec-int(dec))*60
                        des = (dem-int(dem))*60
                        opmdata_ra.append('%s:%s:%s' % (int(rah),int(ram),ras))
                        if int(ded) == 0 and ded < 0:
                            opmdata_de.append('-%s:%s:%s' % (int(ded),int(dem),des))
                        else:
                            opmdata_de.append('%s:%s:%s' % (int(ded),int(dem),des))
                        break

                #for i in range(len(tmass_ra_sel)):
                #   if (float(opmcoo_x1[i]))**2 + (float(opmcoo_y1[i]))**2 < Halfsize**2:
                #       n += 1
                #       if float(opmout_data[6]) == n:
                #           rah = float(tmass_ra_sel[i])/360.*24
                #           ram = (rah-int  (rah))*60
                #           ras = (ram-int(ram))*60
                #           ded = float(tmass_dec_sel[i])
                #           if ded < 0:
                #               dec = - ded
                #           else:
                #               dec = ded
                #           dem = (dec-int(dec))*60
                #           des = (dem-int(dem))*60
                #           opmdata_ra.append('%s:%s:%s' % (int(rah),int(ram),ras))
                #           opmdata_de.append('%s:%s:%s' % (int(ded),int(dem),des))
                #           break
                #for i in range(len(tmass_ra_sel)):
                #   if opmout_data[9] == '%0.3f' % tmass_mag_sel[i]:
                #       rah = float(tmass_ra_sel[i])/360.*24
                #       ram = (rah-int  (rah))*60
                #       ras = (ram-int(ram))*60
                #       ded = float(tmass_dec_sel[i])
                #       if ded < 0:
                #           dec = - ded
                #       else:
                #           dec = ded
                #       dem = (dec-int(dec))*60
                #       des = (dem-int(dem))*60
                #       opmdata_ra.append('%s:%s:%s' % (int(rah),int(ram),ras))
                #       opmdata_de.append('%s:%s:%s' % (int(ded),int(dem),des))
                #       break
        file = open('%sopmsf.dat' % outfile,"w")
        for i in range(len(opmdata_x2)):
            file.write("%s %s\n" % (opmdata_x2[i],opmdata_y2[i]))
        file.close()
        if os.path.exists('%sopmsf_wcs.dat' % outfile):
            os.system('rm %sopmsf_wcs.dat' % outfile)
        iraf.wcsctran('%sopmsf.dat' % outfile, '%sopmsf_wcs.dat' \
   % outfile, infile, 'logical', 'world', columns="1 2", formats="%.6f %.6f")
        i = 0
        opmdata_x2_wcs=[]
        opmdata_y2_wcs=[]
```

```
                for line in open('%sopmsf_wcs.dat' % outfile, 'r'):
                        i += 1
                        if i > 3:
                                opmout_data = line.split(' ')
                                opmdata_x2_wcs.append(opmout_data[0])
                                opmdata_y2_wcs.append(opmout_data[1])

                ###___for match file
                file = open('%s.match' % outfile,"w")
                for i in range(len(opmdata_x1)):
                        file.write("%s %s %s %s\n" % (opmdata_x1[i],opmdata_y1[i],opmdata_ra[i],opmdata_de[i]))
                file.close()
                file = open('%smatch.reg' % outfile,"w")
                file.write('global color=green font=\"helvetica 10 normal\" \
        select=1 edit=1 move=1 delete=1 include=1 fixed=0 source\n')
                for i in range(len(opmdata_x1)):
                        file.write("fk5;circle(%s,%s,0.0005) # color=cyan\n" % (opmdata_ra[i],opmdata_de[i]))
                        file.write("physical;circle(%s,%s,10)\n" % (opmdata_x1[i],opmdata_y1[i]))
                file.close()
                if os.path.exists('%s.fits' % outfile):
                        os.system('rm %s.fits' % outfile)
                iraf.imcopy(infile, outfile)
                file = open('%s.plt' % outfile,"w")
                file.write('f\n')
                file.write(': .snap eps\n')
                file.write('q\n')
                file.close()
                if os.path.exists('%s.ccmap' % outfile):
                        os.system('rm %s.ccmap' % outfile)
                iraf.ccmap('%s.match' % outfile, '%s.db' % outfile,xcolumn=1,ycolumn=2, \
        lngcolumn=3,latcolumn=4,lngunit='hours',latunits='degrees', \
        projection='tnx', xxorder=2, xyorder=2, yxorder=2, yyorder=2, \
        results='%s.ccmap' % outfile, maxiter=3, reject=3, interactive='no', \
        cursor='%s.plt' % outfile)
                iraf.ccsetwcs(outfile, '%s.db' % outfile, '%s.match' % outfile)

                if clean == 'yes':
                        os.system('rm %sopm.param' % infile)
                        os.system('rm %stmpdata.par' % infile)
                        os.system('rm %stmpcenter.par' % infile)
                        os.system('rm %stmpfitsky.par' % infile)
                        os.system('rm %stmpphot.par' % infile)
                        os.system('rm %sdao.coo' % infile)
                        os.system('rm %s.phot' % infile)
                        os.system('rm %s.cent' % infile)
                        os.system('rm %slocal.cent' % infile)
                        os.system('rm %sopm.coo' % infile)
                        os.system('rm %sphot.dat' % infile)
                        os.system('rm %sopmout.dat' % outfile)
                        os.system('rm %sopmsf.dat' % outfile)
                        os.system('rm %sopmsf_wcs.dat' % outfile)
                        #os.system('rm %s.match' % outfile)
                        #os.system('rm %s.ccmap' % outfile)
                        #os.system('rm %s.db' % outfile)
                        #os.system('rm %s.plt' % outfile)

                logger.debug("'{0:s}' map wcs using opm.".format(outfile))
                self._add_history(os.path.basename(outfile))
                return

         #___ get_catalog ____________________________________________________________
         def get_catalog(self, outfile=None, imSIZE=300):
                infile = self._get_infilename()
                RA = iraf.hselect(infile,"RA2000","yes",Stdout=-1)
                DEC = iraf.hselect(infile,"DEC2000","yes",Stdout=-1)
                imRA = RA[0].split(':')
                imDEC = DEC[0].split(':')
                url = "http://irsa.ipac.caltech.edu/cgi-bin/Gator/nph-query? \
       outfmt=1&objstr=%sh%sm%ss+%sd%sm%ss&spatial=Cone&radius=%s&radunits=arcsec&catalog=fp_psc" \
        % (imRA[0],imRA[1],imRA[2],imDEC[0],imDEC[1],imDEC[2],imSIZE)
                if outfile is None :
```

```
                        if not os.path.exists("./2mass/%s.tbl" % self.__history[0]):
                                urllib.urlretrieve(url,"./2mass/%s.tbl" % self.__history[0])
                else:
                        if not os.path.exists("./2mass/%s.tbl" % outfile):
                                urllib.urlretrieve(url,"./2mass/%s.tbl" % outfile)
                return

        #___ cos_clean ____________________________________________________________
        def cos_clean(self):
                """Remove cosmic ray.

                This function produces object masks by using run objmask().

                Args:
                        dist_map: a distosion map file (file).
                        Default: rcParams["DIST"]

                Returns:
                        None

                Intermediate files:
                        None

                Raises:
                        logger.error: An error occurred when no distosion map found."""

                infile = self._get_infilename()
                outfile = self._get_outfilename(rcParams['CO'])
                if os.path.exists('%s.fits' % outfile):
                        os.system('rm %s.fits' % outfile)
                if os.path.exists('%stmp1.fits' % outfile):
                        os.system('rm %stmp1.fits' % outfile)
                if os.path.exists('%stmp2.fits' % outfile):
                        os.system('rm %stmp2.fits' % outfile)
                iraf.median(infile,'%stmp1.fits' % outfile,5,5)
                iraf.imarith(infile,'-','%stmp1.fits' % outfile,'%stmp2.fits' % outfile)
                Repthres = float(iraf.imstat('%stmp2.fits' % outfile,nclip=3, \
       fields='stddev',format='no',Stdout=-1)[0])
                iraf.imreplace('%stmp2.fits' % outfile, 0, upper='%s'% (Repthres*3))
                iraf.imreplace('%stmp2.fits' % outfile, 1, lower='%s'% (Repthres*3))
                iraf.imcopy(infile,outfile)
                iraf.fixpix(outfile,'%stmp2.fits' % outfile)
                logger.debug("'{0:s}' remove cosmic rays.".format(outfile))
                self._add_history(os.path.basename(outfile))
                return


        #___ cos_remove ____________________________________________________________
        def cos_remove(self):
                """Remove cosmic ray.

                        This function produces object masks by using run objmask().

                        Args:
                        dist_map: a distosion map file (file).
                        Default: rcParams["DIST"]

                        Returns:
                        None

                        Intermediate files:
                        None

                        Raises:
                        logger.error: An error occurred when no distosion map found."""

                infile = self._get_infilename()
                outfile = self._get_outfilename(rcParams['CO'])
                if os.path.exists('%s.fits' % outfile):
                        os.system('rm %s.fits' % outfile)

                iraf.noao(Stdout=-1)
                iraf.imred(Stdout=-1)
                iraf.crutil(Stdout=-1)
                #iraf.cosmicrays(infile,outfile,npasses=3,fluxratio=0.01,interactive='No')
                #iraf.cosmicrays(infile,outfile,npasses=3,fluxratio=0.1,interactive='No')
```

```
            iraf.cosmicrays(infile,outfile,interactive='No')

            logger.debug("'{0:s}' remove cosmic rays.".format(outfile))
            self._add_history(os.path.basename(outfile))
            return


    #___ cp_image ______________________________________________________________
    def cp_image(self, outfile=None):
            """Copy a file to a directory.

            Copy or rename a FITS file.
            The file to be created will be overwritten if exists.

            Args:
                    outfile: a FITS filename of output frame to be copyed (string).
                    Default: rcParams["OUTPUT_DIR"]

            Returns:
                    None

            Intermediate files:
                    None

            Raises:
                    logger.error: An error occurred when no rcParams["OUTPUT_DIR"] found."""

            if outfile is None:
                    if "OUTPUT_DIR" in rcParams:
                            outfile = rcParams["OUTPUT_DIR"]
            infile = rcParams["DATA_DIR"] + "/" + self.__history[-1]
            outfile = rcParams["OUTPUT_DIR"] + "/" + self.__history[-1]
            self._remove("%s.fits" % outfile)
            iraf.imcopy(infile, outfile)
            logger.debug("'%s' ---> '%s' copy." % (infile,outfile))
            return

    #___ sub_dark ______________________________________________________________
    def sub_dark(self, dark_frame=None):
            """Subtracts dark from the data.

            Subtracts dark level from the data, and creates a FITS file prefixed
            with rcParams["DARK"].
            The file to be created will be overwritten if exists.

            Args:
                    dark_frame: a FITS filename of dark frame to be used (string).
                    Default: rcParams["DARK"]

            Returns:
                    None

            Intermediate files:
                    None

            Raises:
                    logger.error: An error occurred when no dark frame found."""

            if dark_frame is None:
                    if "DARK" in rcParams:
                            dark_frame = rcParams["DARK"]
            if dark_frame is None:
                    logger.error("No dark frame found.")
                    raise ValueError("No dark frame found.")
            elif not os.path.exists(dark_frame):
                    logger.error("No such dark frame.")
                    raise ValueError("No such dark frame.")
            infile = self._get_infilename()
            outfile = self._get_outfilename(rcParams["DF"])
            self._remove("%s.fits" % outfile)
            iraf.imarith(infile, "-", dark_frame, outfile)
            logger.debug("'{0:s}' dark subtracted done.".format(outfile))
            self._add_history(os.path.basename(outfile))
            return

    #___ sub_sky _______________________________________________________________
    def sub_sky(self, infile, skyfile=None, selfsky=True, imsurf=False, clean=True):
```

```
        """Subtracts sky from the data.

        Subtracts sky level from the data, and creates a FITS file prefixed
        with rcParams["SS"]. If file name of sky frame is set as option, the sky
        subtraction is done by it. By setting a list of fits number as input
        parameter, a self-sky flat can be produced with using the list.
        The file to be created will be overwritten if exists.

        Args:
            sky_frame: a FITS filename of sky frame to be used (string).
            Default: file list with full path

        Returns:
            None

        Intermediate files:
            tmp_sky: combined sky frame

        Raises:
            logger.error: An error occurred when no dark frame found."""

        outfile = self._get_outfilename(rcParams["SS"])

        if selfsky is False:
            if not "SKY" in rcParams:
                logger.error("No such skyfile and skyframe.")
                raise ValueError("No such skyfile and skyframe.")
            else:
                tmpsky_frame = rcParams["SKY"]
                if os.path.exists('%s/tmp_sky.fits' % rcParams['OUTPUT_DIR']):
                    self._remove('%s/tmp_sky.fits' % rcParams['OUTPUT_DIR'])
                med_infle = iraf.imstatistics(infile, nclip='10', fields='mean', Stdout=-1)
                med_sky = iraf.imstatistics(tmpsky_frame, nclip='10', fields='mean', Stdout=-1)
                diff_med = float(med_infle[1]) - float(med_sky[1])
                iraf.imarith(tmpsky_frame, "+", diff_med, '%s/tmp_sky.fits' % rcParams['OUTPUT_DIR'])
                sky_frame = '%s/tmp_sky' % rcParams['OUTPUT_DIR']

        if selfsky is True:
            if skyfile is None:
                logger.error("No skyfile.")
                raise ValueError("No skyfile.")
            else:
                tmpsky_frame = ','.join(skyfile)
                if os.path.exists('%s/tmp_sky.fits' % rcParams['OUTPUT_DIR']):
                    self._remove('%s/tmp_sky.fits' % rcParams['OUTPUT_DIR'])
                if iraf.hselect(infile,'OBJMASK','yes',Stdout=-1) != ['']:
                    imcomlog = iraf.imcombine(tmpsky_frame,'%s/tmp_sky.fits'%rcParams['OUTPUT_DIR'],\
        combine='average',masktype='!OBJMASK',maskvalue=0, reject='avsigclip', Stdout=-1)
                else:
                    print tmpsky_frame
                    imcomlog = iraf.imcombine(tmpsky_frame,'%s/tmp_sky.fits'%rcParams['OUTPUT_DIR'],\
         combine='median',masktype='none',reject='avsigclip', Stdout=-1)
                sky_frame = '%s/tmp_sky' % rcParams['OUTPUT_DIR']

        self._remove("%s.fits" % outfile)
        iraf.imarith(infile, "-", sky_frame, outfile)
        #if imsurf == 'yes':
        #       iraf.imcopy(tmpsky.fits, tmpsky2.fits)
        #       imsurfit tmpsky2.fits tmpsky3.fits function=chebyshev xorder=2 \
        #   yorder=2 type_output="fit" niter=10
        #       imarith tmpsky.fits - tmpsky3.fits sky_ANIA000${FITSN}.fits

        logger.debug("'{0:s}' sky subtracted done.".format(outfile))
        #logger.debug("%s" % ('\n'.join(imcomlog)))
        self._add_history(os.path.basename(outfile))
        if clean is True:
            if os.path.exists('%s/tmp_sky.fits' % rcParams['OUTPUT_DIR']):
                self._remove('%s/tmp_sky.fits' % rcParams['OUTPUT_DIR'])
        return

    def sub_sky0(self, infile, skyfiles=None, skyframe=None):
        logger.info(" Sky subtraction for '{0}'.".format(infile))
```

```
        outfile = self._get_outfilename(rcParams["SS"])

        selfsky_frame = '%s/tmp_sky.fits' % rcParams['OUTPUT_DIR']
        tmpfiles = [selfsky_frame]
        _remove(tmpfiles)

        if skyframe is None and skyfiles is None:
            _error(ValueError, "Either 'skyfiles' or 'skyframe' must be set.")

        if skyframe is True:
            if "SKY" in rcParams:
                skyframe = rcParams["SKY"]
            else:
                ### How do you handle this case? ###
                skyframe

        if skyframe is None:
            skyframe = '%s/tmp_sky' % rcParams['OUTPUT_DIR']
            skyfiles = ','.join(skyfiles)
            logger.info("  Making a self sky frame using [{0}] ...".format(skyfiles))
            if iraf.hselect(infile, 'OBJMASK', 'yes', Stdout=-1) != ['']:
                imcomlog = iraf.imcombine(skyfiles, selfsky_frame, combine='average', \
       masktype='!OBJMASK', maskvalue=0,  reject='avsigclip', Stdout=-1)
            else:
                imcomlog = iraf.imcombine(skyfiles, selfsky_frame, combine='median', \
      masktype='none', reject='avsigclip', Stdout=-1)
            logger.debug("\n".join(imcomlog))


        logger.info("  Subtracting the sky frame...")
        _remove("%s.fits" % outfile)
        iraf.imarith(infile, "-", skyframe, outfile)

        self._add_history(os.path.basename(outfile))
        _remove(tmpfiles)
        logger.info(" Done.")
        return

    #___ div_flat _____________________________________________________________
    def div_flat(self, flat_frame=None, overwrite=True):
        """Divided by flat from the data.

        Divide image by flat fram. You can set flat frame as input parameter.
        If you set flat frame as input parameter, the input file deal with it as
        priority, and If rcParam['FLAT'] is not set and input file equals None,
        pro_flat() is run in this function at first. After running pro_flat(),
        'self flat.fits' file is produced, and use the output as flat frame.
        You can set pro_flat() parameters as option in this function. After this
        procedure, the prefix character 'ff' is added to the default output filename.

        Args:
            dark_frame: a FITS filename of flat frame to be used (string).
            Default: rcParams["FLAT"]

        Returns:
            None

        Intermediate files:
            None

        Raises:
            logger.error: An error occurred when no flat frame found."""

        if flat_frame is None:
            if "FLAT" in rcParams:
                flat_frame = rcParams["FLAT"]

        if flat_frame is None:
            logger.error("No flat frame found.")
            raise ValueError("No flat frame found.")
        elif not os.path.exists(flat_frame):
            logger.error("No such flat frame.")
            raise ValueError("No such flat frame.")
        infile = self._get_infilename()
        outfile = self._get_outfilename(rcParams["FF"])
```

```
            if overwrite == True:
                self._remove("%s.fits" % outfile)

            try:
                iraf.imarith(infile, "/", flat_frame, outfile)
            except iraf.IrafError as err:
                logger.exception(err)
                raise

            logger.debug("'{0:s}' flat divided done.".format(outfile))
            self._add_history(os.path.basename(outfile))
            return

    #___ cor_dist ______________________________________________________________
    def cor_dist(self, dist_map=None):
        """Correct Distorsion with distorsion map.

        This function correct distorsion with distorsion map. You can set
        distorsion map file as input parameter. If you do not set it, and error
        is occured. After this procedure, the prefix character 'dc' is added to
        the default output file name.

        Args:
            dist_map: a distosion map file (file).
            Default: rcParams["DIST"]

        Returns:
            None

        Intermediate files:
            None

        Raises:
            logger.error: An error occurred when no distosion map found."""
        """
        if dist_map is None:
            if "DIST" in rcParams:
                dist_map = rcParams["DIST"]

        if dist_map is None:
            logger.error("No flat frame found.")
            raise ValueError("No flat frame found.")
        elif not os.path.exists(flat_frame):
            logger.error("No such flat frame.")
            raise ValueError("No such flat frame.")

        infile = rcParams["OUTPUT_DIR"] + "/" + self.__history[-1]
        outfile = rcParams["OUTPUT_DIR"] + "/" + rcParams["FF"] + self.__history[-1]

        self._remove("%s.fits" % outfile)

        iraf.imarith(infile, "/", flat_frame, outfile)
        logger.debug("'{0:s}' flat divided done.".format(outfile))
        self._add_history(os.path.basename(outfile))
        """
        return

    #___ run_sextractor _______________________________________________________
    def run_sextractor(self):
        """Create object mask with sextractor.

        This function produces object masks by using run sextractor().

        Args:
            dist_map: a distosion map file (file).
            Default: rcParams["DIST"]

        Returns:
            None

        Intermediate files:
            None

        Raises:
            logger.error: An error occurred when no distosion map found."""
        """

```

```
        """
        return

    #___ run_objmask __________________________________________________________
    def run_objmask(self,infile_name=None,outfile_name=None):
        """Create object mask with iraf objmasks.

        This function produces object masks by using run objmask().

        Args:
            dist_map: a distosion map file (file).
            Default: rcParams["DIST"]

        Returns:
            None

        Intermediate files:
            None

        Raises:
            logger.error: An error occurred when no distosion map found."""

        if infile_name is None:
            infile = self._get_infilename()
        else:
            infile = rcParams["OUTPUT_DIR"] + "/" + infile_name
        if outfile_name is None:
            outfile = rcParams["OUTPUT_DIR"] + "/" + rcParams["OBJMASK"] + self.__history[-1]
        else:
            outfile = rcParams["OUTPUT_DIR"] + "/" + rcParams["OBJMASK"] + infile_name
        self._remove("%s.pl" % outfile)
        iraf.noao.nproto(Stdout=-1)
        iraf.objmasks(infile, "%s.pl" % outfile, omtype='boolean', masks='', hsigma=5)
        logger.debug("'{0:s}' create objectmask done.".format(outfile))
        #self._add_history(os.path.basename(infile))
        return

    #___ pro_register _________________________________________________________
    def pro_register(self):
        """Shift Images.

        This function produces object masks by using run objmask().

        Args:
            dist_map: a distosion map file (file).
            Default: rcParams["DIST"]

        Returns:
            None

        Intermediate files:
            None

        Raises:
            logger.error: An error occurred when no distosion map found."""

        infile = self._get_infilename()
        outfile = self._get_outfilename(rcParams["RE"])
        if os.path.exists('%s.fits' % outfile):
            os.system('rm %s.fits' % outfile)
        if os.path.exists('%s_bpm.pl' % outfile):
            os.system('rm %s_bpm.pl' % outfile)
        iraf.mscred(Stdout=-1)
        iraf.mscimage(infile,outfile,fluxcon='yes',ntrim=10)
        logger.debug("'{0:s}' shift images.".format(outfile))
        self._add_history(os.path.basename(outfile))
        return


    #___ Calculate magzero and system efficiency ______________________________
    def calc_sys(self,tmass_file,infile_name=None, filter_band='Ks', \
   mag_thrsh=12.0, mag_thrsl=17.5, apert=10, unit='ADU', display=True):
        """Shift Images.

            This function produces object masks by using run objmask().

```

```
                Args:
                dist_map: a distosion map file (file).
                Default: rcParams["DIST"]

                Returns:
                None

                Intermediate files:
                None

                Raises:
                logger.error: An error occurred when no distosion map found."""
        if infile_name is None:
                infile = self._get_infilename()
                outfile = self._get_outfilename(rcParams["CAL"])
        else:
                infile = rcParams["OUTPUT_DIR"] + "/" + infile_name
                outfile = rcParams["OUTPUT_DIR"] + "/" + rcParams["CAL"] + infile_name

        if os.path.exists('%s.fits' % outfile):
                os.system('rm %s.fits' % outfile)

        tmass_ra, tmass_dec = [], []
        tmass_ra2, tmass_dec2 = [], []
        tmass_ra_sel, tmass_dec_sel, tmass_mag_sel1, tmass_mag_sel2= [], [], [], []
        tmass_mag1, tmass_mag2, tmass_magj, tmass_magh, tmass_magk = [], [], [], [], []
        tmass_flag_phqual, tmass_flag_rdflg, tmass_flag_blflg, tmass_flag_ccflg = [], [], [], []
        center_x, center_y, center_flg = [], [], []
        magzero, syseff, mag_ab = [], [], []
        magzero_error, syseff_error = [], []
        x_axis, y_axis = [], []

        h = 6.62606957e-34
        convf = 3.4

        i = 0
        for line in open('./2mass/%s.tbl' % tmass_file, 'r'):
                if i > 100 and line.split(' ')[0] != '\\' and line.split(' ')[0] != '|':
                        tmass_data = line.split(' ')
                        while tmass_data.count('') > 0:
                                tmass_data.remove('')
                        tmass_ra.append(tmass_data[0])
                        tmass_dec.append(tmass_data[1])
                        tmass_magj.append(float(tmass_data[8])+0.893845) #ABmag-J
                        tmass_magh.append(float(tmass_data[12])+1.37432) #ABmag-H
                        tmass_magk.append(float(tmass_data[16])+1.84024) #ABmag-K
                        tmass_flag_phqual.append(tmass_data[20])
                        tmass_flag_rdflg.append(tmass_data[21])
                        tmass_flag_blflg.append(tmass_data[22])
                        tmass_flag_ccflg.append(tmass_data[23])
                i += 1

        exptime = float(iraf.hselect('%s.fits' % infile,"EXPTIME","yes",Stdout=-1)[0])


        #___ Filter selection
        if filter_band is 'Y':
                LAM=1.03779
                DLAM=0.0993
                BAND1 = 'J'
                BAND2 = 'H'
        elif filter_band is 'J':
                LAM=1.275
                DLAM=0.1586
                BAND1 = 'J'
                BAND2 = 'H'
        elif filter_band is 'H':
                LAM=1.673
                DLAM=0.297
                BAND1 = 'J'
                BAND2 = 'H'
        elif filter_band is 'Ks':
                LAM=2.14879
                DLAM=0.3215
                BAND1 = 'H'
                BAND2 = 'Ks'
        elif filter_band is 'N207':
```

```
			LAM=2.074
			DLAM=0.041
			BAND1 = 'H'
			BAND2 = 'Ks'
		elif filter_band is 'Paa':
			LAM=1.87539
			DLAM=0.0079
			BAND1 = 'H'
			BAND2 = 'Ks'
		elif filter_band is 'Paaoff':
			LAM=1.90925
			DLAM=0.0326
			#DLAM=0.309
			BAND1 = 'H'
			BAND2 = 'Ks'
		elif filter_band is 'Pab':
			LAM=1.28126
			DLAM=0.024
			BAND1 = 'J'
			BAND2 = 'H'
		elif filter_band is 'Paboff':
			LAM=1.326
			DLAM=0.034
			BAND1 = 'J'
			BAND2 = 'H'
		else:
			print "Please set filter_band"
			print "Y,J,H,Ks,N207,Paa,Paaoff,Pab,Paboff"

		#___ Set 2MASS Filter Parameters
		if BAND1 is 'H':
			LAM1=1.662
			tmass_mag1 = tmass_magh
			match_num = 1
		elif BAND1 is 'Ks':
			LAM1=2.159
			tmass_mag1 = tmass_magk
			match_num = 2
		else:
			LAM1=1.235
			tmass_mag1 = tmass_magj
			match_num = 0

		if BAND2 is 'H':
			LAM2=1.662
			tmass_mag2 = tmass_magh
		elif BAND2 is 'J':
			LAM2=1.235
			tmass_mag2 = tmass_magj
		else:
			LAM2=2.159
			tmass_mag2 = tmass_magk


		file = open('%s/%s.coo' % (rcParams['OUTPUT_DIR'],tmass_file),"w")
		for i in range(len(tmass_ra)):
			if list(tmass_flag_ccflg[i])[match_num].isdigit(): # Contamination check
				if list(tmass_flag_phqual[i])[match_num]=='A' or \
		list(tmass_flag_phqual[i])[match_num]=='B' or \
		list(tmass_flag_phqual[i])[match_num]=='C' or \
		list(tmass_flag_phqual[i])[match_num]=='D' or \
		list(tmass_flag_phqual[i])[match_num]=='E': # Quality check
						if float(list(tmass_flag_blflg[i])[match_num])==1: # Blend flag
							if tmass_mag1[i] <= mag_thrsl and tmass_mag1[i] >= mag_thrsh:
								file.write("%s %s\n" % (tmass_ra[i],tmass_dec[i]))
								tmass_ra_sel.append(tmass_ra[i])
								tmass_dec_sel.append(tmass_dec[i])
								tmass_mag_sel1.append(tmass_mag1[i])
								tmass_mag_sel2.append(tmass_mag2[i])

		file.close()

		file = open('%stmass.reg' % infile,"w")
		file.write('global color=cyan font=\"helvetica 10 normal\" \
	select=1 edit=1 move=1 delete=1 include=1 fixed=0 source\n')
		for i in range(len(tmass_ra_sel)):
			rah = float(tmass_ra_sel[i])/360.*24
			ram = (rah-int(rah))*60
```

```
                ras = (ram-int(ram))*60
                ded = float(tmass_dec_sel[i])
                if ded < 0:
                        dec = - ded
                else:
                        dec = ded
                dem = (dec-int(dec))*60
                des = (dem-int(dem))*60
                file.write("fk5;circle(%s:%s:%s,%s:%s:%s,0.0005)\n" \
    % (int(rah),int(ram),ras,int(ded),int(dem),des))
        file.close()

        #___ photometery
        if os.path.exists('%s.phot' % infile):
                os.system('rm %s.phot' % infile)
        iraf.noao(Stdout=-1)
        iraf.digiphot(Stdout=-1)
        iraf.apphot(Stdout=-1)

        iraf.phot('%s.fits' % infile, output='%s.phot' % infile, apertures=apert, \
coords='%s/%s.coo' % (rcParams['OUTPUT_DIR'],tmass_file), annulus=(apert+1), \
dannulu='20',wcsin='world',verify='NO',inter='NO')
        flux = iraf.pdump('%s.phot' % infile, 'FLUX', 'yes', Stdout=-1)
        stdev = iraf.pdump('%s.phot' % infile, 'STDEV', 'yes', Stdout=-1)
        area = iraf.pdump('%s.phot' % infile, 'AREA', 'yes', Stdout=-1)
        xcenter = iraf.pdump('%s.phot' % infile, 'XCENTER', 'yes', Stdout=-1)
        ycenter = iraf.pdump('%s.phot' % infile, 'YCENTER', 'yes', Stdout=-1)

        for i in range(len(flux)):
                if float(flux[i]) > 0:
                        inp_mag = np.log10(LAM)*(tmass_mag_sel1[i]-tmass_mag_sel2[i])/(np.log10(LAM1) \
       -np.log10(LAM2)) + (np.log10(LAM1)*tmass_mag_sel2[i]-np.log10(LAM2)* \
       tmass_mag_sel1[i])/(np.log10(LAM1)-np.log10(LAM2))
                        mag_ab.append(inp_mag)
                        magzero_tmp = inp_mag + 2.5*np.log10(float(flux[i])/exptime)
                        magzero_tmp_error = inp_mag + 2.5*np.log10( (float(flux[i]) + \
       float(stdev[i])*np.sqrt(float(area[i])))/exptime) - magzero_tmp
                        magzero.append( magzero_tmp )
                        magzero_error.append( magzero_tmp_error )
                        syseff.append( convf*h*LAM/(np.pi*0.5**2*3630*10**(-26)*DLAM*10**(-magzero_tmp/2.5)) )
                        syseff_error.append( convf*h*LAM/(np.pi*0.5**2*3630*10**(-26)* \
       DLAM*10**(-magzero_tmp_error/2.5) ) )
                        x_axis.append( float(xcenter[i]) )
                        y_axis.append( float(ycenter[i]) )

        file = open('%s.photlst' % infile,"w")
        for i in range(len(x_axis)):
                file.write("%s\t%s\t%s\n" % (x_axis[i],y_axis[i],syseff[i]))
        file.close()

        magzero_tmp = []
        magzero_error_tmp = []
        syseff_tmp = []
        syseff_error_tmp = []
        magzero_clp = magzero
        magzero_error_clp = magzero_error
        syseff_clp = syseff
        syseff_error_clp = syseff_error
        n = 0
        while n <5:
                magzero_clp = np.array(magzero_clp)
                magzero_error_clp = np.array(magzero_error_clp)
                syseff_clp = np.array(syseff_clp)
                syseff_error_clp = np.array(syseff_error_clp)
                magzero_ave = np.average(magzero_clp)
                syseff_ave = np.average(syseff_clp)
                magzero_std = np.std(magzero_clp)
                syseff_std = np.std(syseff_clp)
                for i in range(len(magzero_clp)):
                        if np.abs(magzero_clp[i]-magzero_ave) <= magzero_std*5:
                                magzero_tmp.append(magzero_clp[i])
                                magzero_error_tmp.append(magzero_error_clp[i])
```

```
                        for i in range(len(syseff_clp)):
                                if np.abs(syseff_clp[i]-syseff_ave) <= syseff_std*3:
                                        syseff_tmp.append(syseff_clp[i])
                                        syseff_error_tmp.append(syseff_error_clp[i])
                        magzero_clp = magzero_tmp
                        magzero_error_clp = magzero_error_tmp
                        syseff_clp = syseff_tmp
                        syseff_error_clp = syseff_error_tmp
                        n += 1


                if unit == 'jy':
                        cal_factor = 3630/(10**(0.4*np.average(magzero_clp)))/exptime
                        iraf.imarith('%s.fits' % infile,'*',cal_factor,'%s.fits' % outfile)
                        iraf.hedit('%s.fits' % outfile, fields='CAL_UNIT', value='Jy', add='Yes', verify='No')
                        print "Set unit = Jy"
                else:
                        cal_factor = exptime
                        iraf.imarith('%s.fits' % infile,'/',cal_factor,'%s.fits' % outfile)
                        iraf.hedit('%s.fits' % outfile, fields='CAL_UNIT', value='ADU/s', add='Yes', verify='No')
                        print "Set unit = ADU/sec"


                iraf.hedit('%s.fits' % outfile, fields='ZMAG_AB', \
       value=np.average(magzero_clp), add='Yes', verify='No')
                iraf.hedit('%s.fits' % outfile, fields='ZMAG_ERR', \
       value=np.std(magzero_clp), add='Yes', verify='No')
                iraf.hedit('%s.fits' % outfile, fields='SYS_EFF', \
       value=np.average(syseff_clp), add='Yes', verify='No')
                iraf.hedit('%s.fits' % outfile, fields='SYS_ERR', \
       value=np.std(syseff_clp), add='Yes', verify='No')
                #print np.average(magzero), np.average(syseff)


                if display is True:
                        from matplotlib.pyplot import *
                        ax1 = subplot(2,1,1)
                        ax1.errorbar(mag_ab,magzero,yerr=[magzero_error,magzero_error],xerr=None,fmt='ko')
                        ax1.plot([0,25],[np.average(magzero_clp),np.average(magzero_clp)],'r-')
                        ax1.set_xlim(10,19)
                        ax1.set_ylim(np.min(magzero_clp)*0.95,np.max(magzero_clp)*1.05)
                        ylabel('MagZero')
                        figtext(0.15,0.85,'MagZero = %0.2f$\pm$%0.2f' \
          % (np.average(magzero_clp),np.std(magzero_clp)),fontsize='10')
                        setp( ax1.get_xticklabels(), fontsize='15')
                        setp( ax1.get_yticklabels(), fontsize='15')

                        ax2 = subplot(2,1,2)
                        ax2.errorbar(mag_ab,syseff,yerr=[syseff_error,syseff_error],xerr=None,fmt='ko')
                        ax2.plot([0,25],[np.average(syseff_clp),np.average(syseff_clp)],'r-')
                        ax2.set_xlim(10,19)
                        ax2.set_ylim(np.min(syseff_clp)*0.8,np.max(syseff_clp)*1.2)
                        ylabel('SysEff')
                        xlabel('AB Magnitude (%s)' % filter_band)
                        figtext(0.15,0.4,'SysEff = %0.2f$\pm$%0.2f' \
          % (np.average(syseff_clp),np.std(syseff_clp)),fontsize='10')
                        setp( ax2.get_xticklabels(), fontsize='15')
                        setp( ax2.get_yticklabels(), fontsize='15')
                        savefig('%s.png' % outfile)
                        clf()
                return


#___ Main Function ____________________________________________________________
if __name__ == "__main__":
        imagegroup = ImageGroup(range(15831,15839))
        imagegroup.sub_dark()
        print "Class ImageGroup is O.K.!"
```